



Norwegian University of  
Science and Technology

# Numerical and Experimental Study of the Airflow Distribution in Close Proximity to a Human Body with a Downward Plane Jet

**Marie Steffensen**

Master of Science in Mechanical Engineering

Submission date: June 2017

Supervisor: Guangyu Cao, EPT

Norwegian University of Science and Technology  
Department of Energy and Process Engineering



EPT-M-2017-83

**MASTER THESIS**

for

Student Marie Steffensen

Spring 2017

Numerical and experimental study of the airflow distribution in close proximity to a human body with a downward plane jet

*Numerisk og eksperimentell studie av luftstrømningsfordelingen nær en menneskekropp med en nedadgående plan jet*

**Background and objective**

Indoor thermal comfort environment aims at keeping more than 80% of the occupants satisfied with the thermal conditions. An acceptable thermal condition is taken as being one in which no more than 10% of the occupants would be dissatisfied as a result of their overall thermal sensation, and between 5 and 10% of the occupants would be dissatisfied according to local thermal discomfort. In the case of draughts, which are referred to as unwanted local cooling of the body caused by air movement, however, a typical maximum permissible dissatisfaction rate is 20%. In fact, a sensation of draught is determined by many factors, including the effect of the ambient environment and people's activities. As for the environmental factors which contribute to draught sensation, air temperature, air velocity, airflow direction, and turbulence intensity have been studied by many researchers. People's activity factors, such as exposure time and metabolic rate, have been shown to play an important role in the sensation of draught.

The objective of this study is to characterise numerically and experimentally the airflow distribution in close proximity to a human body with a downward plane jet.

**The following tasks are to be considered:**

1. Literature review: state of the art analysis of the airflow distribution close to a human body with a downward plane jet.
2. Model and simulate the interaction of a downward plane jet and thermal plumes from a human body.
3. Conduct experimental measurements of air velocity distribution close to a human body.
4. Analyse the effect of thermal plume on a downward plane jet and validate numerical models with measurement results.
5. Provide suggestions and guidance to design airflow distribution close to the human body to avoid draught sensation and improve local air quality.

Within 14 days of receiving the written text on the master thesis, the candidate shall submit a research plan for his project to the department.

When the thesis is evaluated, emphasis is put on processing of the results, and that they are presented in tabular and/or graphic form in a clear manner, and that they are analyzed carefully.

The thesis should be formulated as a research report with summary both in English and Norwegian, conclusion, literature references, table of contents etc. During the preparation of the text, the candidate should make an effort to produce a well-structured and easily readable report. In order to ease the evaluation of the thesis, it is important that the cross-references are correct. In the making of the report, strong emphasis should be placed on both a thorough discussion of the results and an orderly presentation.

The candidate is requested to initiate and keep close contact with his/her academic supervisor(s) throughout the working period. The candidate must follow the rules and regulations of NTNU as well as passive directions given by the Department of Energy and Process Engineering.

Risk assessment of the candidate's work shall be carried out according to the department's procedures. The risk assessment must be documented and included as part of the final report. Events related to the candidate's work adversely affecting the health, safety or security, must be documented and included as part of the final report. If the documentation on risk assessment represents a large number of pages, the full version is to be submitted electronically to the supervisor and an excerpt is included in the report.

Pursuant to “Regulations concerning the supplementary provisions to the technology study program/Master of Science” at NTNU §20, the Department reserves the permission to utilize all the results and data for teaching and research purposes as well as in future publications.

The final report is to be submitted digitally in DAIM. An executive summary of the thesis including title, student's name, supervisor's name, year, department name, and NTNU's logo and name, shall be submitted to the department as a separate pdf file. Based on an agreement with the supervisor, the final report and other material and documents may be given to the supervisor in digital format.

- Work to be done in lab (Water power lab, Fluids engineering lab, Thermal engineering lab)  
 Field work

Department of Energy and Process Engineering, 15. January 2017



---

Guangyu Cao  
Academic Supervisor

Research Advisor: Risto Kosonen <risto.kosonen@aalto.fi>

# Preface

This master's thesis has been conducted at Norwegian University of Science and Technology, NTNU, during the spring semester of 2017. The basis of the thesis work have been experiments done in the climate and energy laboratory at the university and computer simulations.

I would like to thank my supervisor, Guangyu Cao, for always answering my questions in times of need and for lending me a powerful computer. I would also like to thank Amar Aganovic for good advice and help during the project and master's thesis. Lastly, I would like to thank my parents for their support and for helping me correcting mistakes and improving the readability of the work.

Marie Steffensen  
Trondheim, 11th June, 2017



# Abstract

This study has investigated the airflow distribution close to a thermal manikin situated next to a downward plane isothermal air jet. Three cases have been investigated by experiments in the laboratory, computational fluid dynamics (CFD) simulations and mathematical models. In case 1, airflow characteristics for an isothermal plane jet were investigated. In case 2, airflow characteristics for the thermal plume rising from a thermal manikin were investigated. In case 3, the plane jet and thermal plume interaction were investigated with a thermal manikin at two locations next to the plane jet. Case 3 also explored the draught the manikin would supposedly have felt at the two locations next to the jet. The two locations corresponded to the locations the manikin would experience draught rates of 20% and 10%. The distances from the occupant's shoulder to the jet's centerline have been referred to as comfort distances. The results gained in this study are presented as vector-plots from the simulation, and velocity distribution contour plots, both from experiments and simulations. The experimental results were finally compared to the simulation results and the mathematical models. Neither of the models fitted the experimental results very well, although there was significant correlation in some areas.

The proposed comfort distances have been verified by the experiments and are regarded as the main findings of the draught rate study. The comfort distances were 0.14 m and 0.27 m from centerline of jet to shoulder of manikin, resulting in a draught rate of 20% and 10% respectively. The conditions assumed during the deduction of these comfort distances were an ambient air temperature of 23°C, a plane jet outlet velocity of 1.5 m/s and a metabolic heat rate of 1.2 MET for a sitting thermal manikin next to the jet.

The deduction of comfort distances next to a plane jet for the different comfort criteria of 20% and 10% draught rate can benefit the protected occupied zone ventilation business with valuable recommendations. Additionally, the results presented in this thesis can hopefully be utilized in several other applications, as studies of the human plume and the plane jet were also conducted.



# Sammendrag

Denne studien har undersøkt luftfordelingen rundt en termisk dukke plassert i nærheten av en plan isoterm luftgardin. Tre tilfeller av interesse har blitt undersøkt med eksperimenter i lab, numeriske fluiddynamikksimuleringer og matematiske modeller. I tilfelle 1 har aspekter rundt luftfordelingen til en plan luftgardin blitt undersøkt. I tilfelle 2 har aspekter rundt luftfordelingen til varmestrømmen fra en sittende termisk dukke blitt undersøkt. I tilfelle 3 har samhandlingen mellom luftgardinen og dukkens varmestrøm blitt studert for to dukkeplasseringer ved siden av luftgardinen. I tillegg har tilfelle 3 studert trekkraten dukken liksom ville ha følt i de to plasseringene ved siden av luftgardinen. Avstandene mellom dukkens skulder og luftgardinens senterlinje ble omtalt som komfort-avstander, og gjaldt for avstander som ville tilsvare trekkrate på 20% og 10%. Resultatene fra de eksperimentelle og de numeriske undersøkelsene ble blant annet presentert med kontur-plots. De numeriske undersøkelsene kunne også produsere vektor-plots for å vise luftbevegelsen i et område av interesse. Til slutt ble de eksperimentelle dataene sammenliknet med de numeriske og de matematiske modellene. Ingen av modellene passet de eksperimentelle resultatene vesentlig godt selv om det var merkbar korrelasjon i flere områder.

De foreslåtte komfort-avstandene har blitt verifisert av eksperimentelle data og regnes for å være det viktigste funnet gjort i trekkratestudien. Komfort-avstandene var henholdsvis 0.27 m mellom skulderen til dukken og luftgardinens senterlinje for en trekkrate på 20% og 0.14 m mellom skulderen til dukken og luftgardinens senterlinje for en trekkrate på 10%. Grensebetingelsene brukt i forbindelse med komfort-avstandene var 23°C i rommet, utløpshastighet for luftgardin på 1.5 m/s og en aktivitetsintensitet på den sittende dukken tilsvarende 1.2 MET.

Anbefalingene av komfort-avstander fra en sittende person til en luftgardin for komfort-kriteriene på 20% og 10% trekkrate kan være fordelaktig i forbindelse med bruk av "protected occupied zone"-ventilasjon. I tillegg kan resultatene fra masteroppgaven forhåpentligvis også bli brukt i andre sammenhenger, da luftgardiner og menneskelig varmestømmer har blitt studert.



# Contents

<b>Master's thesis description</b>	<b>I</b>
<b>Preface</b>	<b>III</b>
<b>Abstract</b>	<b>V</b>
<b>Sammendrag</b>	<b>VII</b>
<b>List of Figures</b>	<b>XV</b>
<b>List of Tables</b>	<b>XVII</b>
<b>List of Symbols</b>	<b>XIX</b>
<b>Abbreviations</b>	<b>XXI</b>
<b>1 Introduction</b>	<b>1</b>
1.1 Objective and motivation . . . . .	1
1.2 Structure and methodology . . . . .	2
1.2.1 Planning before and during the master's thesis . . . . .	3
1.3 Data acquisition and information retrieval . . . . .	3
<b>2 Theory on plane jets, the human thermal plume and draught</b>	<b>5</b>
2.1 Literature review on plane jets . . . . .	5
2.1.1 Protected occupied zone ventilation . . . . .	6
2.2 Theory on plane jets . . . . .	7
2.2.1 Velocity distribution . . . . .	8
2.2.2 Maximum velocity decay . . . . .	10
2.3 Theory on the human thermal plume . . . . .	13

2.3.1	Centerline velocity development . . . . .	14
2.4	Thermal comfort and draught . . . . .	17
<b>3</b>	<b>Experimental setup</b>	<b>21</b>
3.1	Experimental facility . . . . .	22
3.2	Air diffuser . . . . .	22
3.2.1	Measuring the outlet flow velocity . . . . .	25
3.3	Thermal manikin . . . . .	25
3.3.1	Calibration of manikin . . . . .	25
3.4	Measurement setup . . . . .	27
3.4.1	Calibration of anemometers . . . . .	29
<b>4</b>	<b>Experimental results</b>	<b>33</b>
4.1	Case 1: 2D downward plane jet . . . . .	33
4.2	Case 2: Thermal plume from thermal manikin . . . . .	35
4.3	Case 3: Interaction between thermal plume and downward plane jet . . . . .	37
<b>5</b>	<b>Theory on Computational Fluid Dynamics (CFD)</b>	<b>43</b>
5.1	Literature review on CFD in indoor environment scenarios . . . . .	44
5.2	Mesh . . . . .	45
5.2.1	Mesh quality indices . . . . .	45
5.2.2	Grid independence . . . . .	46
5.3	Boundary layers . . . . .	46
5.3.1	y+ . . . . .	47
5.4	Turbulence Models . . . . .	47
5.4.1	RNG k- $\epsilon$ model . . . . .	50
5.4.2	Enhanced wall treatment . . . . .	51
5.5	Thermal plume considerations . . . . .	51
5.6	Solution methods in Fluent . . . . .	52
5.7	Simulation errors . . . . .	53
5.7.1	Roundoff errors . . . . .	53
5.7.2	Iteration errors . . . . .	53
5.7.3	Solution errors . . . . .	53
5.7.4	Model errors . . . . .	54
<b>6</b>	<b>Simulation setup</b>	<b>55</b>
6.1	Geometrical models . . . . .	55
6.2	Meshes . . . . .	57
6.2.1	Grid independence check . . . . .	59

6.3	Setup in Fluent . . . . .	60
<b>7</b>	<b>Simulation results</b>	<b>63</b>
7.1	Case 1: 2D downward plane jet . . . . .	63
7.2	Case 2: Thermal plume from thermal manikin . . . . .	64
7.3	Heat transfer . . . . .	68
7.4	Case 3: Interaction between thermal plume and downward plane jet . . . . .	69
7.4.1	Manikin below jet . . . . .	70
7.4.2	Simulation results for case 3.1 and 3.2 . . . . .	71
<b>8</b>	<b>Discussion</b>	<b>77</b>
8.1	Comparison of results . . . . .	77
8.2	Limitations of the experimental setup . . . . .	80
8.3	Momentum evaluation . . . . .	83
8.4	Draught related discussion . . . . .	84
8.5	Validity of equations and deduction of comfort distances . . . . .	85
8.6	Applicability for real life scenarios . . . . .	86
8.7	Further work . . . . .	88
<b>9</b>	<b>Conclusion</b>	<b>89</b>
	<b>Appendix A: Technical drawing, diffuser</b>	<b>91</b>
	<b>Appendix B: Gantt chart</b>	<b>92</b>
	<b>Appendix C: Conference paper</b>	<b>93</b>
	<b>Appendix D: Additional experimental results</b>	<b>100</b>
	<b>Appendix E: Risk assessment report</b>	<b>102</b>



# List of Figures

1.1	Example of how to narrow down a search in Scopus . . . . .	4
1.2	Example of how to narrow down a search in WoS . . . . .	4
2.1	Workers in a foundry being cooled by an air douche. Source: Fundamentals of Industrial Ventilation, (Baturin, 1972) . . . . .	6
2.2	A plane, vertical jet in 2D and 3D . . . . .	7
2.3	Equation 2.1 gives the distribution of velocity, $U$ , along the $x$ -axis at various distances downstream of the nozzle, $y_j$ . $U(x = 0) = U_m$ . The value of $x$ is the lateral distance from the centerline. . . . .	9
2.4	Velocity distribution from equation 2.1 compared with equation 2.2 ( $y = 1.0$ m) . . . . .	9
2.5	Representation of the principal flow regions of a plane jet. Source: Baturin (1972) . . . . .	11
2.6	Flow through different shaped outlets. a) has a sharp opening, b) and c) have curved openings. c) is displaying the shape of the nozzle used in the experiment. . . . .	12
2.7	Simplified plume development from horizontal plate. Source: Industrial ventilation - Design guidebook, (Goodfellow and Tähti, 2001) . . . . .	16
3.1	Simplified setup in the lab . . . . .	21
3.2	Smoke visualization of the jet's profile . . . . .	23
3.3	3D-model of the diffuser, full view . . . . .	24
3.4	3D-model of the diffuser, sectioned view. The long plate along the middle is perforated . . . . .	24
3.5	The thermal manikin . . . . .	26
3.6	Measurement points for the experiments . . . . .	28
3.7	Setups in experimental facility . . . . .	29
3.8	Calibration setup for anemometer calibration . . . . .	31

4.1	Maximum velocity decay at jet centerline, mean values and standard deviations displayed . . . . .	34
4.2	Spread angle of experimental jet (a) and velocity contours of jet in xy-plane (b) . . . . .	35
4.3	Velocity contours of plume in xy-plane, facing the manikin, (a), and in yz-plane, manikin facing east, (b) . . . . .	36
4.4	Spread angle of experimental plume, xy-plane (a) and yz-plane (b) . . . . .	37
4.5	Maximum velocity decay at plume centerline, mean values and standard deviations displayed . . . . .	38
4.6	Smoke visualization of the jet and manikin for case 3.1 (a) and smoke machine setup (b) . . . . .	39
4.7	Maximum velocity decay at jet centerline, mean values and standard deviations displayed . . . . .	40
4.8	Velocity contours of jet and plume in xy-plane, manikin at $x=0.34$ m, (a), and manikin at $x=0.47$ m, (b) . . . . .	40
4.9	Velocity distribution at shoulder height, $y = 1.1$ m, with manikin positions at $x = 0.34$ m for case 3.1 and $x = 0.47$ m for case 3.2 . . . . .	41
5.1	The 4 different 3D mesh elements . . . . .	45
5.2	Comparison of velocity contours (a) and dimensionless velocity (b) for different turbulence models for an indoor flow situation. The model error can be seen as the variations between the turbulence models. (a) Source: Rong and Nielsen (2008), (b) Source: Wang and Chen (2009) . . . . .	54
6.1	CFD, geometrical setup . . . . .	57
6.2	Distribution of $y^+$ at the manikin . . . . .	57
6.3	Mesh used for the CFD analysis of case 1, jet scenario, (a)+(b), case 2, plume scenario, (c)+(d), case 3.1, manikin at 0.34 m from jet (e)+(f) . . . . .	58
6.4	Manikin surface mesh (a) and case 3.1 surface mesh, manikin placed 0.34 m next to jet (b) . . . . .	59
6.5	Percentage change in velocity at the point of interest from one mesh refinement to the next . . . . .	60
7.1	Velocity and Turbulence intensity contours close to the diffuser outlet of case 1 . . . . .	64
7.2	MATLAB deduced jet spread angle . . . . .	65
7.3	Velocity distributions at various heights above the floor (a), dimensionless representation (b) . . . . .	65
7.4	Jet centerline velocity development [m/s] . . . . .	66
7.5	Velocity contours [m/s], turbulence intensity [%] and temperature [ $^{\circ}$ C] contours, xy-plane . . . . .	67
7.6	Plume centerline velocity development from head of manikin . . . . .	67

7.7	Velocity distribution for plume at seven different heights, case 2, xy-plane (a) and yz-plane (b) . . . . .	68
7.8	Calculated plume spread from simulation, case 2, xy-plane (a) and yz-plane (b) . . . . .	68
7.9	Monitored velocity at 1.6 m above ground shows the flow is very unstable . . . . .	70
7.10	Velocity contours (a) and (b), pressure contour (c) and turbulence intensity (d) . . . . .	71
7.11	Velocity vectors colored by static temperature close to shoulder for manikin below jet . . . . .	72
7.12	Velocity streamlines of manikin below jet . . . . .	72
7.13	Velocity contours [m/s] and turbulence intensity, case 3.1 (a) and (c) and case 3.2 (b) and (d) . . . . .	73
7.14	Jet centerline maximum velocity decay for case 3 . . . . .	74
7.15	Velocity distribution laterally from shoulders at $y = 1.1$ m for case 3.1 ( $x=0.34$ m) and 3.2 ( $x=0.47$ m) . . . . .	75
7.16	Velocity vectors colored by temperature, case 3.1 (a) and case 3.2 (b) . . . . .	75
7.17	Velocity vectors colored by temperature, close-up at shoulder, case 3.1 . . . . .	76
7.18	Velocity vectors colored by temperature, close-up at shoulder, case 3.2 . . . . .	76
8.1	Jet centerline maximum velocity decay for case 1, comparison . . . . .	78
8.2	Plume centerline velocity development for case 2, comparison . . . . .	80
8.3	Jet centerline maximum velocity decay for case 1, comparison . . . . .	81
8.4	Velocity contour for 4 different iterations of case 3.1. The chosen case is at top right . . . . .	82
8.5	Jet centerline maximum velocity decay for case 1, comparison . . . . .	82
8.6	Deduction of comfort distances for DR = 10% and DR = 20% . . . . .	87



# List of Tables

2.1	Parameters to be used in equation 2.3 taken from the experimental setup . . . . .	11
2.2	The values of the parameters and variables used in calculations in the thesis . . . .	19
3.1	Measured manikin surface temperatures . . . . .	26
3.2	Measurement requirements from NS-EN 13182 (2002) . . . . .	29
3.3	Useful data about the measuring instruments used in the experiment . . . . .	30
4.1	Draught rate at shoulder for case 3.1 and 3.2 . . . . .	39
5.1	Mesh quality indices (ANSYS, 2016) . . . . .	46
5.2	Turbulence model overview . . . . .	48
5.2	Turbulence model overview . . . . .	49
5.2	Turbulence model overview . . . . .	50
6.1	The 3D model's human body components . . . . .	56
6.2	Important CFD aspects for the study. OQ = Orthogonal quality, SK = Skewness, AR = Aspect ratio . . . . .	62
7.1	Draught rate at shoulder for case 3.1 and 3.2 . . . . .	74
8.1	Draught rate at shoulder for case 3.1 and 3.2 . . . . .	85
A1	Parameters of interest for the jet flow, case 1 . . . . .	101



# List of Symbols

$\alpha$	Spread angle of jet/plume between centerline and edge [°]
$A_0$	Cross-sectional area of diffuser outlet [ $m^2$ ]
$A_i$	Cross-sectional area of jet at vena contracta [ $m^2$ ]
$A_{pers}$	Surface area of a person [ $m^2$ ]
$A_s$	Cross-sectional area of the jet/plume for a certain $y_j/y_p$ [ $m^2$ ]
$\beta$	Volumetric thermal expansion coefficient [ $K^{-1}$ ]
$b$	Length of the half width of the jet for a certain $y_j$ [ $m$ ]
$C_b$	Proportionality constant, dependent on spread angle, $\alpha$ [-]
$c_p$	Specific heat capacity of room air [ $\frac{kJ}{kgK}$ ]
$clo$	Clothing insulation [ $\frac{m^2K}{W}$ ]
$\Delta T_m$	Temperature difference between centerline of plume for a given $y_p$ and the room temperature [°C]
$D_{pers}$	Diameter of a person based on a cylinder approximation [ $m$ ]
$DR$	Draught rate [%]
$\epsilon$	Contraction coefficient [-]
$\varepsilon$	Eddy dissipation rate [ $J/(kg \cdot s)$ ]
$e$	The base of the natural logarithm [-]
$G_b$	Generation of turbulent kinetic energy due to buoyancy [ $J/(m^3s)$ ]
$G_k$	Generation of turbulent kinetic energy due to mean velocity gradients [ $J/(m^3s)$ ]
$Gr$	Grashof number [-]
$g$	Acceleration due to gravity [ $\frac{m}{s^2}$ ]
$h$	Height of the experimental facility [ $m$ ]
$h_0$	Height of diffuser outlet cross section [ $m$ ]
$h_c$	Convective heat transfer coefficient [ $W/m^2K$ ]
$h_{pers}$	Height of a person [ $m$ ]
$i$	Impulse coefficient [-]
$I_n$	Integral regularly used in jet equations [-]
$K$	Constant related to jet centerline velocity [-]
$k$	Turbulent kinetic energy [ $J/kg$ ]
$l$	Length [ $m$ ]

$m$	Body mass [ $kg$ ]
$\dot{m}$	Air mass flow rate [ $kg/s$ ]
$\mu_{eff}$	Effective dynamic viscosity [ $Pa \cdot s$ ]
$MET$	Metabolic rate [ $W/m^2$ ]
$n$	Subscript, an integer $\geq 1$ [-]
$N$	Number of readings in the given location [-]
$\nu$	Kinematic viscosity [ $Pa \cdot s$ ]
$p$	Static pressure [ $Pa$ ]
$Q$	Volume flow [ $\frac{m^3}{s}$ ]
$Re$	Reynolds number [-]
$\rho_0$	Air density at diffuser outlet [ $\frac{kg}{m^3}$ ]
$\rho_r$	Air density of the ambient room air [ $\frac{kg}{m^3}$ ]
$S$	User-defined source term [ $J/(m^3s)$ ]
$t_{a,l}$	Local air temperature used in DR-equation [ $^{\circ}C$ ]
$T_{room}$	Room temperature [ $^{\circ}C$ ]
$TU$	Turbulence intensity [%]
$U$	Velocity at a location (x,y) for either the jet or the plume [ $m/s$ ]
$U_0$	Nozzle outlet velocity [ $m/s$ ]
$U_m$	Velocity at the centerline for the jet/plume flow [ $m/s$ ]
$u$	Velocity in flow direction in RNG-model equations [ $m/s$ ]
$\bar{v}$	Average velocity of flow readings in a given location [ $m/s$ ]
$\bar{v}_{a,l}$	Local mean air velocity used in DR-equation [ $m/s$ ]
$w$	Width of the experimental facility [ $m$ ]
$\dot{W}_c$	Convective heat release [ $kW$ ]
$x$	Horizontal distance from the centerline of the jet/plume [ $m$ ]
$x_{0,5}$	Distance to the centerline where $U$ is equal to $0.5 \cdot U_m$ [ $m$ ]
$Y_M$	Contribution of fluctuating dilatation in compressible turbulence to the overall dissipation rate [ $J/(m^3s)$ ]
$y$	Vertical distance from the floor [ $m$ ]
$y_0$	Distance from the source of either jet or plume to outlet or heat emitting surface respectively [ $m$ ]
$y_i$	Length of initial/core zone of the jet [ $m$ ]
$y_j$	Vertical distance from the source of the jet [ $m$ ]
$y_p$	Vertical distance from the source of the plume [ $m$ ]
$y_t$	Length of transitional zone of the jet [ $m$ ]
$y+$	Non-dimensional height related to mesh [-]
$\emptyset$	Diameter [ $m$ ]

# Abbreviations

<b>POV</b>	Protected occupied zone ventilation
<b>PV</b>	Personalized ventilation
<b>ppm</b>	Parts per million
<b>WoS</b>	Web of Science
<b>DR</b>	Draught rate
<b>CFD</b>	Computational fluid dynamics
<b>CAD</b>	Computer assisted drawing
<b>CO<sub>2</sub></b>	Carbon dioxide
<b>MET</b>	Metabolic heat rate
<b>VariAC</b>	Variable transformer unit
<b>SD</b>	Standard deviation
<b>TU</b>	Turbulence intensity
<b>CtoC</b>	Centerline to centerline
<b>CtoS</b>	Centerline to shoulder
<b>RNG</b>	Re-normalization group
<b>SST</b>	Shear stress transport
<b>RSM</b>	Reynold stress model
<b>RKE</b>	Realizable k- $\epsilon$ model
<b>SKE</b>	Standard k- $\epsilon$ model
<b>LRN</b>	Low Reynolds number model
<b>DES</b>	Detached eddy simulation
<b>LES</b>	Large eddy simulation
<b>DNS</b>	Direct numerical simulation
<b>BL</b>	Boundary layer
<b>BC</b>	Boundary condition
<b>RANS</b>	Reynolds averaged Navier Stokes models
<b>OQ</b>	Orthogonal quality
<b>SK</b>	Skewness
<b>AR</b>	Aspect ratio



# Introduction

Indoor climate has been crucial to our well-being ever since the dawn of humankind. Even though the first humans lived outdoors, they were still driven by the same needs as we are today in terms of indoor climate – clean air and thermal comfort. Unlike us, the first humans breathed air of excellent quality all year round. However, they did not always live in thermal comfort, and had to use fires and animal hide to keep warm on cold days – just the way we today rely on ovens, floor heating, air conditioning and other sources to create a satisfying indoor climate. Despite abundant ways to heat or cool, we struggle to achieve continuous thermal comfort and supply of fresh air to breathe. One way to achieve a satisfying indoor climate can be to focus on attaining thermal comfort. Factors that can disrupt this comfort, can be thermal stratification, draught, radiative asymmetry, too cold or too hot floors etc. Out of all these kinds of possible ways to induce thermal discomfort, this master’s thesis will especially focus on draught in an indoor environment and how to prevent it. A practical asset gained from investigating the air flow distribution around a human body from a downward plane jet, is knowledge of draught, which can be applied in the field.

## 1.1 Objective and motivation

Recently, there has been developed a way to protect certain areas in a room from pollution sources using a plane vertical jet. This kind of ventilation is called Protected Occupied Zone Ventilation (POV) and has a goal of limiting the spread of airborne contaminants in a room or zone. The jet can block off or separate two zones from each other. Applications can be in hospitals to shield reception staff from sick patients or to shield patients susceptible to infections from pollution from doctors, or in office spaces to separate office cubicles from each other again to prevent spread of contagious diseases (Cao et al., 2014). By investigating the air distribution around a

human sitting next to such a plane air jet, this master's thesis can be used as a base for how to prevent draught in locations with POV. One interesting question is, how close to the jet can a person reside before feeling uncomfortable due to draught? The jet's outgoing velocity, the room's air temperature and the strength of the thermal plume rising from a human being will influence the answer, and are therefore thoroughly investigated.

As seen in the master thesis' description on page II, the objective of this study is to characterize both numerically and experimentally the airflow distribution in close proximity to a human body with a downward plane jet. To structure and limit the master's thesis to a comprehensible size, and to be able to extensively answer the main objective, some sub-objectives have been specified to ease the complexity of the task:

1. Making a mathematical model of the jet and the human thermal plume
2. Simulate numerically the flow interactions between the jet and the plume flow
3. Conducting measurements of the velocity distribution of a plane isothermal air jet under the influence of an occupant's thermal plume
4. Comparing the experimental results with the numerical results and the mathematical model
5. Assessing how far from the air curtain a person can reside without feeling thermally uncomfortable
6. Evaluating how such an air curtain can be applied in the field and how to prevent draught

## 1.2 Structure and methodology

The master's thesis is divided into two main parts after the two main scientific methods used. The main methods consist of an experimental part and a numerical part. Each part elaborates on theory, scientific setup and results regarding three situational cases. The three cases that are studied both by experiment and by simulation are:

1. 2D downward plane jet
2. Thermal plume from thermal manikin
3. Interaction between thermal plume from thermal manikin and downward plane jet
  - 3.1. Distance from thermal manikin centerline to jet centerline that corresponds to 20% draught rate
  - 3.2. Distance from thermal manikin centerline to jet centerline that corresponds to 10% draught rate

More specifically, case 1 studies the flow from a plane isothermal air jet. Case 2 studies the thermal plume from a sitting thermal manikin, resembling an occupant. Case 3 is divided into two sub-cases that investigates how close a manikin's centerline can be to the plane jet's centerline

without sensing a draught rate of more than 20% for sub case 3.1 and 10% for sub-case 3.2. Case 3 is the main interest of the study. Case 1 and 2 have the purpose of increasing the understanding of the different flow fields present in the case 3 scenario. It is easier to understand how the flows interact when their basic behavior is known by having case 1 and 2 as reference cases. After the cases have been studied separately in the experimental and the numerical part, the two parts and the three cases are compared in the discussion chapter together with a mathematical model to validate the results. Due to the fact that all research methods have their limitations and sources of errors, the trustworthiness of the results will increase if the results of comparing empirical data to a mathematical model coincide. Assessment of the draught sensed by a human close to the plane jet is also included in the discussion chapter. Finally, a conclusion will sum up the important aspects and findings of the thesis. The reader should have a basic understanding of typical indoor flows and ventilation techniques as well as some knowledge on computational fluid dynamics (CFD) to be able to comprehend the totality of this thesis.

### **1.2.1 Planning before and during the master's thesis**

To plan ahead, a Gantt chart was developed during the first 2 weeks of the semester, covering the 19 weeks left until the final delivery, 11.06.2017. The chart included time frames for the various stages of the thesis: literature study, development of a simulation model, experimental setup, conducting the experiment, interpreting experimental results, interpreting simulation results, writing the thesis, and proof reading. The Gantt chart can be found in appendix B. Generally, the three stages related to the experiment was initiated later than planned, due to a desire to use particle image velocimetry, PIV, as a flow visualization technique. Unfortunately, not enough time was available to perform the PIV, and the same measuring method used for the project work, which is described in a conference paper based on the results from the project work in appendix C had to be used. A full description of the thesis' experimental setup can be found in chapter 3.

## **1.3 Data acquisition and information retrieval**

Writing any kind of scientific paper requires a thorough literature study, because it is crucial for the paper's credibility. The quality of the paper will increase if the author is updated on the latest technology in the field. Oria.no is a gateway to the literature found in the various Norwegian scientific libraries, and it is accessible for anyone that has an oria-account (Bibsys, 2016) - this means practically all students in Norway. Oria gives full text access to papers and e-books from many renowned scientific databases. However, not all the papers accessible by NTNU are found in Oria. Therefore, databases like Scopus and Web of Science (WoS) were searched to get a more complete picture of available literature (Storleer, 2016). Citations have been exported to .bib-files from the respective publisher's page (for online literature). These files were imported into JabRef, a BibTex referencing program in the same style as EndNote. Book referencing has

Search history	Combine queries... e.g. #1 AND NOT #3	Q ?
3 TITLE ( convective boundary flow AND human* )		1 document results
2 TITLE-ABS-KEY ( convective boundary flow AND human* )		84 document results
1 TITLE-ABS-KEY ( convective boundary flow )		9,346 document results

Figure 1.1: Example of how to narrow down a search in Scopus

Search History: Web of Science™ Core Collection				Edit Sets	Combine Sets AND OR	Delete Sets Select All Delete
# 3	1	TITLE: (convective boundary flow AND human*) <small>Indexes=SCI-EXPANDED, SSCI, A&amp;HCI, CPCI-S, CPCI-SSH, ESCI Timespan=All years</small>		Edit	<input type="checkbox"/>	<input type="checkbox"/>
# 2	52	TOPIC: (convective boundary flow AND human*) <small>Indexes=SCI-EXPANDED, SSCI, A&amp;HCI, CPCI-S, CPCI-SSH, ESCI Timespan=All years</small>		Edit	<input type="checkbox"/>	<input type="checkbox"/>
# 1	7,246	TOPIC: (convective boundary flow) <small>Indexes=SCI-EXPANDED, SSCI, A&amp;HCI, CPCI-S, CPCI-SSH, ESCI Timespan=All years</small>		Edit	<input type="checkbox"/>	<input type="checkbox"/>
					AND OR	Select All Delete

Figure 1.2: Example of how to narrow down a search in WoS

been done manually by inserting citation information in JabRef.  $\LaTeX$ , the typesetting system used to write the thesis, collects the citations from the JabRef library.

As mentioned, WoS and Scopus are convenient databases. They both have millions of indexed items in virtually all science areas. They are easy to use, especially by the use of boolean operators, proximity operators or the use of \*-sign or "-sign. The use of operators will considerably narrow down a search, and ease the pursuit for relevant literature. Figure 1.1 and 1.2 shows how a search has been narrowed down by the use of different operators and search fields in both Scopus and WoS. The same search entry was used to show that the two databases have different literature contents. Oria.no, WoS and Scopus are peer-reviewed databases, which means that the articles found here have been approved by real people. This maintains the standard of the literature available (Bar-Ilan, 2008)

The university library has also been useful, especially when fundamental theories on fluid dynamics and turbulence were needed in the study. Journal research papers do not usually include the basics that are sometimes needed to fully understand the phenomena at hand. The chance to borrow a wide range of good books was therefore appreciated. Knowledge on performing experiments and using measuring instruments and air handling unit was mainly gathered during the project work the previous semester, which contributed to a swift completion of the experiment.

# Theory on plane jets, the human thermal plume and draught

This master's thesis has investigated a downward free isothermal plane jet and its influence on an occupant's thermal comfort close to the jet. This chapter includes a literature review on the use of isothermal plane jets and looks into the theory on plane jets, on the human thermal plume and on draught. Mathematical models and parameters to be used in calculations for comparison to the experimental and numerical results in chapter 8 are also determined.

## 2.1 Literature review on plane jets

The master's thesis has investigated the isothermal plane jet. The use of an isothermal plane jet in an indoor environment is not very common. The non-isothermal plane jet is, however, used in many areas, for instance to separate two areas of different temperatures from each other (Foster et al., 2006). Examples of non-isothermal plane jet applications are, for instance, to use a plane jet over the entrance to a shopping center with automatic doors, over the door to a cold storage or over the door to other places where it is desired to maintain a specific climatic environment (hot, cold or clean), but where people frequently have to go in and out of the door. Non-isothermal downward jets can also be used for cooling of workers and hot processes (Baturin, 1972; Yang et al., 2009), see figure 2.1. Isothermal plane jets have been found applied in protected occupied zone ventilation (POV), which is a ventilation system very relevant for this study. No other mentionable application that favors the isothermal jet over the non-isothermal jet was found.

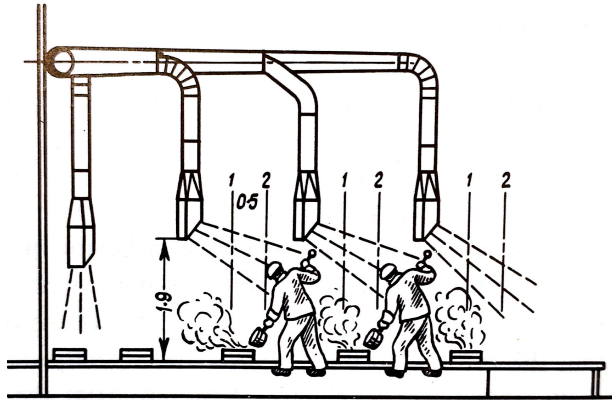


**Figure 2.1:** Workers in a foundry being cooled by an air douche. Source: *Fundamentals of Industrial Ventilation*, (Baturin, 1972)

### 2.1.1 Protected occupied zone ventilation

The protected occupied zone ventilation (POV) is a novel kind of ventilation that specializes in creating healthy zones of clean air inside a larger area usually with varying air quality. The POV normally takes advantage of vertical plane air jets to isolate the zones (Cao et al., 2015). One of the motivational factors for this kind of ventilation, is to hinder the spread of epidemic respiratory diseases, which are threatening our health today (Cao et al., 2014). These plane jets can, for instance, be used in waiting rooms in hospitals to separate sick patients and healthy staff and visitors, or in big offices to separate office booths from each other. The POV can prevent cross-contamination across booths, which is normal in offices today where mixing ventilation is used. The theory on POV has been developed quite recently, and not many studies have been conducted in this field. Therefore, the few studies published are important pieces in the understanding of this ventilation technique.

Especially the studies by Cao et al. (2014, 2015) on this area are central. One of the studies (Cao et al., 2014) investigated protected occupied zone ventilation (POV) with varying air flows and furniture arrangements. A traceable gas,  $CO_2$ , was used to simulate the pollution flow in the room. The optimal setup proved to separate the protected occupied zone from the polluted zone by up to 2800 ppm. The protection efficiency was defined in this study as: 1 minus the ratio of  $CO_2$ -concentration in the protected zone and the  $CO_2$ -concentration in the polluted zone. This efficiency specified how well the POV performed in shielding occupants from the pollution at the other side of the plane jet. This efficiency ranged from 8-50%. This journal article has been very useful in the thesis, mostly due to its use of a downward plane jet, but also due to the fact that it made the author realize that the results from this master's thesis' experiments can be of importance in this field.

## 2.2 Theory on plane jets

All the equations in this chapter regarding air jets are referring to a plane vertical jet with y-axis along the jet, and x-axis normal to the jet. Figure 2.2 shows a typical isothermal downward plane jet. A plane jet is defined as the jet coming out of an outlet with an aspect ratio of length,  $l$ , over width,  $h_0$  of at least 40 (Gutmark and Wygnanski, 1976; Awbi, 2003). Due to the high aspect ratio, the jet is considered uniform along the length of the nozzle, and we can treat the jet as a 2D jet as seen in figure 2.2. The diffuser outlet used in this thesis has an outlet width,  $h_0$ , and a diffuser length,  $l$ , of 0.02 m x 2.0 m respectively. This gives an aspect ratio of 100, thus the thesis's jet can be characterized as a plane jet. The 2D plane jet will henceforth be the considered dimensions for the plane jet throughout the thesis. As the jet develops, shear forces at the jet and room air interface entrains ambient air into the jet, increasing the jet's mass and volumetric flow rate. This is why the jet expands as it moves through the room. Due to the conservation of momentum, mass times velocity, throughout the the jet, the jet's velocity decreases as the mass increases (Skåret, 2000).

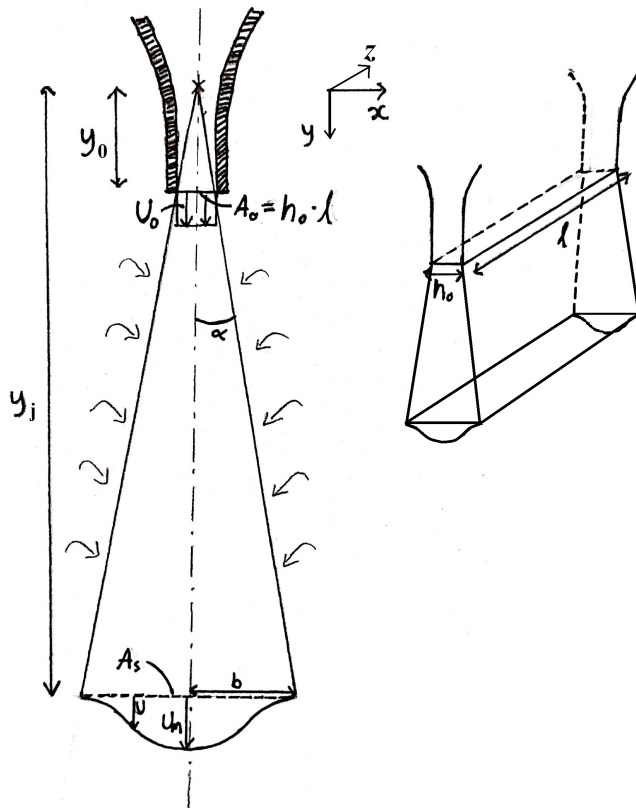


Figure 2.2: A plane, vertical jet in 2D and 3D

## 2.2.1 Velocity distribution

According to Abramovich (1963), the velocity profile of the vertical jet for a given  $y$ -location can be expressed as:

$$\frac{U}{U_m} = \left(1 - \left(\frac{x}{b}\right)^{1.5}\right)^2 \quad (2.1)$$

Where,  $U$  is the velocity at a certain distance  $x$  from the centerline,  $U_m$  is the velocity at the centerline, the maximum velocity for a given  $y_j$ , and  $b$  is the horizontal distance from the centerline to the jet's outer boundary.  $y_j$  is defined as the distance from the source of the jet to a desired height downstream, which can be seen in figure 2.2. The distance from the source of the jet to the outlet,  $y_0$ , is constant, and can be calculated by using Pythagoras' theorem. Hence, for half the outlet width,  $0.02 \cdot \frac{1}{2} = 0.01$  m, and a jet spread angle,  $\alpha$ , of  $13.4^\circ$ , we get:

$$y_0 = \frac{0.01}{\tan(13.4)} = 0.042m$$

An  $\alpha = 13.4^\circ$  was found by measuring the spread angle of the jet used in the experiment.

Equation 2.1 correlates well with early experimental results for velocity distributions for the main region of plane jets and axial jets, both isothermal and non-isothermal (Abramovich, 1963). This equation is also frequently used by Skåret (2000) who has written one of the syllabus books for the technical course: "Ventilation for fire, industry and safety" at Norwegian University of Science and Technology (NTNU). Figure 2.3 displays, using equation 2.1, the change in velocity distribution for  $(y_j - y_0)$  ranging from 0.5 m to 1 m. As the jet propagates, its profile widens and flattens. This coincides with the fact that the velocity decreases as the jet moves through still air, and the mass increases, resulting in a wider and wider jet ( $b$  increases).

According to Awbi (2003), the following equation, a Gaussian distribution, also produces velocity distribution profiles very close to earlier experimental results:

$$\frac{U}{U_m} = e^{-\ln 2 \left(\frac{x}{x_{0.5}}\right)^2} \quad (2.2)$$

Where  $U$  is the velocity at the location of interest,  $U_m$  is the maximum velocity decay,  $x$  is the distance to the centerline at a given  $y_j$  and  $x_{0.5}$  is the distance to the centerline for the same  $y_j$  where  $U = 0.5 \cdot U_m$ . Skåret (2000) also lists this equation as trustworthy. However, he mentions that for areas very close to the jet boundary, its precision decreases, as seen in figure 2.4. Due to Skåret's reasoning, equation 2.2 was only used to validate results from equation 2.1.

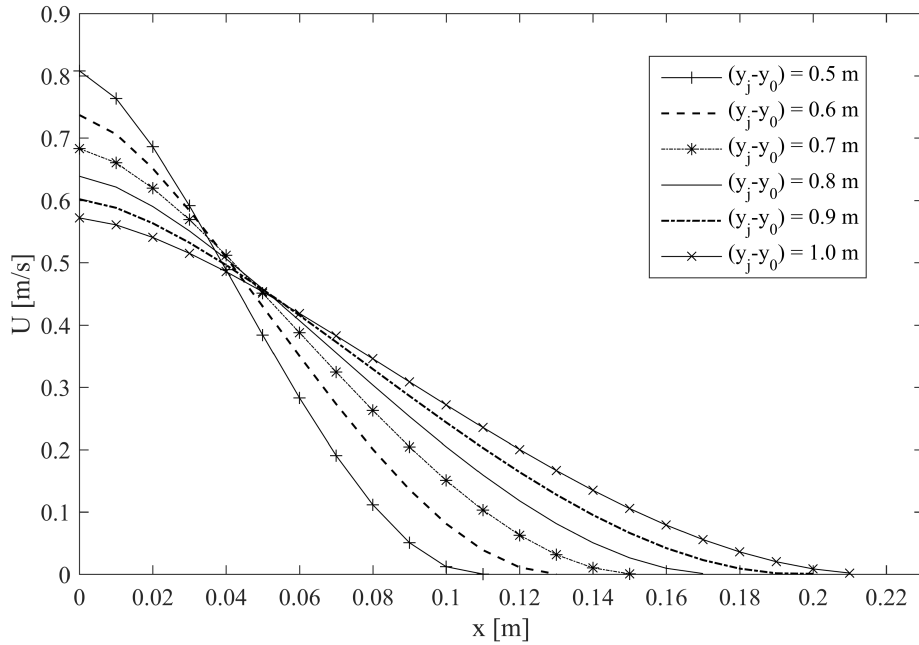


**Figure 2.3:** Equation 2.1 gives the distribution of velocity,  $U$ , along the  $x$ -axis at various distances downstream of the nozzle,  $y_j$ .  $U(x=0) = U_m$ . The value of  $x$  is the lateral distance from the centerline.

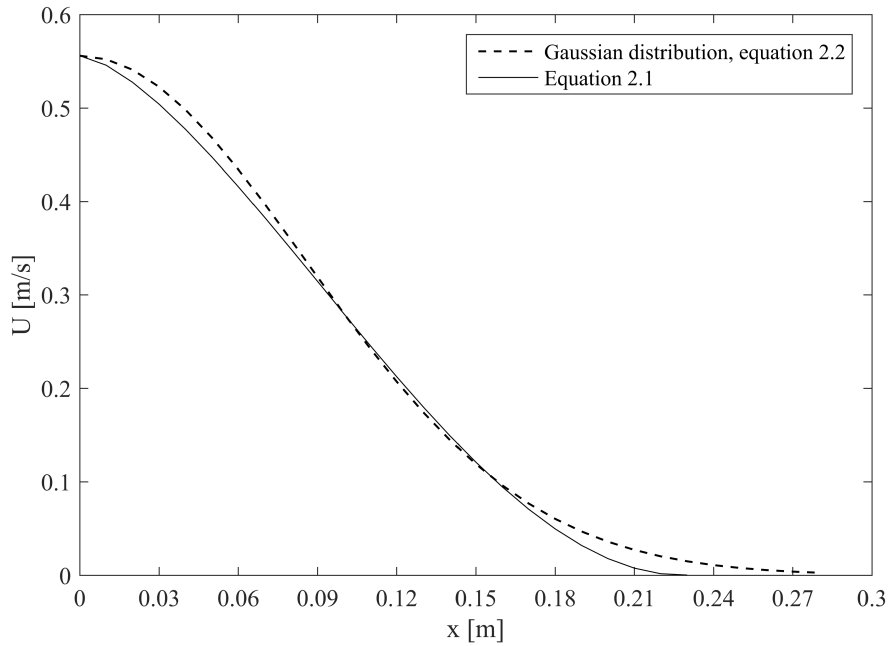


**Figure 2.4:** Velocity distribution from equation 2.1 compared with equation 2.2 ( $y = 1.0$  m)

## 2.2.2 Maximum velocity decay

As the jet develops downstream, more and more air gets entrained at the jet's boundary due to increasing surface area. In other words, the air jet's mass increases. To uphold the momentum, the velocity has to decrease. The maximum velocity decay equation by Skåret (2000) gives the correlation between outlet velocity,  $U_0$ , taken as 1.5 m/s, which is a common outlet velocity for plane jets used in POV, and the maximum decayed velocity at the centerline,  $U_m$ :

$$\frac{U_m}{U_0} = \sqrt{\frac{h_0 \cdot \rho_0 \cdot i}{y_j \cdot \rho_r \cdot \epsilon \cdot I_4 \cdot 2 \tan \alpha}} = K \sqrt{\frac{h_0}{y_j}} \quad (2.3)$$

Where,  $h_0$  is the width of the diffuser opening,  $y_j$  is the distance downstream from the source of the jet,  $\rho_0$  is the air density at the diffuser outlet,  $\rho_r$  is the air density of the ambient room air,  $\epsilon$  is the contraction coefficient,  $I_4$  is a constant related to the free, plane jet, and is equal to 0.316 (Skåret, 2000),  $i$  is a coefficient relating to eventual impact losses the jet might experience at the outlet and  $\alpha$  is the spread angle of the jet from the centerline, in this study measured to be  $13.4^\circ$ . For this master's thesis, the K for a free plane jet was found to be 2.58. In other studies, Gutmark and Wagnanski (1976) has found K to yield 2.43, while Skistad (1995) and Awbi (2003) used a K equal to 2.7 and 2.67 respectively.

Equation 2.3 is valid for the fully developed/main region of the plane jet. As displayed in figure 2.5, a plane jet consists of two principal regions: the core/initial region and the main region (Baturin, 1972; Awbi, 2003). Between them, a smaller transitional region bridges the two regions. In the core region,  $U_0 = U_m$ . The region extends to roughly 10 times the half-width of the outlet,  $\frac{h_0}{2} = 0.01$  m (Abramovich, 1963), and can be seen in figure 2.5 as  $y_i$ . The transitional region,  $y_t$ , extends to a length of 1.2 times the core region. The main region of the plane jet comes after this, roughly 15 times the half-width, and is considered to have a fully developed flow. Equations modeling the transitional region have not been found by the author. More about this can be found in chapter 8.

To use equation 2.3 as an approximation of the maximum velocity decay of the experiment, all the parameters in the equation had to be evaluated correctly to fit the experiment.  $h_0$ ,  $y_0$ ,  $\rho_0$  and  $\rho_r$  are parameters taken from the experimental setup (chapter 3). These values, which are used in calculations specifically for this study, are given in table 2.1.

The other parameters,  $\epsilon$ ,  $I_4$ ,  $i$  and  $\alpha$ , will henceforth be determined.

### Contraction coefficient, $\epsilon$

A flow in a nozzle follows the streamline principle of Bernoulli. Therefore, for  $90^\circ$  edged nozzle outlets (like in figure 2.6a) the flow will not fill the outlet opening due to the streamline's inability to instantly turn  $90^\circ$ . To do this, an infinitely high pressure gradient had to act across

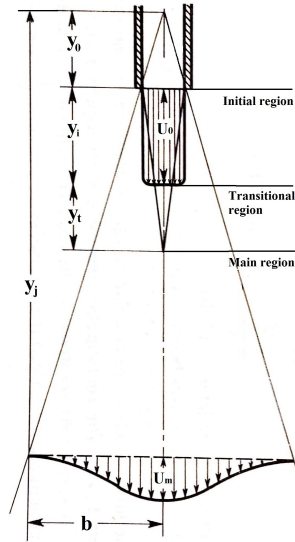


**Figure 2.5:** Representation of the principal flow regions of a plane jet. Source: Baturin (1972)

**Table 2.1:** Parameters to be used in equation 2.3 taken from the experimental setup

Parameter	Value
$h_0$	0.02 m
$y_0$ , part of $y_j$	0.042 m
$\rho_0 = \rho_r$	$1.19 \frac{kg}{m^3}$

the streamlines. Instead, the cross-section of the jet will contract slightly a little distance away from the outlet, into what is called a *vena contracta* (Munson et al., 2002). The *contraction coefficient*,  $\epsilon$ , is the ratio between the vena contracta's cross-sectional area,  $A_i$ , and the nozzle outlet's cross-sectional area,  $A_0$ , (Crowe et al., 2010):

$$\epsilon = \frac{A_i}{A_0} \quad (2.4)$$

As seen in figure 2.6, figure 2.6a) has a sharp opening. This kind of opening yields a contraction coefficient,  $\epsilon$ , of around 0.62 (Crowe et al., 2010). Figure 2.6b and 2.6c however, have curved openings, allowing the streamlines to follow the geometry, thus  $\epsilon \approx 1$ .  $\epsilon \approx 1$  is optimal to use, since  $U_0$  for  $\epsilon < 1$  is taken as the velocity at the vena contracta, while for  $\epsilon \approx 1$ ,  $U_0$  equals the outlet velocity. The outlet velocity is much easier both to calculate and to measure in an experiment. Therefore, the nozzle was made to have an  $\epsilon$  as close to 1 as possible.  $\epsilon = 1$  is the value used in equation 2.3.

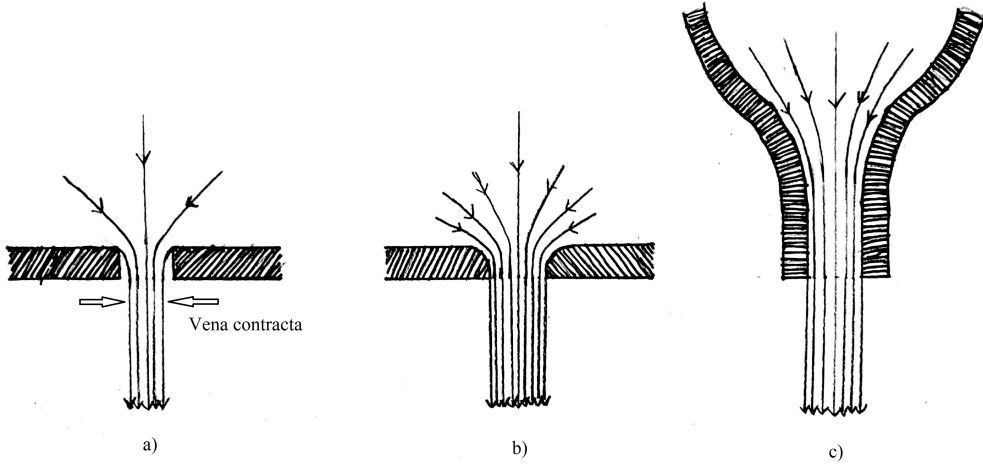


**Figure 2.6:** Flow through different shaped outlets. a) has a sharp opening, b) and c) have curved openings. c) is displaying the shape of the nozzle used in the experiment.

### The jet characteristic, $I_4$

$I_n$  is an integral found in various jet flow equations, like in equation 2.3 for the maximum velocity decay. It is short for:

$$I_n = \int_0^1 \left(1 - \left(\frac{x}{b}\right)^{1.5}\right)^n \frac{dA}{A_s} = \int_0^1 \left(\frac{U}{U_m}\right)^{\frac{n}{2}} \frac{dA}{A_s} \quad (2.5)$$

Where  $x$  is the horizontal distance from the jet's centerline for a corresponding velocity,  $U$ ,  $b$  is the horizontal distance from the jet's centerline to the edge of the jet,  $n$  is an integer  $\geq 1$ ,  $A_s$  is the cross-sectional area of the jet at a given distance,  $(y_j - y_0)$ , downstream of the nozzle.

For a plane, free jet,  $I_4$  has been calculated to be 0.316 (Abramovich, 1963).

Inside this integral,  $I_n$ , we find the equation for the jet's velocity distribution (equation 2.1). By looking closely at this integral, it is observable that the integral used in the maximum velocity decay equation (equation 2.3),  $I_4$ , is actually the velocity distribution squared.

### Impact loss coefficient, $i$

Skåret (2000) does not elaborate much on this coefficient. He explains it as the impact loss a flow can have if it passes through a grid or something similar in the nozzle opening. The impact loss will induce a loss in momentum, and is a number between 0 and 1.

Since the outlet velocity for the plane jet,  $U_0$ , is assumed to be 1.5 m/s just AFTER the opening,  $i$  will be taken as 1 in equation 2.3.

**Discharge angle,  $\alpha$** 

The jet's discharge angle is semi-empirically found (Skåret, 2000). Thus, the  $\alpha$  used by different researchers varies. Baturin (1972) states that a plane jet's spread angle can vary between  $12^\circ - 16^\circ$ , while Abramovich (1963) uses  $\alpha = 12.3^\circ$  in his study, Skåret (2000) uses  $\alpha = 13.2^\circ$ , Skistad (1995) uses  $\alpha = 11^\circ$  and Awbi (2003) uses  $\alpha = 12.5^\circ$ . The span of different values makes it difficult to know which  $\alpha$  to use, especially since very few of the researchers elaborate on the experimental setup used to find the value. Therefore, both the experiment and the simulation did a measurement of the jet's spread angle to find the correct  $\alpha$  for the study. The simulation yielded a spread angle of  $\alpha = 13.1^\circ$ , while the experiment got an  $\alpha = 13.4^\circ$

## 2.3 Theory on the human thermal plume

For the experiment to be as realistic as possible, the occupant's thermal plume has been taken into consideration. Temperature differences between the occupant and the ambient air create density differences in the air around the occupant. Due to the buoyancy effect, heated air surrounding the occupant rises up above the occupant's head. Naturally, this plume will interact with the plane jet if the occupant is sitting close by, which is precisely the reason why knowledge on the human thermal plume is equally as important as jet theory (section 2.2) in this study. The larger the temperature difference between the ambient air and the body surface temperature, the more powerful the plume will become, and the more it can affect the downward jet. In the case where the natural convective flow, the plume, and the forced convection from the jet is more or less equal, the heat transfer from the manikin is referred to as *mixed* convection. According to Zhai et al. (2007), the most common air-conditioned indoor flow scenario is mixed convection. It is characterized when the Grashof number divided by the Reynolds number squared is approximately equal ( $Gr/Re^2 \approx 1$ ). This can be the case in case 3 where the jet flow and the plume flow are studied together. A location of interest would be at the occupant's shoulder which is the most probable area of impact from the jet on the occupant. Calculating the total convective heat transfer from a human body at a certain distance to a plane jet is possible if the surface areas of the body subjected to mixed, forced and natural convection is known. Due to the complex human geometry, however, and uncertainties regarding characteristic lengths for the various areas subject to the different types of convection, calculating the total convective heat released in this way is difficult. Unfortunately, a relationship between heat transfer in W, being the result of such an evaluation, and draught rate was not found, or else more could have been done in this area. Since draught rate has been the focus of study in this thesis, an evaluation of the heat transfer from different types of convection has not been conducted. Instead, metabolic heat rate, surface area and the typical percentage of convective heat for a manikin have been used to approximate convective heat transfer.

Exactly what is happening in the plume-air jet interaction and how they affect each other, studied

by case 3, is currently impossible to accurately model mathematically. No mathematical models have been found describing this kind of flow situation. This is the reason why case 3 with jet and plume is only investigated by experiment and simulation with computational fluid dynamics, CFD. Deducing mathematical models for this interaction is a natural way forward if investigated further.

The focus will now be on the human thermal plume. According to Turner (1973); Skåret (2000); Awbi (2003), the thermal plume from a heat source in a quiescent environment has approximately the same velocity and temperature distribution as an air jet, in other words, a Gaussian distribution. However, the section of the plume they are referring to is the plume's fully developed region where the flow is self-similar. In this region, thermal stratification is negligible, and is usually located 1 m or more above the heat source (Borges et al., 2002). No equations were found for the human thermal plume explicitly. Equation 2.1 will therefore be used for the velocity distribution calculations regarding the human plume due to the lack of alternatives.

Part of the literature claims that the spread of a thermal plume is equal to that of an axisymmetrical jet of roughly  $12.5^\circ$  (Baturin, 1972; Awbi, 2003; Goodfellow and Tähti, 2001). However, according to Zukowska (2011) the edge of the plume for a certain cross-section is positioned at a distance from the location of  $U_m$  where  $U = U_m/e$  (where  $e \approx 2.71828$ ). By fitting this to the experimental data acquired in this thesis, a spread angle of  $11.3^\circ$  was found.

### 2.3.1 Centerline velocity development

There was, as mentioned, not found any mathematical models in the literature for the thermal plume from the complex geometry of the human body. Typically, the literature approximated a human geometry by the use of a cylinder (Goodfellow and Tähti, 2001; Zukowska et al., 2007; Dokka TH, 2002; Makhoul et al., 2013). When approximating a human as a thermal cylinder, an appropriate height and diameter of the cylinder should be found. Dokka TH (2002) used this correlation for the cylinder diameter,  $D_{pers}$ :

$$D_{pers} = 2 \left( -h_{pers} + \sqrt{h_{pers}^2 + \frac{A_{pers}}{\pi}} \right) = 0.363m \quad (2.6)$$

Where  $h_{pers}$  is the the cylinder height equal to the height of the sitting thermal manikin, measured to be 1.4 m.  $A_{pers}$  is the surface area of a person, which is on average  $1.8 \text{ m}^2$ . However, by the use of equation 2.7, the more specific Du-Bois surface area could be found (Jones, 2001):

$$A_{pers} = 0.202m^{0.425}h^{0.725} \quad (2.7)$$

Where  $A_{pers}$  is the surface area of the person,  $m$  is the body mass [kg],  $h$  is the height [m]. For the thermal manikin used in the experiment, the standing height was roughly 1.72 m, and

supposed body mass was roughly 60 kg. This gave an  $A_{pers} = 1.705 \text{ m}^2 \approx 1.7 \text{ m}^2$ . This value was used for  $A_{pers}$  in equation 2.6.

Various mathematical models from the literature have been explored to find an appropriate model of the maximum velocity at a certain height above a person's head. The well-known point and line source equations could be used. Vertical plumes from horizontal plates are more similar to the plume from a human head than from points or lines. Goodfellow and Tähti (2001) describes a horizontal plate approach. It is fairly similar to the point source approach, but rather approximates a virtual plume source,  $y_0$ , below the horizontal heat source of interest, here the manikin's head, instead of assuming the source point was at the top of the manikin's head. The horizontal plate approach uses the virtual source together with the point source equation. The virtual source is the point where the plume boundaries meet. Figure 2.7 describes the way of thinking. Two point source equations, eq. 2.8 and eq. 2.9 have been compared. Heskestad (1984) introduces this correlation for an axisymmetric plume's centerline velocity development for a point source:

$$U_m = 3.4 \left( \frac{g}{\rho c_p T} \right)^{\frac{1}{3}} \cdot \left( \frac{\dot{W}_c}{y_p} \right)^{\frac{1}{3}} \quad (2.8)$$

Where  $U_m$  is the plume's centerline velocity for a certain  $y_p$ , where  $y_p$  now is the distance from the virtual source and not from the top of the plate, to a desired height,  $y$  [m],  $g$  is the acceleration due to gravity,  $T$  is equal to  $T_{room}$  [K],  $\rho$  is the density of the room air,  $c_p$  is the specific heat capacity of the room air,  $\dot{W}_c$  is the convective heat power emitted from the source [kW]. The numerical factor 3.4 was found experimentally from experiments regarding fire plumes.

Skåret (2000) uses this correlation for a point source:

$$U_m = \frac{1.63}{C_b^{\frac{2}{3}}} \cdot \left( \frac{g\beta}{\rho c_p} \right)^{\frac{1}{3}} \cdot \left( \frac{\dot{W}_c}{y_p} \right)^{\frac{1}{3}} = C \cdot \left( \frac{\dot{W}_c}{y_p} \right)^{\frac{1}{3}} \quad (2.9)$$

The definitions of  $U_m$ ,  $\rho$ ,  $c_p$ ,  $g$ ,  $y_p$  and  $\dot{W}_c$  are the same for equation 2.8 and 2.9.  $C_b$  is equal to  $\tan \alpha = 0.238$  for  $\alpha = 13.4^\circ$ ,  $\beta$  is equal to  $\frac{1}{T_{room}}$ .

The two equations, 2.8 and 2.9, are, in fact, equal except for the empirical coefficient C, which for eq. 2.8 is 1.027 and for eq. 2.9 is 1.28. 1.28 is a value used a lot in the literature (Awbi, 2003; Goodfellow and Tähti, 2001; Skåret, 2000) for plume centerline velocity development.

It is possible to find  $y_0$  using Pythagoras' theorem, like Abramovich (1963); Goodfellow and Tähti (2001) and Skistad (1995) as for the jet. Heskestad (1984) has a different approach, and refers to a  $y_0$  as a function of the heat released (kW). Skåret (2000) uses a  $y_0$  which is 0-0.5 times the diameter or width of a horizontal plate,  $D$  or  $D_{pers}$  in this case, while Goodfellow and Tähti (2001) suggest that  $y_0$  is somewhere between 1.7-2.1 times  $D$ . Due to the extreme variations in definitions of  $y_0$ , the definition by Awbi (2003) of  $y_0 = 1.2 \text{ m}$  was chosen in the thesis because this was meant for cylinders, which are closer to a human than a horizontal plate. The results

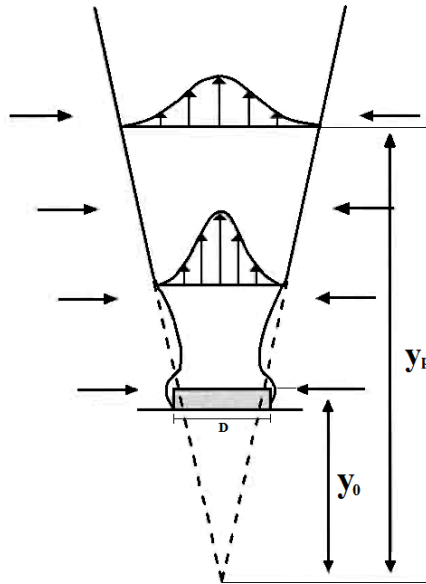


**Figure 2.7:** Simplified plume development from horizontal plate. Source: *Industrial ventilation - Design guidebook*, (Goodfellow and Tähti, 2001)

should anyhow be viewed critically, as well as the results from the plume equations 2.8 and 2.9 for using the virtual source assumption for horizontal plate sources.

The manikin was assumed to have a metabolic rate of 1.2 MET which is equal to  $1.2 \cdot 58.2 W/m^2 = 69.84 W/m^2$ . A total heat release was therefore assumed to be  $69.84 \cdot 1.7 = 118.7 W$ , where  $1.7 = A_{pers}$ . The body's surface temperatures were assumed to be  $33^\circ C$  for the head and neck,  $32^\circ C$  for the upper body and  $31^\circ C$  for the lower body. To find the convective heat release,  $\dot{W}_c$ , the types of heat release had to be classified. A real human emits both latent heat (evaporation and respiration (21%) plus heat loss from heating of intake of air and food (4%)) and sensible heat (convection (31%), and radiation (44%)) (Baturin, 1972). A manikin, on the other hand, only releases sensible heat, where roughly 40% comes from convection and 60% from radiation (Sørensen and Voigt, 2003; Murakami et al., 2000). The total convective heat output released from the thermal manikin should therefore equal  $\dot{W}_c = 0.4 \cdot 118.7 = 47.5 W$ .

Knowing the strength of the plume can be difficult since it can vary a lot between different indoor conditions. Typical values in the literature for maximum plume velocities are around 0.3 m/s (Homma and Yakiyama, 1988; Licina et al., 2014). According to Licina et al. (2015) the thermal plume above a sitting person in a quiescent environment at  $23^\circ C$  will be destroyed by a downward flow of 0.425 m/s at the manikin's surface. This implies that the manikin will not be protected by its thermal plume while being exposed to an airflow of 0.425 m/s at its body. It also means that the plume produced by the manikin in Licina et al.'s experiment only reached velocities lower than 0.425 m/s. Homma and Yakiyama (1988) measured a plume velocity of

0.25 m/s at a distance of 0.15 m above an occupant's head. For the same height, Licina et al. (2014) got a plume velocity of 0.30 m/s.

## 2.4 Thermal comfort and draught

As explained in 1.1, the thesis will consider the possible draught a person might experience when residing close to a downward plane jet, for instance in the case of POV being used in an indoor space. To investigate draught, some knowledge on thermal comfort is needed. According to Norwegian standard NS-EN7730 (2005):

*"Thermal comfort is the condition of mind which expresses satisfaction with the thermal environment"*

Thermal comfort is an important term in the field of thermal environment. An occupant's thermal comfort can be influenced by six factors. Two are personal factors, namely metabolic rate and clothing insulation, and the other four are the environmental parameters air temperature, mean radiant temperature, air velocity and relative humidity (Corgnati and da Silva, 2011). Several different combinations of these factors may be used to achieve thermal comfort. There is no clear answer. However, Fanger (1972) has a general theory that for sedentary situations, a person experiences thermal comfort as long as:

- The air temperature is between 23°C and 26°C
- The vertical thermal stratification from 0.1 m to 1.1 m in a room is less than 3°C
- The mean air velocity subject to a person is less than 0.25 m/s

If these guidelines are followed, a typical occupant with an activity of 1.2 MET (sedentary activity) and a clothing insulation of 1 clo ( $= 0.155 \frac{m^2 K}{W}$ ) in a room with these conditions should be thermally comfortable. A bad combination of these parameters, for example too low temperature and high mean air velocity, can cause the sensation of draught. It is a sensation most people can relate to and is one of the most frequent causes of complaint in heated or cooled buildings and transport vehicles (Awbi, 2003). Draught is a type of local thermal discomfort, and is usually referred to as unwanted local convective cooling of a person. Typically, draught from below on the head and draught on the back of the neck is easier felt than draught downward on the head or draught towards the face. Also, the magnitude of the unwanted convective cooling is affected by the temperature difference between skin and room air, air velocity and turbulence intensity (Awbi, 2003). Studies show that as long as a person is normally clothed (1 clo) and is thermally neutral, exposure of air of high velocity is usually of minor importance (Fanger, 1972). This also agrees with the fact that people can feel thermally comfortable outdoors where the air velocity usually is higher than indoors. However, personal differences are big in this area. Especially skin exposed to air of high velocity can be uncomfortable.

According to NS-EN7730 (2005), calculating the draught rate, DR, can give a percentage of

people dissatisfied due to draught:

$$DR = (34 - t_{a,l})(\bar{v}_{a,l} - 0.05)^{0.62} \cdot (0.37 \cdot \bar{v}_{a,l} \cdot Tu + 3.14) \quad (2.10)$$

For  $\bar{v}_{a,l} < 0.05 \text{ m/s}$  : use  $\bar{v}_{a,l} = 0.05 \text{ m/s}$

For  $DR > 100\%$  : use  $DR = 100\%$

Where  $t_{a,l}$  is the local air temperature [ $^{\circ}\text{C}$ ] between  $20^{\circ}\text{C}$  and  $26^{\circ}\text{C}$ ,  $\bar{v}_{a,l}$  is the local mean air velocity [ $\text{m/s}$ ]  $< 0.5 \text{ m/s}$ ,  $Tu$  is the local turbulence intensity [%] between 10% and 60% (if unknown, 40% may be used). The equation is valid for people at sedentary activities, and concerns a typical draught sensation felt at the neck. The draught rate can give an indication of the possible draught the manikin will supposedly feel during the experiment.

The draught rate is a very central part of the thesis, and case 3 is, as introduced, investigating two manikin locations next to a plane jet that will yield a DR of 20% and 10% for comfort categories B and A respectively (case 3.1 and 3.2). The comfort categories are defined in NS-EN7730 (2005), where category B is usually applied to new buildings used by normal, healthy occupants, while category A is mostly used in buildings or rooms with sensitive and fragile occupants, like the young and the elderly. The two distances between the manikin's location and the plane jet centerline is referred to as comfort distances. These comfort distances had to be calculated before conducting measurements to know where to place the manikin. The calculation of the comfort distances consisted of two steps: calculations of the maximum velocities allowed for the desired comfort criteria (20% and 10% DR) and finding the location that these velocities corresponded to in the jet's velocity distribution. Step one used equation 2.10 to calculate the velocities for a DR of 10% and 20%. An ambient temperature of  $23^{\circ}\text{C}$  and a turbulence intensity (TU) of 10% were used in these calculations. A TU of around 10% was experimentally found close to and in the jet in the project work, hence this value was used. The maximum allowed velocities found were 0.143 m/s and 0.278 m/s for a DR of 10% and 20% respectively. In step two, the respective x-locations at the shoulder height of 1.1 m were found from the plane jet simulations of the jet's velocity distribution. A more detailed description of the deduction of the comfort distances can be found in chapter 8.5. The comfort distances calculated were 0.34 m for a DR of 20% and 0.47 m for a DR of 10% for case 3.1 and 3.2 respectively. A distance from centerline of manikin to upper arm/shoulder of 20 cm was included in the comfort distances. The real distances between the shoulder of the manikin and the jet centerline were 0.14 m for 20% DR and 0.27 m for 10% DR.

Table 2.2 is included to give a quick summary over the specific parameters used in thesis that were introduced in this chapter.

**Table 2.2:** The values of the parameters and variables used in calculations in the thesis

<i>Air jet relevance</i>		<i>Plume relevance</i>	
<b>Parameter</b>	<b>Value</b>	<b>Parameter</b>	<b>Value</b>
$U_0$	1.5 m/s	$h_{pers}$	1.4 m
$h_0$	0.02 m	$A_{pers}$	$1.7 \text{ m}^2$
$\alpha$	$13.4^\circ$	$T_{amb}$	$23^\circ\text{C} = 296\text{K}$
$I_4$	0.316	$y_{0,plume}$	1.2 m
$\epsilon$	1	$\dot{W}_c$	47.5 W
$\rho_r$	$1.19 \frac{\text{kg}}{\text{m}^3}$	$\alpha$	$11.3^\circ$
$\rho_0$	$1.19 \frac{\text{kg}}{\text{m}^3}$	$\rho$	$1.19 \frac{\text{kg}}{\text{m}^3}$
$i$	1	$c_p$	$1.007 \frac{\text{kJ}}{\text{kgK}}$
$y_{0,jet}$	0.042 m	$C_b$	0.238
		$\beta$	$0.0034 \text{ K}^{-1}$



## Experimental setup

This chapter will provide an overview of the experimental setup, the measuring methods and the calibration of equipment.

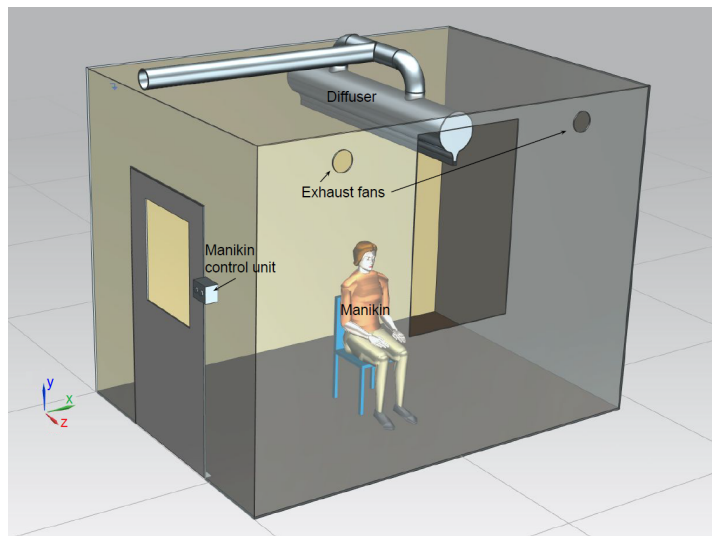


*Figure 3.1: Simplified setup in the lab*

As introduced in chapter 1, the thesis investigates 3 different cases both experimentally, in this chapter, and numerically, in chapter 6:

1. 2D downward plane jet
2. Thermal plume from thermal manikin
3. Interaction between thermal plume from thermal manikin and downward plane jet

- 3.1. Distance from thermal manikin centerline to jet centerline that corresponds to 20% draught rate
- 3.2. Distance from thermal manikin centerline to jet centerline that corresponds to 10% draught rate

The cases are further evaluated in chapter 8 with a comparison of experimental data, numerical data and data from the mathematical models.

## 3.1 Experimental facility

The facility used during the experiment resembled a small office located inside a laboratory at NTNU, with room dimensions of 3.50 m · 2.50 m · 2.65 m (l·w·h). The diffuser was placed in the middle of the ceiling to fill the width of the room, as seen in figure 3.1. A plexi-glass window enabled a good view of the air jet's profile from the outside, and was placed in the wall right in between the two exhaust fans. Looking at the jet through the plexi-glass instead of viewing the jet from inside, avoided the experimental operator influencing the flow pattern. A flow test of the diffuser with smoke mixed with supply air visualized the contours of the jet, as seen in figure 3.2, for case 1. A black cloth was hung on the back wall to improve the contrast of the smoke jet. A smoke test of case 3 was also conducted and is explained more in chapter 4. The exhaust fans were set to have the same volume flow rate as the diffuser to balance the air change rate and to get a steady-state situation. Finding the correct rpm for the fans was done by making sure the pressure difference between the room and the outside was approximately zero. The pressure difference was measured by a DPM TT570 Low-Res manometer, and the fans were controlled with a dimmer switch. During the experiment, the room temperature was kept at  $23 \pm 0.3^\circ\text{C}$ , which was frequently checked by temperature measurements from a TSI VelociCalc 9565-P multi-function ventilation meter. The room had little thermal stratification as the vertical temperature difference from floor to ceiling was 0.02 K. The surface temperatures were measured with a Bosch PTD 1 thermo detector.

## 3.2 Air diffuser

The air diffuser was modeled in Siemens NX, a CAD-software, before construction. The diffuser was constructed from a machine drawing made from the 3D-model, which can be found in appendix A. The diffuser was completed during the project work last semester. The only change done during the thesis was to increase the distance to the floor with 0.45 m to a total of 2.2 m to the ground. The diffuser consisted mainly of a 250 mm diameter duct 2 m long with blocked ends, two smaller incoming air ducts and a nozzle outlet at the lower end. The final design is displayed in full in figure 3.3 and sectioned in figure 3.4.



*Figure 3.2: Smoke visualization of the jet's profile*

All the components inside the diffuser had the purpose to even out the outgoing flow in such a way that the velocity at the outlet was 1.5 m/s all along the length of the nozzle. For instance, inside the diffuser, the two smaller plates below the incoming 160 mm ducts spread the air to the sides to avoid local high velocity below at the nozzle outlet. A perforated plate with  $\text{Ø}4$  mm holes and a solid ratio of 54% was fitted along the the middle of the duct. The plate induced a pressure drop dependent on the local flow velocity squared, meaning that in areas with high velocity, the flow would retard more than in areas with low velocity. This would even out the flow overall. To straighten the flow and to reduce the turbulence, a honeycomb pattern made of straws were inserted in the nozzle outlet. The final diffuser design unfortunately still produced uneven velocities along the nozzle. High velocities were observed especially in the middle of the diffuser. To reduce the velocity in this area, three plexi-glass rectangles, each with a 10 cm width, were placed between the two inlet ducts. See figure 3.4. The open lamellas at the bottom of the duct were openings in the duct for leading the air flow down the nozzle. A continuous slot opening was avoided due to a consequential loss in the duct's stiffness and shape which could result in problems with adhering the nozzle mouth properly to the duct.

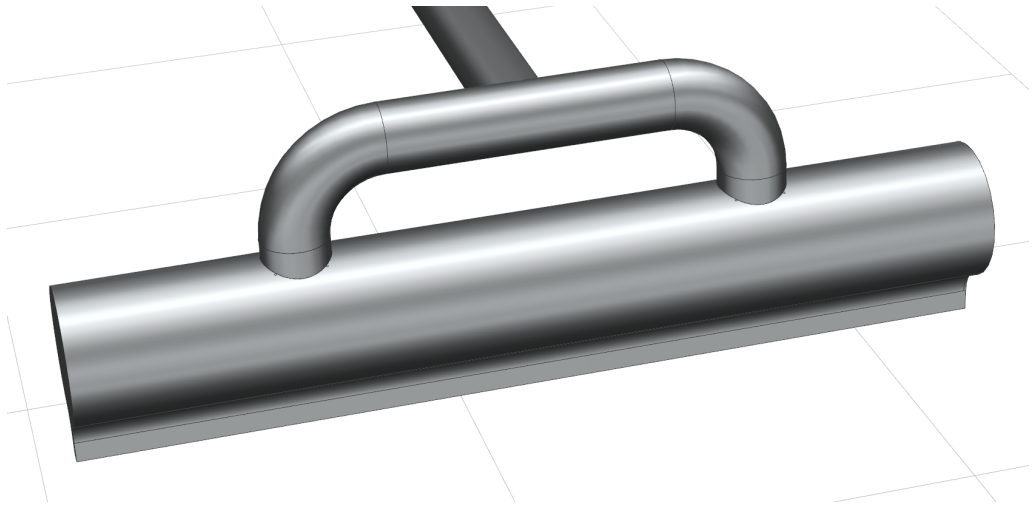


*Figure 3.3: 3D-model of the diffuser; full view*

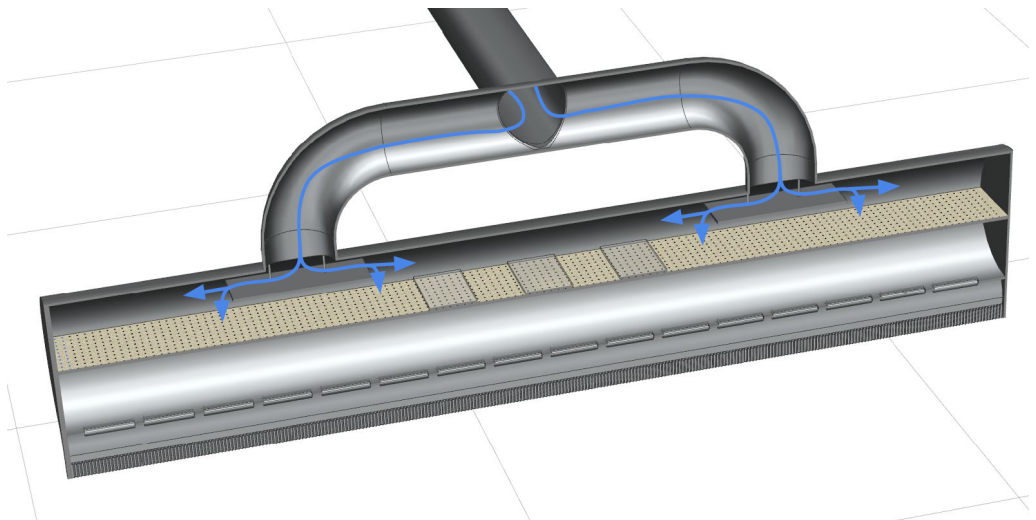


*Figure 3.4: 3D-model of the diffuser; sectioned view. The long plate along the middle is perforated*

### 3.2.1 Measuring the outlet flow velocity

To be able to treat the air jet as a 2D jet, the outlet velocity along the nozzle had to be as close to the desired 1.5 m/s as possible. 21 locations along the nozzle were measured with a TSI VelociCalc anemometer. Over 2 3-minute log time, each location had 180 measurements (one measurement every second). The variations in the outflow velocity proved to be  $\pm 0.1$  m/s. The variations should preferably have been somewhat lower. The faulty regions were just below the small plates below the incoming ducts and just below the plexi-glass plates. To improve the design, another perforated plate could be placed slightly higher or lower than the present one. Also, smaller pieces of plexi-glass would block the flow less than big pieces.

## 3.3 Thermal manikin

The manikin, a female version, was of the type that is used for exhibiting clothes in a clothing store. It was made of fiber glass with a hard white exterior. The body posture was sitting, however slightly bent forward. A small box was put under the feet to make her upright. A sedentary activity, equal to 1.2 MET, was assumed. With a total surface area of  $1.7 \text{ m}^2$ , a total heat release of 118.7 W was therefore the total desired heat output, as previously calculated in chapter 2. To achieve this, a dimmable 100 W light bulb was positioned in the stomach, and functioned as part of the metabolic heat generation. A fan inside the manikin above the light bulb contributed to a more even heat distribution inside the manikin. The rest of the metabolic heat came from heat foil that was wrapped around the manikin's body to simulate the hot human skin, as seen in figure 3.5. The heat foil had a specific power of  $60 \frac{\text{W}}{\text{m}^2}$ .  $0.855 \text{ m}^2$  was used, resulting in a total output of 51.3 W. To have the ability to control the surface temperature of the head region, the upper body and the lower body, the heat foil was connected in three separate circuits each with a dimmer.

Some safety issues had to be considered when the heat foil was used, due to the fact that it was actually made for floor heating. The foil drew a current of 230 V, which meant that it was not as user-friendly as hoped and could potentially cause shocks if handled irresponsibly. Therefore, a safety door switch was installed to cut the power when a person entered the room with the manikin. This way, the manikin was safe to handle. The internal heat from the light bulb plus the heating of the skin made the manikin function similar to a human body in terms of heat generation.

### 3.3.1 Calibration of manikin

The manikin's heat output was adjusted by changing the surface temperature. The temperature was measured with a Bosch PTD 1 thermo detector regularly to make sure the surface temper-

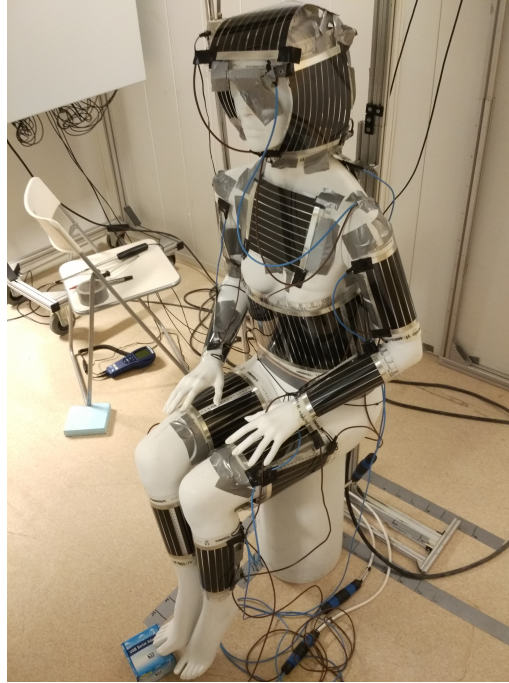


**Figure 3.5:** *The thermal manikin*

**Table 3.1:** *Measured manikin surface temperatures*

	<b>Head region</b>	<b>Upper body</b>	<b>Lower body</b>
<b>Measured temperature</b>	$32.7 \pm 0.4 \text{ }^\circ\text{C}$	$32.4 \pm 0.6 \text{ }^\circ\text{C}$	$30.8 \pm 0.3 \text{ }^\circ\text{C}$

ature was close to the desired temperatures of  $33^\circ\text{C}$  on the head,  $32^\circ\text{C}$  on the upper body and  $31^\circ\text{C}$  at the lower body. The body surface temperatures were measured every time the airflow measurements were performed. Table 3.1 shows the average value of the surface temperature measurements.

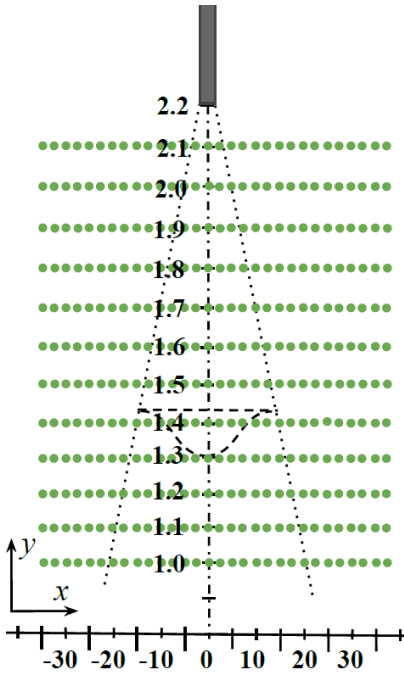
The temperature was controlled by adjusting the voltage to the light bulb. The heat foil was set to full power, yielding a total heat output of 51.3 W. This meant that the light bulb would have to supply 67.4 W to fill the desired total heat output of 118.7 W. The main goal was to achieve correct surface temperature, and the light bulb was adjusted accordingly. A VariAC, a variable transformer unit, controlled the light bulb. The VariAC supplied voltage values from 0-230 V to the light bulb. The max amount of power of the bulb was 100 W. This meant that the bulb was using 100 W when the VariAC was turned to 230 V. After a quick calibration of the VariAC, it was discovered that the output was correct at low values, but as the voltage output exceeded 100 V, there was a deviation that grew larger and larger. At the most, the VariAC was outputting 230 V when set to 220 V. The maximum set-point on the VariAC was therefore 220 V and not 230 V. The VariAC is not listed in table 3.3, since no specifications sheet was found. Due to the slight

error in the VariAC output, the voltage set point used to find the correct manikin heat output was critically considered. After several tries, a VariAC set point of 151 V together with the heat foil proved to yield the correct surface temperature.

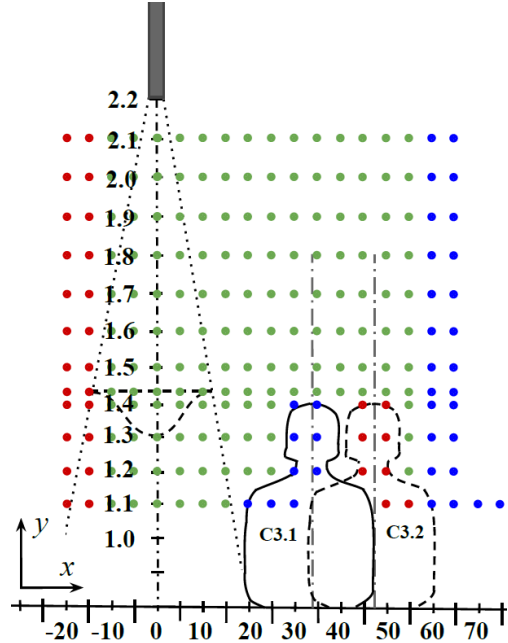
### 3.4 Measurement setup

Omnidirectional anemometers were used to measure the magnitude of air velocity. An adjustable stand was made for the anemometers where 7 probes were aligned horizontally 10 cm apart. The long horizontal rod with the anemometers could be adjusted up and down along the stand. The stand was placed in the middle of the room below the diffuser with one probe directly in the jet's centerline. Figures 3.7a and 3.7b show the setups in the laboratory. The setup was sequentially moved 5 cm to both sides to fill the points in between the first probe locations at each height. Totally 11 heights between the diffuser outlet at 2.2 m and the shoulder of the manikin at 1.1 m were measured with the heights being 10 cm apart. The measuring points for the three cases can be seen in figures 3.6a, 3.6b, 3.6c and 3.6d. For case 3.1, the centerline of the manikin was located 0.34 m to the side of the jet centerline, coinciding with the location where a human supposedly would feel a draught rate of 20%. For case 3.2, the centerline of the manikin was located 0.47 m to the side of the jet centerline, coinciding with the location where a human supposedly would feel a draught rate of 10 %. For calculating these distances, a maximum velocity was found from equation 2.10 assuming a turbulence intensity of 10 % and an ambient temperature of 23 degrees. Next, the respective x-locations in the jet velocity distribution for the shoulder height of 1.1 m were found.

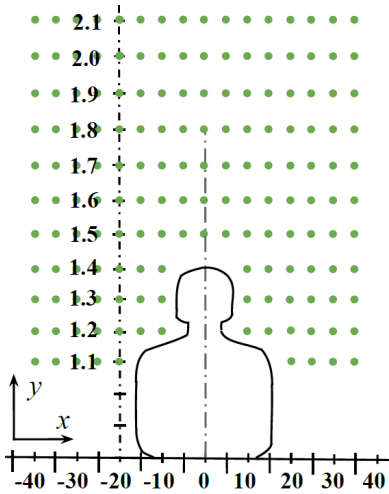
Two sets of anemometers were secured to the stand: 5 SensoAnemo 5100LSF velocity transducers, part of the air distribution measurement system AirDistSys 5000 by Sensor Electronic, and 3 TSI Velocity transducers model 8475. Additionally, a hand-held TSI VelociCalc 9565-P multi-function ventilation meter was used for the initial outlet velocity measurements, and regular control measurements of the diffuser outlet velocity every hour or so. Each velocity measurement was conducted through 10 minutes to make sure the logging time was sufficient to capture the turbulence air flow fluctuations. The SensoAnemo transducers had a log time of 2s, of which 16 velocity samples were averaged over the 2 seconds. The SensoAnemo also calculated the standard deviation, turbulence intensity and draught rate 8 times a second to get precise results. The values were averaged each 2s and logged the same way as the velocity reading. For the TSI Velocity transducers model 8475 a log time of 1 s was chosen, of which a sample of 20 readings were averaged each second. Both anemometers fulfilled the requirements given by the standard NS-EN 13182:2002 - instrumentation requirements for air velocity measurements in ventilated spaces. A comparison of the NS-EN 13182 requirements and the technical specification of the SensoAnemo 5100LSF transducers and the TSI Velocity transducers model 8475 can be found in table 3.2.



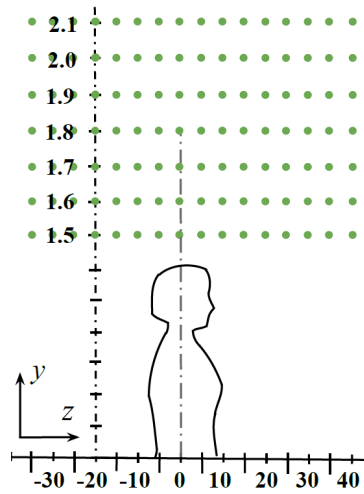
(a) Measuring points for case 1



(b) Measuring points for case 3. Green = common points, red = case 3.1, blue = case 3.2



(c) Measuring points for case 2. Front plane,  $xy$

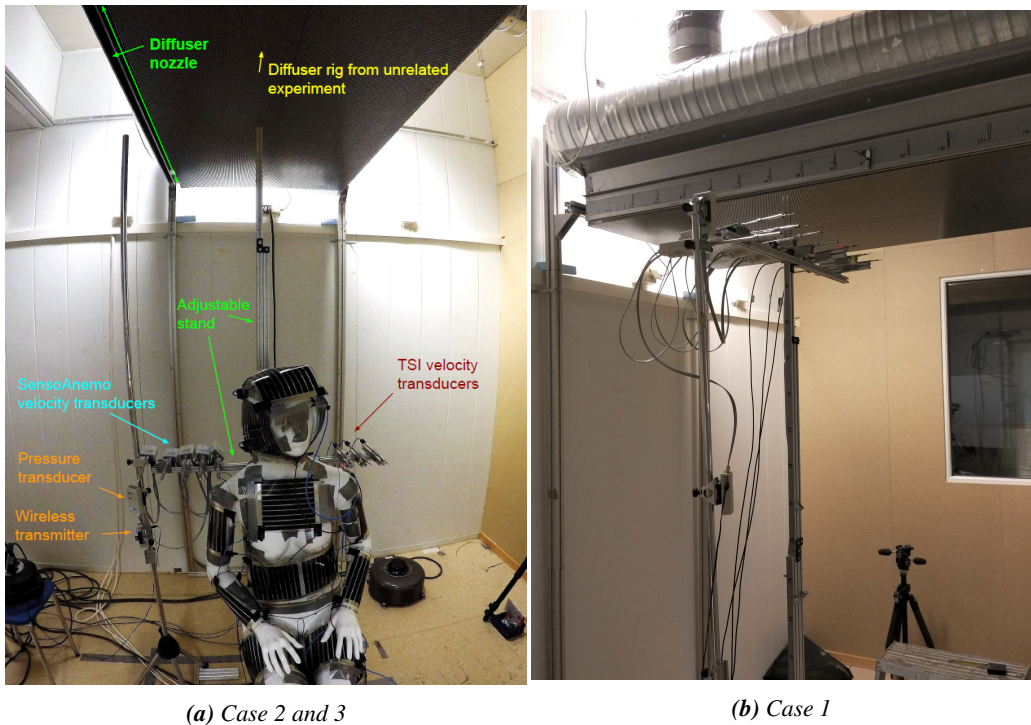


(d) Measuring points for case 2. Side plane,  $yz$

**Figure 3.6:** Measurement points for the experiments

**Table 3.2:** Measurement requirements from NS-EN 13182 (2002)

Parameter	Measurements in jet flow	Measurements in occupied zone	SensoAnemo 5100LSF transducers	TSI transducers, model 8475
Instantaneous velocity range	0.25-12 m/s	0.05-1.0 m/s	0.05-5 m/s	0.05-5.0 m/s
Upper response frequency	N/A	>1.0 Hz	min. 1.0 Hz, typ. 1.5 Hz	1 Hz
Measuring period	$\geq 60$ s	$\geq 180$ s	600 s	600 s
Sampling rate	$\geq 1$ Hz	$\geq 5$ Hz	8 Hz	20 Hz

**Figure 3.7:** Setups in experimental facility

### 3.4.1 Calibration of anemometers

The SensoAnemo Velocity Transducers model 5100LSF and the VelociCalc 9565-P unit were recently calibrated by the manufacturer. The TSI Velocity Transducers model 8475 however, were calibrated a long time ago, and had to be verified. The calibration was done by using a constant pressure drop velocity chamber. See figure 3.8. A DPM TT570 manometer was used to measure the gauge pressure between the pressurized chamber and the ambient environment. Compressed air was heated to room temperature in the calibrator and hence channeled through a

**Table 3.3:** Useful data about the measuring instruments used in the experiment

<b>Model</b>	<b>Measuring variable</b>	<b>Range</b>	<b>Accuracy</b>	<b>Resolution</b>
SensoAnemo5100LSF	Velocity	0.05-5.0m/s	$\pm 0.02$ m/s or $\pm 1.5\%$ of readings	0.001 m/s
SensoAnemo5100LSF	Temperature	-10°C-50°C	$\pm 0.2^\circ\text{C}$	0.1°C
TSI Velocity Transducer model 8475	Velocity	0.05-2.54 m/s	$\pm 3.0\%$ of reading or $\pm 0.025$ m/s	0.002 m/s
TSI VelociCalc 9565-P	Velocity	0-50 m/s	Greatest of $\pm 3\%$ of reading or $\pm 0.015$ m/s	0.01 m/s
TSI VelociCalc 9565-P	Temperature	-18°C-93°C	$\pm 0.3^\circ\text{C}$	0.1°C
Bosch PTD 1	Temperature	-20°C-200°C	$\pm 1^\circ\text{C}$ (10-30°C)	0.1°C
DPM TT570 Low-Res version	Pressure	0-7.5 kPa	Readings < 100 counts $\pm 2$ counts	1 Pa

cylindrical chamber where the anemometer to be calibrated measured the velocity of the passing flow. The flow exited through a small hole at the top of the chamber. Velocity readings from the anemometer were compared to a calibration graph with gauge pressure over velocity. The velocity measurements did coincide with the correct values at the graph, which meant that the TSI Velocity Transducers model 8475 could be used directly.

Details about all the measurement instruments used in the experiment can be found in table 3.3.



*Figure 3.8: Calibration setup for anemometer calibration*



# Experimental results

The experiment consisted of four different setups, as shown in the previous chapter. The first setup was used to measure the isothermal plane jet, the second setup was used to measure the manikin's thermal plume, and the last two setups were used to measure the jet and plume flow with two different manikin placements. The first sub-case, named case 3.1, had a distance of 0.34 m between the jet centerline and the manikin centerline. The second sub-case, case 3.2, had a distance of 0.47 m between the jet centerline and the manikin centerline as seen in figure 3.6b. Case 2, plume, was measured in two planes, plane  $xy$  and  $yz$ , which are the planes viewing the manikin from the front and from the side respectively and are normal to each other. The reason for measuring over two planes is the 3-dimensional behavior of the plume for a sitting person mentioned by (Zukowska et al., 2010; Borges et al., 2002). Case 3 was only measured in the front plane due to the fact that the front plane was the plane of interest displaying the interaction between the jet flow and the plume flow. The plane jet was also only measured in the front plane due to its 2D characteristics.

## 4.1 Case 1: 2D downward plane jet

For the plane jet, a higher density of measurement points was used. Velocity was measured at a total of  $29 \times 11$  points in the  $xy$ -plane, each over the course of 10 minutes. Roughly 600 samples for each point were used to identify the average flow and for calculating the respective turbulence intensity. At the centerline, additionally standard deviation and draught rate were estimated. Figure 4.1 shows the experimental values for the maximum velocity decay of the jet, which for a plane jet is at the centerline. Standard deviation bars have also been added to show the spread of the velocity measurements in each point. Both experimental data from this semester's experiment and last semester's experiment (from the project work) have been added due to coinciding setups

in both cases. The measurements follow the same trend all the way, except close to the diffuser outlet where the old measurements were slightly higher. The centerline velocity will further be evaluated in chapter 8.

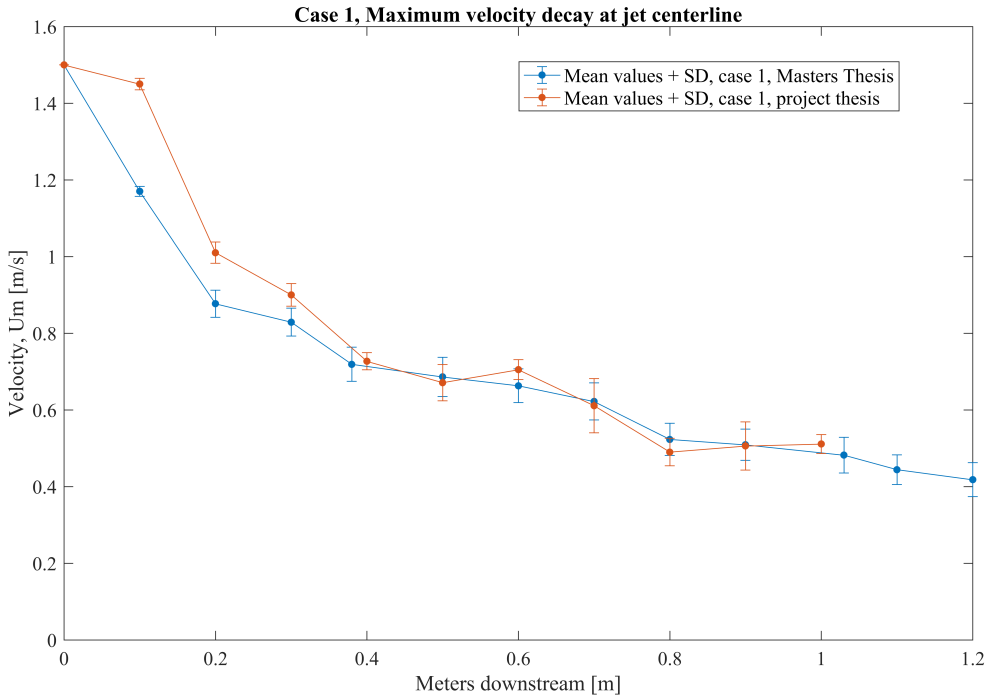


Figure 4.1: Maximum velocity decay at jet centerline, mean values and standard deviations displayed

Figure 4.2a shows where the edge of the jet lies downstream of the nozzle. The results are based on the theory from Abramovich (1963); Awbi (2003) that states that:

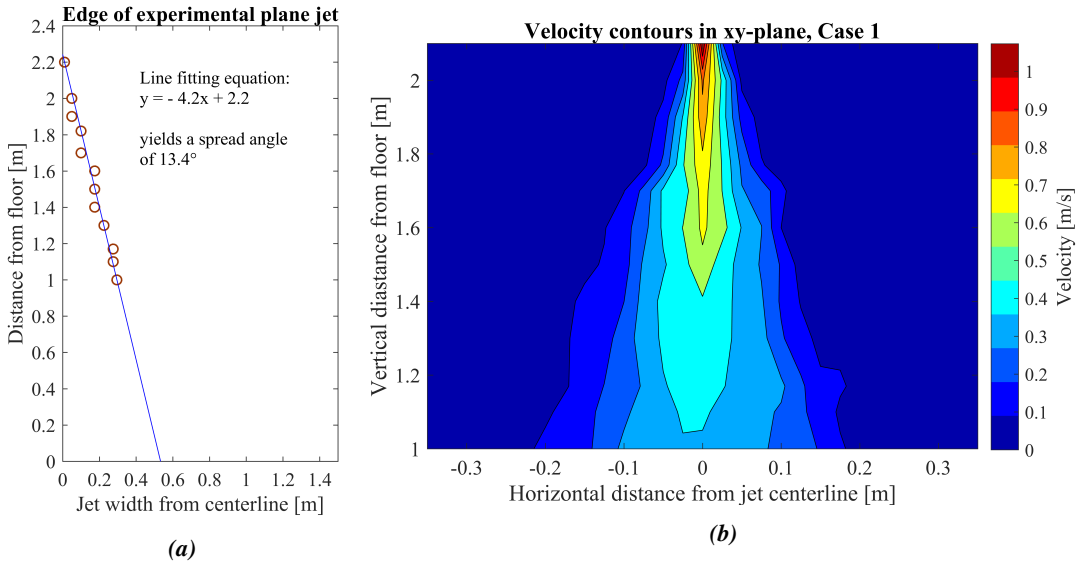
$$U_{0.5} = 0.5U_m \tag{4.1}$$

and

$$x_{0.5} = 0.44b \tag{4.2}$$

Where,  $U_{0.5}$  refers to the velocity that is half of the velocity at the centerline,  $U_m$ , at a given height, and  $x_{0.5}$  is the x-location of  $U_{0.5}$ . An empirical correlation, equation 4.2, links  $x_{0.5}$  to the width of the jet,  $b$ . It is the angle between  $b$  and the centerline that gives the spread angle,  $\alpha$ , of the jet. To be able to find  $\alpha$  for the experiment, the 29 points at 11 different heights measured for the jet were put into a matrix of 11x29 points, each with a unit number and respective velocity in MATLAB. For each height-vector, the respective  $U_m$ , being the point with the highest velocity-value, was found with a MATLAB-script. The script hence divided  $U_m$  by 2, as in equation 4.1, and found  $U_{0.5}$ . The point in the height vector with a velocity value closest to the calculated

$U_{0.5}$  was found by the use of a for-loop and its respective location,  $x_{0.5}$ , was noted. Hence,  $b$  could be found by the use of equation 4.2. The last thing to do, was to find the point in each height-vector with a location closest to the calculated  $b$ . All these  $b$ -locations were then plotted in a graph of x-value in the room vs. height above the floor, together with linear graph fitting, as seen in figure 4.2a. After plotting the location, the spread angle could be found by using a graph fitting function. The equation for the linear graph fit could also be retrieved in MATLAB, and was found to be  $y = -4.2x + 2.2$ , yielding a spread angle of  $\alpha = \tan^{-1}(\frac{1}{4.2}) = 13.4^\circ$ .



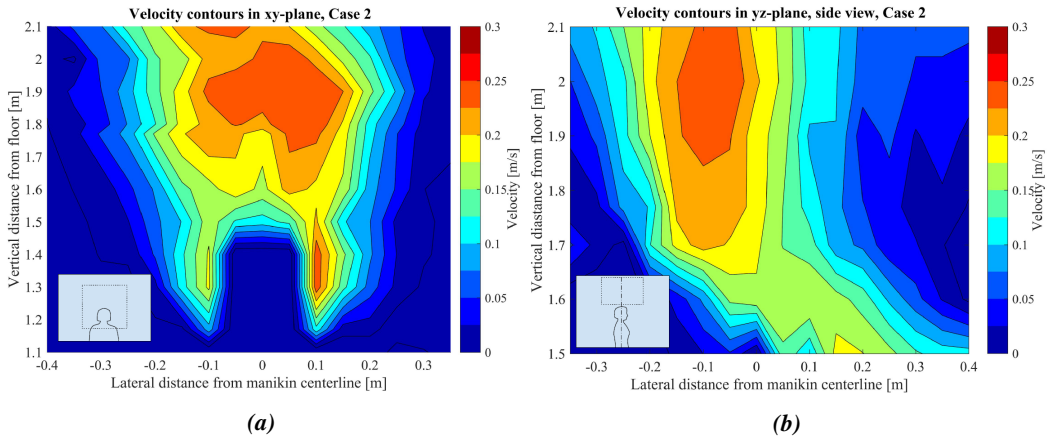
**Figure 4.2:** Spread angle of experimental jet (a) and velocity contours of jet in xy-plane (b)

Figure 4.2b displays the experimental velocity distribution of the jet in the xy-plane with a contour plot from the 29x11 points. The jet's profile can easily be recognized with its initial high velocity core region and its decreasing and widening behavior as the jet develops downstream.

## 4.2 Case 2: Thermal plume from thermal manikin

The plume from the manikin was measured both in the xy-plane and the yz-plane, being the front plane facing the manikin and the side plane with the manikin facing right respectively. A total number of 16x11 points in the xy-plane and 16x7 points in the yz-plane were used to investigate the velocity of the human plume. According to research (Zukowska, 2011; Rouse et al., 1952) the plume axis tend to deviate slightly from the vertical axis as the plume develops. This behavior could also be seen in the experiment, see figure 4.3b, and is the reason why the yz-plane was included in the measurements. The yz-measurements were only measured from  $y = 1.5$  m to  $y =$

2.2 m, because this area was sufficient to cover the manikin's plume axis wandering.



**Figure 4.3:** Velocity contours of plume in  $xy$ -plane, facing the manikin, (a), and in  $yz$ -plane, manikin facing east, (b)

The spread angle of the plume was found roughly in the same way as for the jet, however the equations used to find the edge were different. The equation used for the boundary of the plume was found in the PhD-thesis of Zukowska et al. (2010) that says the boundary of the plume at a certain cross-section lies where the velocity is equal to:

$$U_b = \frac{U_m}{e} \quad (4.3)$$

Where,  $U_b$  is the velocity at the plume boundary for a given cross-section,  $U_m$  is the maximum velocity at that cross-section and  $e$  is the base of the natural logarithm ( $\approx 2.71828$ ). The half width of the plume for a given cross-section is hence the difference in location of  $U_m$  and  $U_b$ . The rest of the deduction procedure of the plume boundary was equal to that of the jet by the use of a MATLAB script. This was done for both the  $xy$ -plane and the  $yz$ -plane, resulting in figure 4.4a and 4.4b. The plume's origin used was a  $y_0 = 1.2$  m below the head of the manikin. This was, as already mentioned, the recommended plume origin to use for a cylinder, which provided a plume more similar to the human plume than a point source (Awbi, 2003). The spread angles deducted from MATLAB proved to be  $11.3^\circ$  and  $10.5^\circ$  for the  $xy$ -plane and the  $yz$ -plane respectively. Because the two spread angles were different, the shape of the plume was not completely circular. The plume seemed to be wider in the  $xy$ -plane than in the  $yz$ -plane, which could be due to the uneven aspect ratio of the human body.

Figure 4.5 displays the centerline velocity of the plume in the  $xy$ -plane. Standard deviation bars have again been added to show the spread of the velocity measurements in each point. The deviation is somewhat larger for the plume than for the jet. The deviation seems much higher due to the lower range of the plume's  $y$ -axis. Figure 4.3a and 4.3b display velocity contours of

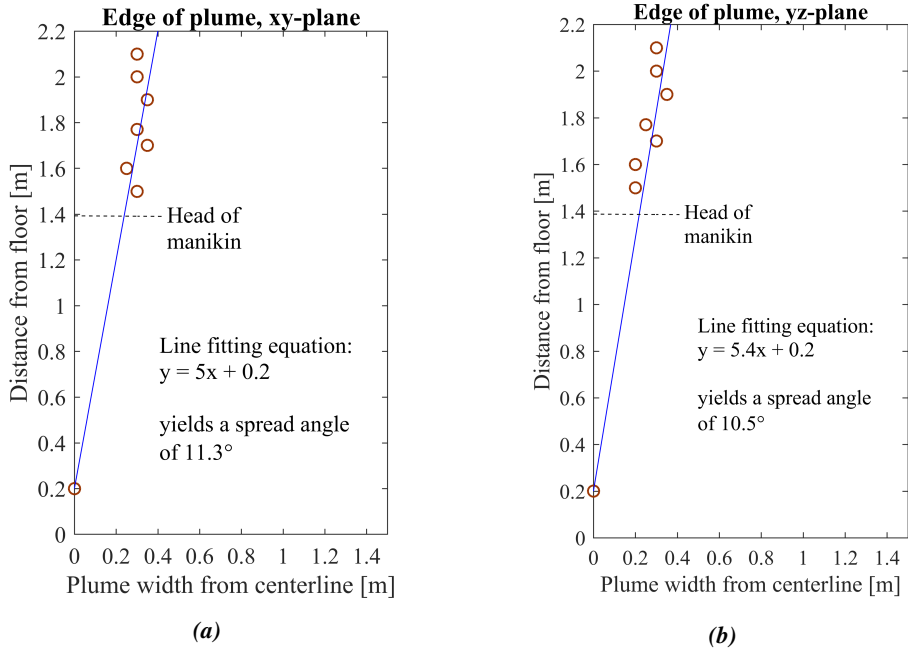


**Figure 4.4:** Spread angle of experimental plume, xy-plane (a) and yz-plane (b)

the plume. In figure 4.3a, the contour of the manikin’s head can be seen at the lower half of the figure. Figure 4.3b displays the velocity contours from 10 cm above the manikin’s head ( $y = 1.5$  m), which is why the manikin cannot be seen in the figure. The manikin’s centerline is set to be 0 in both figures to ease the understanding of the contours.

### 4.3 Case 3: Interaction between thermal plume and downward plane jet

Figure 4.7 displays the jet’s centerline maximum velocity decay for case 3.1 and 3.2. As expected, the results show that the points closely follow the same curve since the jet is equal in strength and position for both sub cases. Figures 4.8a and 4.8b display the velocity contours of the jet and plume flow for case 3.1 and 3.2 respectively. The shape of the manikin can be seen in each figure at the bottom right. In both cases a slight plume can be seen, however compared to the velocities of the jet, the plume velocities are low, and are not as visible in the contour plot as the jet. In both cases, the jet seems to deflect slightly towards the manikins shoulder.

Unfortunately, no direction of the flow at any point was known due to the usage of omnidirectional anemometers. This meant that classifying which velocities were rising as a plume and which were falling with the jet was not possible. The CFD simulation was however, able to

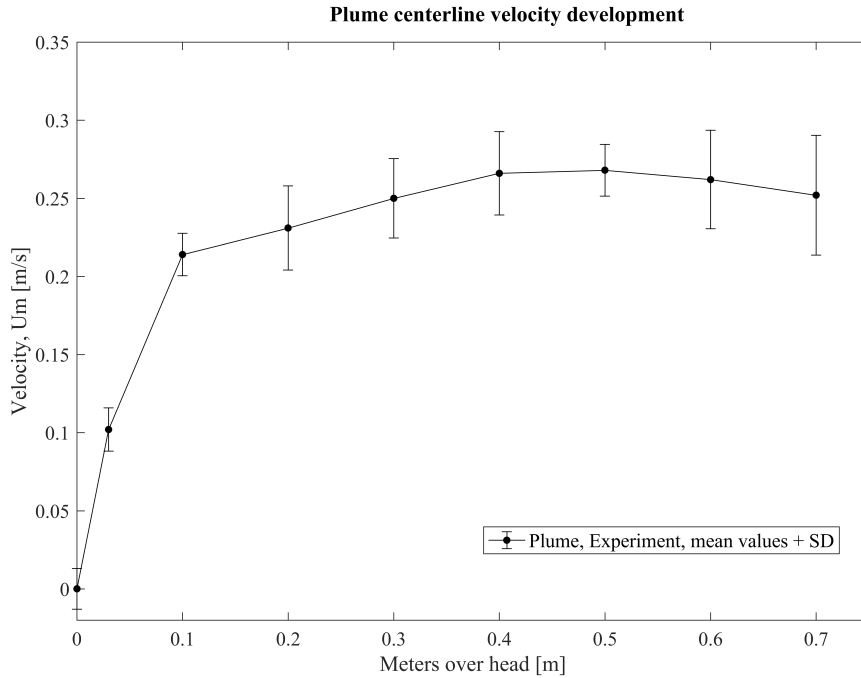


**Figure 4.5:** Maximum velocity decay at plume centerline, mean values and standard deviations displayed

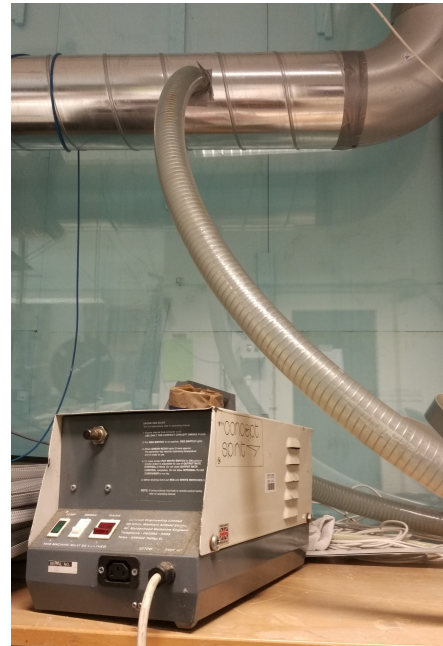
better clarify the flow situation.

Smoke visualization was conducted for case 3 to try to see if the interaction between the plume and the jet could be seen. It seems from figure 4.6a that the jet flow is not influenced by the manikin much. However, the fact that the jet had to be filmed from the outside meant that the smoke in front of the manikin blurred out the area at the cross-section with the manikin. A fully black wall would also increase the quality of the smoke test. Another matter was problems with pertaining smoke in the air for longer than 10 s, as the smoke machine, see figure 4.6b, got too hot after a while and did not supply dense enough smoke. Due to over pressure in the supply duct when the diffuser was supplying air, the smoke machine could not get its smoke to penetrate the flow and follow it out and through the diffuser outlet. Therefore, a damper was inserted in the supply duct prior to the smoke machine's inlet hole to temporarily stall the supply flow while the smoke machine filled the supply duct with smoke. A filling time of 3 minutes gave a smoke profile for 10 s, which was the machine's maximum limit for continuously supplying smoke.

The two manikin centerline positions  $x = 0.34$  m and  $x = 0.47$  m from the jet centerline was calculated to yield a DR of 20 % and 10% respectively according to the DR-equation. In addition to exploring the airflow distribution near the manikin close to a plane jet, the experiment would also verify the coherency of the proposed comfort distances, and the measured and simulated results.



(a) Manikin at 0.47 m from jet centerline



(b)

**Figure 4.6:** Smoke visualization of the jet and manikin for case 3.1 (a) and smoke machine setup (b)

The experiments showed that the velocity measured at the shoulder was below the maximum allowed velocity for both sub-cases, as seen in table 4.1. However, the measured local turbulence intensity was higher than the 10% used in the preliminary DR-calculations, which ended up resulting in a DR slightly higher than the desired DR at the shoulder. The deviation, however, was minimal and considered to be acceptable due to the natural human differences in preferred indoor conditions. This meant that the proposed distances were acceptable for the experimental situation investigated in the thesis. A graph of the measured velocity distribution at shoulder height of  $y = 1.1$  m can be seen in figure 4.9. The placements of the manikin can be seen where the velocity reaches zero. Case 3.1 had slightly lower velocities in the jet than case 3.2. This might be because the manikin was closer to the jet for case 3.1 and the flow got interrupted somewhat by the shoulder of the manikin, which slowed the jet down slightly.

**Table 4.1:** Draught rate at shoulder for case 3.1 and 3.2

DR desired	CtoC distance	CtoS distance	Calc. velocity	Meas. velocity at shoulder	Measured TU	Measured DR
20%	0.34 m	0.14 m	0.278 m/s	0.274 m/s	16.17%	21.7%
10%	0.47 m	0.27 m	0.143 m/s	0.137 m/s	25.81%	10.7%

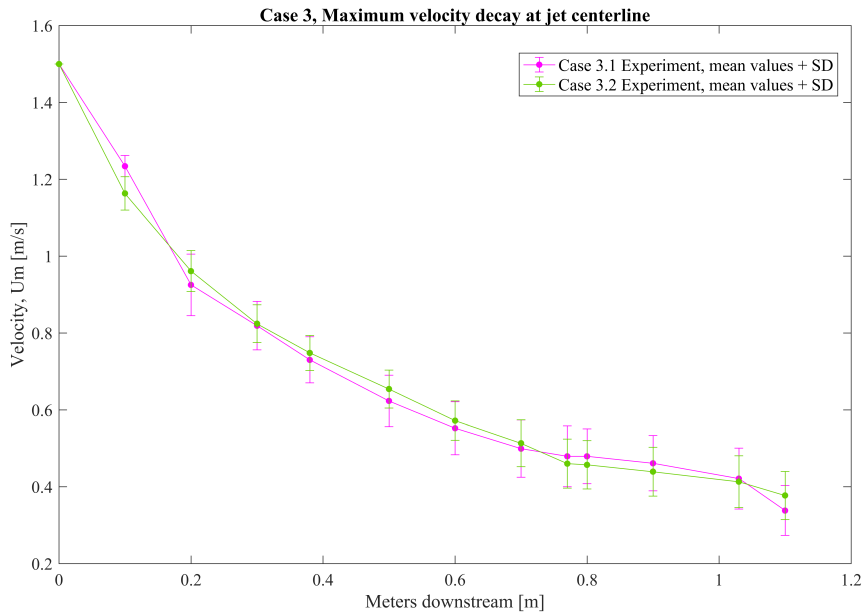


Figure 4.7: Maximum velocity decay at jet centerline, mean values and standard deviations displayed

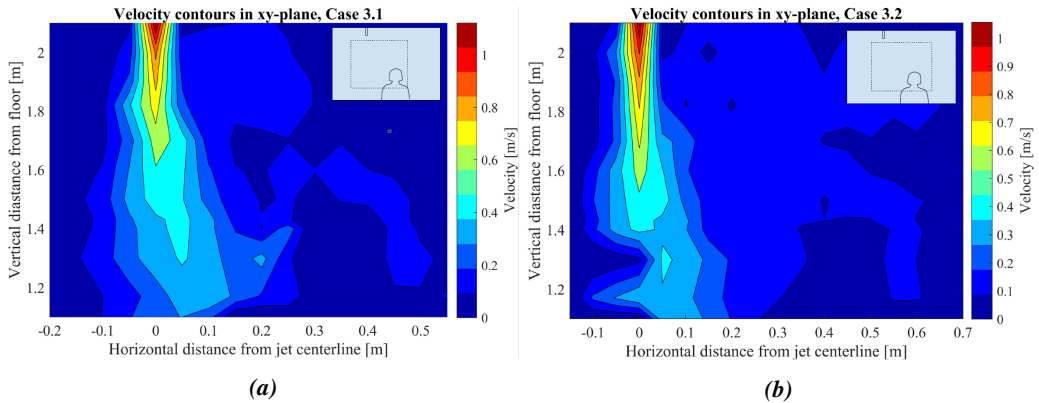
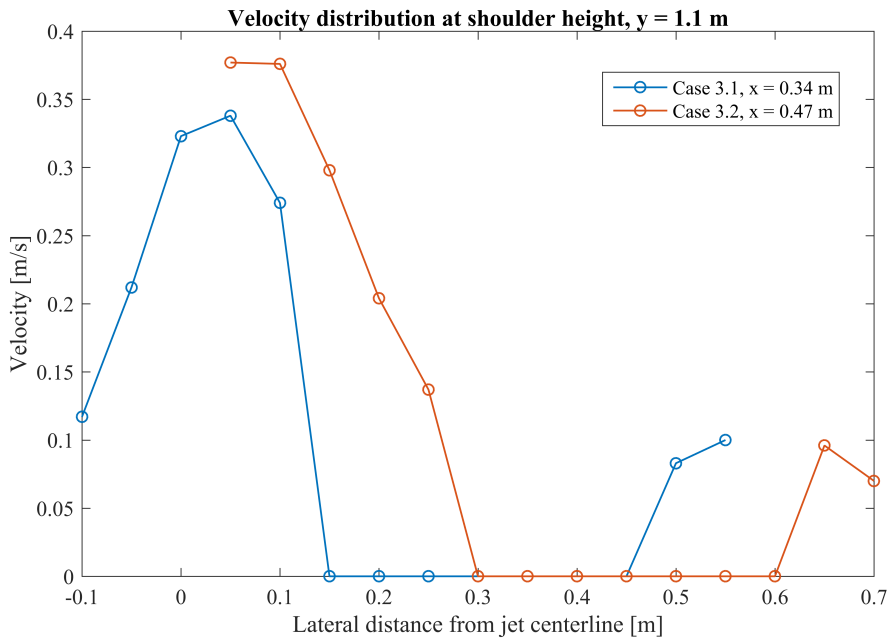


Figure 4.8: Velocity contours of jet and plume in xy-plane, manikin at  $x=0.34$  m, (a), and manikin at  $x=0.47$  m, (b)

In table 4.1, CtoC distance is referring to centerline of jet to centerline of manikin, and CtoS distance is referring to centerline of jet to shoulder of manikin. The difference of 20 cm is due to the width of a shoulder from the manikin centerline. If not stated, the comfort distances referred to in the thesis refers to the centerline of jet to centerline of manikin. In that case, only subtract 20 cm from the distance to get the distance from centerline of jet to shoulder of manikin.



**Figure 4.9:** Velocity distribution at shoulder height,  $y = 1.1$  m, with manikin positions at  $x = 0.34$  m for case 3.1 and  $x = 0.47$  m for case 3.2



# Theory on Computational Fluid Dynamics (CFD)

Ever since its dawn in the late 1960's, Computational Fluid Dynamics (CFD) has had a big impact on engineering solutions and on our understanding of fluid flow. From the early days it proved to be an especially useful tool for the aircraft industry in aircraft design (Cebeci et al., 2005). Back then, what was considered as a complex geometry and a fine mesh, is today considered as trivial. An example of how quick the availability of computational power have progressed since then and the impact this has had on CFD, is described by Chapman (1979). Simulating the flow over an airfoil by solving the Reynolds averaged Navier Stokes equations for a given numerical setup would in 1979 take under half an hour and cost \$1000 (1979-US dollars) in computer time. Doing the same given simulation in the 1960s would take 30 years and cost roughly \$10 million (1979-US dollars) in computer time. The time and cost of doing the same simulation today, is not even worth mentioning. That is how fast this field is developing. As a consequence to this rapid development, many opinions of best practices exist for the same problem. Doing a literature review on CFD has proven that the year of the literature being reviewed is of utter importance. The choice of models used in papers from early 1980'ies are being overruled in the favor of other models in papers written today. Another matter is that flow scenarios differ from each other, and naturally, not all scenarios have been simulated with CFD. Many factors, like temperature, velocity, humidity, heat transfer coefficients, mesh etc., can yield totally different flow scenarios in the same facility. The flow scenario being investigated in this study for instance, has, to the knowledge of the author, not been simulated before. However, there are many CFD studies on thermal plumes rising from human beings, and studies considering plane jets. Still a flow scenario with the same room temperature and the same room size, manikin size and surface temperature, have seemingly not been investigated before.

## 5.1 Literature review on CFD in indoor environment scenarios

There have been many studies of both turbulent jets and human thermal plumes. Launder and Spalding (1974) did a numerical study on the turbulent jet already in 1974. At that time the standard  $k-\epsilon$  turbulence model was the most popular model, while  $k-\omega$  was also used to some extent. The different turbulence models are explained in section 5.4. For a turbulent jet, the  $k-\epsilon$  model proved to yield the best result. Awbi (1989) was also early in using numerical simulations for flow predictions, and this time, room ventilation flow was investigated. He studied a room with a slot inlet supplying cold airflow along the ceiling with and without obstacles, exhaust close to the floor, and floor heating applied. Again the standard  $k-\epsilon$  model was used and overall yielded satisfactory results. However, for natural convection and Low-Reynolds number flow areas, it performed poorly. The RNG  $k-\epsilon$  and the Realizable  $k-\epsilon$  models are used instead when studying natural flow convection problems nowadays. Liu et al. (2015) did a numerical study on the fluctuating flow characteristics of a human's thermal plume in a confined space of the size of an airplane cabin. Kilic and Sevilgen (2008) also investigated the plume from a human with CFD as well as the heat transfer and moisture transport. Several papers have been written about CFD studies of the human plume and compared the results to measurements (Sørensen and Voigt, 2003; Gao and Niu, 2004). Several review articles have also been published on the progress and development of CFD for indoor air distributions and human thermal plumes (Nielsen, 2015; Gao and Niu, 2005). A similar kind of study with two parts by Zhai et al. (2007) and Zhang et al. (2007) investigates eight different turbulence models in four indoor convection scenarios - forced convection in a room with partitions, natural convection in a tall cavity, mixed convection in a square cavity and strong natural convection in a model fire room. The various turbulence models (0 eq. model<sup>1</sup>, RNG  $k-\epsilon^2$ , SST  $k-\omega^3$ , LRN model<sup>4</sup>,  $v^2f$ <sup>5</sup>, RSM<sup>6</sup>, DES<sup>7</sup> and LES<sup>8</sup>) proved to suit some of the scenarios better than others. The models found to perform best overall with satisfying accuracy, computational time and robustness were the RNG  $k-\epsilon$  and the  $v^2f$  model. The Large Eddy Simulation, Reynolds Stress Model and Detached Eddy Simulation models have not been considered for this study due to being computationally expensive and not necessary yielding results with accuracy superior to the typically used Reynolds Averaged Navier Stokes (RANS) models. (Zhang et al., 2007) These models approximate parts of the flow scenario with empirical correlations and model assumptions. The RANS models are the most used turbulence models.

---

<sup>1</sup>by Chen and Xu (1998)

<sup>2</sup>Re-Normalization Group by Yakhot and Orszag (1986)

<sup>3</sup>Shear Stress Transport model by Menter (1994)

<sup>4</sup>Low-Reynolds Number  $k-\epsilon$  model by Launder and Sharma (1974)

<sup>5</sup> $k-\epsilon$  with auxiliary equations for velocity fluctuations,  $v^2$  eq. and relaxation function,  $f$ , by Davidson et al. (2003)

<sup>6</sup>Reynolds Stress Model by Gibson and Launder (1978)

<sup>7</sup>Detached Eddy Simulation by Shur et al. (1999)

<sup>8</sup>Large Eddy Simulation with a dynamic subgrid scale model studied by Germano et al. (1991); Lilly (1992)

## 5.2 Mesh

A mesh is a grid that divides a flow domain into small elements. The governing equations are numerically solved for each element which, put together, yields an approximate representation of the flow domain. For a 3D flow, which is the type used in this thesis, a mesh can be constructed from 4 different types of cells: triangular prism cells, hexahedrons, tetrahedrons and pyramid cells, as seen in figure 5.1. The tree triangular elements are usually used in a tetrahedral mesh. This type of mesh is favorable to use around complex geometries, like a manikin. Another well-known mesh type is structured mesh, consisting only of hexahedrons. This mesh can be packed denser than the tetrahedral mesh, which means that it can have larger element size for the same numerical precision. Structured mesh usually have a higher element quality than tetrahedral mesh. However, structured mesh is usually recommended to be used for simple geometries, like cubes or cylinders as described in the ANSYS Documentation Guide 17.0 ANSYS (2016). Creating a good mesh is vital to get an accurate simulation result. Some important aspects to consider when creating the mesh are: to make sure that eventual boundary layers get properly resolved or modeled, that the grid is independent from the solution, that dense mesh near areas of interest is used, and that the important geometrical details get captured properly. Another important matter is to check the quality of the mesh.

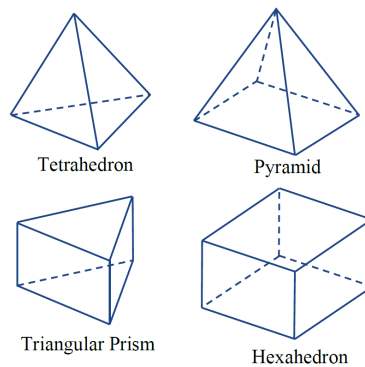


*Figure 5.1: The 4 different 3D mesh elements*

### 5.2.1 Mesh quality indices

The mesh quality will affect the solution of the equations, and is therefore very important. There are several ways to define a good quality mesh. One way is to check mesh quality indices, also called mesh metrics. In ANSYS Meshing, these are available in the statistics-tab after a mesh has been generated. They can be viewed also for inflation layers and surface mesh if these meshes are previewed before constructing the full volume mesh. The mesh quality indices give information about a cell's orientation relative to its neighbor cells or its geometry deficiency compared to

**Table 5.1:** Mesh quality indices (ANSYS, 2016)

Index name	Mesh type	Recommended limit	Notes
Orthogonal Quality	Surface mesh	min. > 0.4-0.5	from 0 (worst) to 1 (perfect)
	Inflation layers	min. > 0.15	
	Volume mesh	min. > 0.1, avg. > 0.7	
Skewness	All	max. < 0.9	Important. from 1 (worst) to 0 (perfect)
	All	avg. < 0.3	
Aspect Ratio	Volume mesh	max. < 100	Large ratios are accepted outside BL
	Surface mesh	max. < 5	

its ideal cell geometry. For this thesis, the orthogonal quality, skewness and aspect ratio have functioned as the mesh quality criteria. The recommended limits for each quality index can be seen in table 5.1. The orthogonal quality refers to how well a cell’s centerline to a face matches the face’s normal vector. In a perfect case the two vectors would coincide. The skewness says something about how skewed a geometry is relative to the perfect shape. For instance, if the perfect shape is a rectangle, then its skewed shape would be a trapezoid. The angles between the edges of the element are larger or smaller than the perfect rectangle’s angles. The aspect ratio refers to the area or length of a reference side to the neighbor side. For instance, for rectangles in 2D, the ratio of length over width.

### 5.2.2 Grid independence

Grid dependence means that a calculated solution does not depend on the mesh resolution. To be sure of this, it is normal to start with a coarse mesh, solve the equations and note the value of a relevant parameter. Hence, the mesh must be made finer, solve the same equations and check whether the value of the relevant parameter has changed. Usually a mesh has to be made finer several times to ensure grid independence. When the relevant parameter has no notable change in its value from one mesh to finer mesh, the solution can be assumed to be independent of the mesh. A grid independence check has been conducted during the CFD simulation preparation and can be found in chapter 6.2.1.

## 5.3 Boundary layers

To be able to capture the flow movement and the heat transfer properly, the manikin’s boundary layer must be considered. The flow in the boundary layer can be divided into several layers. The logarithmic layer, the buffer layer and the viscous sublayer. The logarithmic layer is the layer that connects to the outer flow region. This region can be described by a logarithmic wall law. The viscous sublayer is the layer closest to the wall. Here the friction forces are the leading forces,

and plays the crucial role (Cengel and Cimbala, 2010). This region is also called the linear or laminar layer, due to its linear behavior when plotting  $u$  [m/s] vs.  $y$  [m] close to the wall. The buffer layer is the layer that connects the logarithmic layer to the viscous sublayer, and is neither linear nor logarithmic (White, 2006).

### 5.3.1 $y_+$

$y_+$  is an important parameter in boundary layer flow. It is a non-dimensional parameter based on the distance from a wall to the first element node and the wall shear stress (ANSYS, 2016). For  $y_+ \approx 1$ , the viscous sublayer can be assumed resolved. How small the cell height,  $y$ , needs to be to yield a small enough  $y_+$ , depends on the flow characteristics. The  $y_+$  is defined as:

$$y_+ = \frac{\rho U_\tau y}{\mu} \quad (5.1)$$

Where  $\rho$  is density, the friction velocity,  $U_\tau = \sqrt{\frac{\tau_w}{\rho}}$ , where  $\tau_w$  is the wall shear stress,  $\mu$  is the dynamic viscosity and  $y$  is the height of the first grid layer. Calculating the correct  $y$  on beforehand is troublesome, and only an approximation can be made. This is done by finding the Reynolds number, the skin friction coefficient and the fluid properties. These correlations have been used to be able to find a  $y$  to use in the simulation of the three cases (ANSYS, 2016):

$$Re = \frac{\rho U L}{\mu} \quad (5.2)$$

$$\tau_w = 0.5 C_f \rho U_\infty^2 \quad (5.3)$$

$$C_f = 0.058 Re_L^{-0.2} \quad (5.4)$$

Where,  $Re$  is the Reynolds number,  $U$  is the flow velocity,  $L$  is the specific length,  $\tau_w$  is the wall shear stress,  $C_f$  is the skin friction coefficient,  $U_\infty$  is the free stream velocity. Equation 5.4 is for a flat plate. For the plume flow from the manikin, a  $y = 1$  mm was found to yield a  $y_+ \approx 1$ . Therefore, a first height thickness of the first inflation layer cell was set to be 1 mm in the CFD calculations of case 2 and case 3.

## 5.4 Turbulence Models

A turbulence model should be used to be able to simulate the turbulence transport and development in a flow properly. Their applicability vary from scenario to scenario. For instance, the standard  $k-\epsilon$  model works best for simple flows with not too much swirl, separation or high pressure gradients. It is best for flows of high Reynolds numbers. Other models, like the  $k-\omega$

SST, are more suitable where the boundary layer flows should be captured, heat transfer effects are important and vorticity flows are normal. Most of the models in the summary-table, table 5.2 are Reynolds Averaged Navier Stokes (RANS) models. How many equations are used for each RANS model is listed in table 5.2 as well as the relative computational time needed to solve a problem. The descriptions of the models have been found in the ANSYS workbench help (ANSYS, 2016). The models that numerically solve the entirety of the flow or parts of the flow are the large eddy simulation model (LES), the detached eddy simulation model (DES) and the direct numerical simulation model (DNS). These can be found last in the table 5.2. One important thing to mention, that becomes evident after having reviewed numerous CFD articles, is that even though a turbulence model is recommended by a paper for a certain application, the same model might perform poorly for the same application in a different paper due to different mesh, boundary conditions (BC's), environmental conditions, experimental data, and/or solution method. There are many uncertainties in modeling turbulence, and it is actually one part of the physical world that humans yet have not been able to fully understand. Therefore, turbulence modeling should be viewed critically and not be taken lightly.

*Table 5.2: Turbulence model overview*

Model name	No. of eq.	Typical usage and other aspects	Comput. time	Examples from literature
Spalart-Allmaras	0	Mainly intended for aerodynamic/turbomachinery applications with little separation such as supersonic/transonic flows over airfoils etc.	<i>Very small</i>	Seim (2009) used this turbulence model in his master's thesis when investigating the wake behind a hydrofoil.
Standard k- $\epsilon$ (SKE)	2	Most used turbulence model a few years ago. Robust and quite accurate, however works best for simple flow problems. Not for problems with large pressure gradients, strong separation, high swirl or large streamline curvature.	<i>Small</i>	Launder and Sharma (1974) used this model to study a turbulent jet. The standard k- $\epsilon$ (SKE) were more accurate than the k- $\omega$ and the k-k1 models for modeling the turbulent jet. Awbi (1989) studied room ventilation flow, both cooling and heating, with the SKE model, which performed overall satisfactory, while not too good for natural convection and low-Re number flow areas. Gao and Niu (2004) studied the human thermal plume with the SKE.
Realizable k- $\epsilon$ (RKE)	2	Improved k- $\epsilon$ -model. Performs better than SKE in rotational flows, boundary layer flows under strong adverse pressure gradient and separating flows. Dissipation rate ( $\epsilon$ ) equation is derived differently than for SKE.	<i>Small</i>	Kong et al. (2015) applied a two-layer approach by Xu and Chen (2001) to the realizable k- $\epsilon$ turbulence model instead of a low-Reynolds number approach. The velocity distribution of the flow in an office cubicle with a PV system proved to fit well with experiments. Realizable k- $\epsilon$ fitted a plume situation the best compared to RNG and standard k- $\epsilon$ according to Hargreaves et al. (2012) who investigated plume maximum velocity, entrainment, plume 'laziness' and plume spread.

Table 5.2: Turbulence model overview

Model name	No. of eq.	Typical usage and other aspects	Comput. time	Examples from literature
RNG k- $\epsilon$ (RNG)	2	The constants in the k- $\epsilon$ equations are derived analytically using renormalization group theory. The dissipation rate equation is also modified. It performs better than SKE for more complex shear flows, and flows with high strain rates, swirl, and separation.	Medium	Rohdin and Moshfegh (2007) investigates the appropriate k- $\epsilon$ model to use for the indoor flow situation in a packaging facility with mixing ventilation. Out of SKE, RKE and RNG, RNG yielded the best results compared to experiments both for velocity and temperature, while RKE was also decent. Mazej and Butala (2011) used RNG k- $\epsilon$ in their investigation of the human plume and particle spread under the influence of a PV ventilation solution. According to Zhang et al. (2007) RNG k- $\epsilon$ is not too good for strong buoyant flows (fire plumes etc.) as it underpredicts the fluctuating velocities. Craven and Settles (2006) also studied the human thermal plume with RNG.
Standard k- $\omega$	2	Can resolve the flow in the viscous boundary layer without wall functions. More sensitive to free-stream conditions. Improved behavior under adverse pressure gradients. Usually used in the aerospace industry and with turbomachinery	Medium	Kuznik et al. (2007) tested RNG, SKE and k- $\omega$ turbulence model for simulating room ventilated flow. They all proved to describe the flow in a good manner. Craven and Settles (2006) tried the k- $\omega$ model for simulating plume flow, and the results were not as good as the RNG.
SST k- $\omega$	4	Combination of k- $\epsilon$ in free flow area and k- $\omega$ in wall area. Performs better than standard k- $\omega$ in free stream areas.	Medium	Good for strong buoyant flows, but not so good for weak buoyant flows (which is studied in the thesis). This is because the model sometimes fails to switch from the k- $\omega$ to k- $\epsilon$ if the flow situation far away from the walls has little turbulence, which will under-predict the turbulence kinetic energy. (Zhang et al., 2007)
$v^2f$	4	Promising new model not fully validated yet for all flow scenarios. It is a k- $\epsilon$ model that also uses equations for mean velocity fluctuations, $v^2$ and a damping factor, $f$ . Performs well for impinging flows, heat transfer and separation.	Medium	A paper by Zhang et al. (2007) compared all types of flow regimes and turbulence models and stated that generally for convective flows, whether they are forced, natural, mixed or of strong buoyancy, $v^2f$ and RNG k- $\epsilon$ are the best, due to their accuracy, computing time and robustness. Tieszen et al. (1998) found that the $v^2f$ and a k- $\epsilon$ model with a two-layer wall treatment performs well and on the same level for a heated vertical plate and a hot wall and cold wall box scenario.
Transitional SST	4	Ideal for surfaces that experience transition from laminar to turbulence. Not much research on this yet however. Uses k- $\omega$ equations plus $Re-\theta$ (for the transition onset Re no.) and intermittency, $\gamma$ .	Large	Aftab et al. (2016) studied the flow over a NACA4415 airfoil and used the Transitional SST, also called $\gamma-Re_\theta$ SST, as well as other SST models, to study the formation of separation bubbles on the surface on the airfoil. The $\gamma-Re_\theta$ SST proved to be best for this scenario.

**Table 5.2: Turbulence model overview**

Model name	No. of eq.	Typical usage and other aspects	Comput. time	Examples from literature
Reynolds Stress Model (RSM)	7	For highly swirling flows, e.g. in cyclones or in highly curved flow domains. Solves all terms in the Reynolds stress tensor.	<i>Large</i>	Wang and Chen (2009) deems RSM and RNG k- $\epsilon$ the best overall RANS models for their experiment. Flow in a room entering from the top side and exiting at the bottom opposite side. Heated box simulating 10 people of 700W were placed in the middle of the room.
Large Eddy Simulation (LES)	All	Fully solves the Navier Stokes equations. Sub-grid turbulence modeling of the small eddies below a certain size criteria is done to minimize the computational power needed. Only solves the big eddies. LES captures the flow more accurately than the RANS models. However, the increased computational cost is not always worth the slight increase in accuracy.	<i>Very large</i>	Wang and Chen (2009) deems LES the best overall model for their experiment. Flow in a room entering from the top side and exiting at the bottom opposite side. Heated box simulating 10 people of 700W were placed in the middle of the room. Kuznik et al. (2006) also tested the LES for room ventilation flow together with the RKE model. Actually, the RKE performed better than the LES in describing velocity and temperature in about all cases.
Detached Eddy Simulation (DES)	All	Like LES, but usually coupled with a RANS-model which models parts of the flow region that does not have to be fully resolved.	<i>Very large</i>	Wang and Chen (2010) developed a new DES model that uses a renewed $v^2f$ model in parts of the computational domain. Same flow scenario as used by Wang and Chen (2009).
Direct Numerical Simulation (DNS)	All	Solves the 3D unsteady Navier Stokes equations for all scales (both space and time). Can only be used for simple flows at modest Re numbers before the computational cost becomes too high for normal engineering purposes. The number of details achieved with such a simulation is usually not required.	<i>Huge</i>	DNS is so computationally expensive to complete, and is therefore not normal to perform. None of the articles found during this master's thesis used the DNS solution method.

### 5.4.1 RNG k- $\epsilon$ model

The turbulence model used in this study is the RNG k- $\epsilon$  model. This turbulence model manages to capture the jet properly as well as plume flow, according to several studies (Mazej and Butala, 2011; Zhang et al., 2007; Craven and Settles, 2006; Kuznik et al., 2007). The RNG k- $\epsilon$  model uses about the same k and  $\epsilon$  equations as the standard k- $\epsilon$  model, but with a different approach to modeling the turbulent viscosity. The model was derived using a statistical technique called

the renormalization group theory, hence the abbreviation RNG. Compared to the standard k- $\varepsilon$  model, the RNG model has an additional term in its  $\varepsilon$ -equation that improves the accuracy for rapidly strained flows. The most important adjustment from the standard k- $\varepsilon$ -model is the RNG-model's analytically derived differential formulation for effective viscosity that can account for low-Reynolds number effects, as long as a sensible wall treatment is applied on near-wall regions. RNG also includes the effect of swirl on turbulence, which enhances the accuracy for swirling flows. The transport equations for turbulence kinetic energy,  $k$ , and the turbulent eddy dissipation,  $\varepsilon$ , are as follows:

$$\frac{\delta}{\delta t}(\rho k) + \frac{\delta}{\delta x_i}(\rho k u_i) = \frac{\delta}{\delta x_j}(\alpha_k \mu_{eff} \frac{\delta k}{\delta x_j}) + G_k + G_b - \rho \varepsilon - Y_M + S_k \quad (5.5)$$

and

$$\frac{\delta}{\delta t}(\rho \varepsilon) + \frac{\delta}{\delta x_i}(\rho \varepsilon u_i) = \frac{\delta}{\delta x_j}(\alpha_\varepsilon \mu_{eff} \frac{\delta \varepsilon}{\delta x_j}) + C_{1\varepsilon} \frac{\varepsilon}{k} (G_k + C_{3\varepsilon} G_b) - C_{2\varepsilon} \rho \frac{\varepsilon^2}{k} - R_\varepsilon + S_\varepsilon \quad (5.6)$$

Where,  $\rho$  is density,  $k$  is turbulent kinetic energy,  $u$  is velocity in flow direction,  $\alpha$  is the inverse Prandtl number,  $\mu_{eff}$  is the effective dynamic viscosity,  $G_k$  refers to the generation of turbulence kinetic energy due to the mean velocity gradients,  $G_b$  is the generation of turbulence kinetic energy due to buoyancy,  $\varepsilon$  is the eddy dissipation rate,  $Y_M$  refers to the contribution of the fluctuating dilatation in compressible turbulence to the overall dissipation rate,  $S$  are user-defined source terms, the various  $C$  are model constants.

## 5.4.2 Enhanced wall treatment

To consider the flow near the surface of the manikin, the RNG k- $\varepsilon$  model can use a method called *enhanced wall treatment*. To be able to capture the low-Reynolds number flow along the surface of the manikin, a fine mesh should be used. With a fine mesh, the enhanced wall treatment can resolve the flow all the way down to the wall through the viscous sub-layer, which is the inner part of the boundary layer, see section 5.3. With a mesh so fine that the first node is placed at  $y^+ \approx 1$ , the enhanced wall treatment uses a two-layer approach that specifies both  $\varepsilon$  and the turbulent viscosity in the near-wall cells. For areas between the viscous sub-layer and the fully turbulent region, an enhanced wall function will be used that blends the logarithmic wall law with the laminar viscous sub-layer law. The rest of the domain ( $y^+ > 200$ ) is assumed a fully turbulent region where the RNG k- $\varepsilon$  model is used (ANSYS, 2016).

## 5.5 Thermal plume considerations

Natural convective flows, also known as thermal plumes, arise from density differences in air volumes, as presented in chapter 2. This kind of flow is very complex, and to be able to simulate

it, several density approximations can be considered. One of them is the Boussinesq density approximation (Incropera et al., 2013). The approximation is only valid for small variations in density, when  $\beta(T - T_0) \ll 1$ , which makes it suitable for human plume flow in normal ambient conditions.

$$(\rho_\infty - \rho) \approx \rho\beta(T - T_\infty) \quad (5.7)$$

This approximation is used for the pressure term in the momentum equation, which will go from this form, in y-direction (which is the main flow direction for this study):

$$u \frac{\delta v}{\delta x} + v \frac{\delta v}{\delta y} = -\frac{1}{\rho} \frac{\delta P_\infty}{\delta y} - g + \nu \frac{\delta^2 v}{\delta x^2} \quad (5.8)$$

... to this form, where the first term on the right hand side proves that the buoyancy effect is being considered:

$$u \frac{\delta v}{\delta x} + v \frac{\delta v}{\delta y} = g\beta(T - T_\infty) + \nu \frac{\delta^2 v}{\delta x^2} \quad (5.9)$$

This density approximation can be applied in the CFD software, ANSYS Fluent.

## 5.6 Solution methods in Fluent

To be able to solve a CFD problem, a solver must be chosen. There are several kinds, but the pressure-based and the density-based solvers are the two most common, and both can be used in Fluent. The pressure-based solvers give satisfying results for most kinds of flow problems (ANSYS, 2016). Density-based solvers are typically used for high-speed compressible flows with shocks. Therefore, the pressure-based solver is used in this study. The pressure-based solver works by following one of two algorithms: The segregated solver or the coupled solver. The segregated solver solves the governing equations in a structured manner quickly summed up like this:

1. Update the fluid properties, like density, viscosity, specific heat transfer coefficients etc.
2. Solve momentum equations and find velocities (by using the results from step 1)
3. Solve pressure-correction continuity equation (by using the results from step 2)
4. Update values for mass flux, pressure and velocity
5. Solve energy, species, turbulence and other scalar equations
6. Check convergence against a convergence criteria
7. Iterate the whole process if not converged

This type of solver has a low memory use since it only has to store one variable at a time. However, this is at the cost of higher computational time and slower convergence. The coupled solver solves step 2 and 3 simultaneously, which yields a faster convergence, but demands a greater use of memory. This is because several variables have to be stored at the same time. The

computer used for this master's thesis has a high memory capacity, which means that the coupled solver was the preferred solver.

## **5.7 Simulation errors**

Performing a CFD simulation can be a cumbersome affair, due to the many possible pitfalls. Typical errors that can arise during a CFD study are:

- Roundoff errors
- Iteration errors
- Solution errors
- Model errors

### **5.7.1 Roundoff errors**

Every computer calculates numbers to a certain numerical precision. No number stored by a computer can have infinitely many decimals, and naturally, a small roundoff error will arise. This kind of error can cause high grid aspect ratios, large differences in length scales and large variable ranges. The error can be minimized by using a double precision solver, which can be chosen during the ANSYS Fluent startup. The double precision solver can store more information per calculation than the single precision solver. Consequentially, the double precision solver demands a higher computational cost, and uses longer time to calculate than the single precision solver. (ANSYS, 2016)

### **5.7.2 Iteration errors**

To avoid a large iteration error, the user can pick a few target variables, like mass flow rate, efficiency, maximum velocity etc., and follow the solution to convergence. If the variables do not change in value for the last iterations, the iteration error is minimized.

### **5.7.3 Solution errors**

The typical solution error is the discretization error. This error will be low for good meshes, but is inevitable for discretized solution methods, like the finite element method, finite volume method and finite difference method. The error can be defined as the error between the solution for a given mesh and the "exact" solution for an infinitely fine mesh.

### 5.7.4 Model errors

Model errors are errors related to inadequacies in the mathematical models. If unsuitable choices of for instance turbulence models, base equations like steady-state vs. unsteady-state, Euler vs. RANS equations and so on, model errors can be substantial. This kind of error can typically be viewed in research where a situation has been modeled with different kinds of turbulence models, and their solutions are compared. The difference in the solutions are usually due to model errors. An example can be seen in figure 5.2a where an indoor flow situation has been evaluated with different turbulence models. The inlet to the room is at the upper left and the outlet at the lower right (Rong and Nielsen, 2008). Another example of different performance of different turbulence models can be seen in figure 5.2b. Here, the flow characteristics at a certain point in a room with an incoming plane horizontal jet close to the ceiling and exhaust at the opposite wall by the floor have been studied (Wang and Chen, 2009).

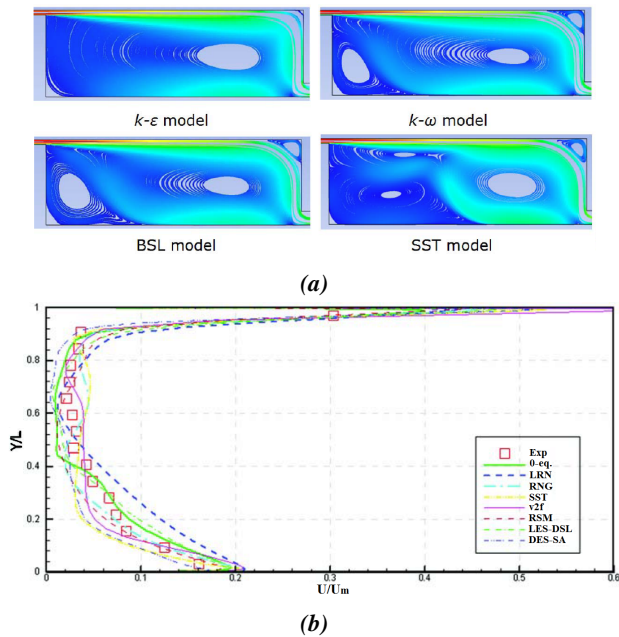


**Figure 5.2:** Comparison of velocity contours (a) and dimensionless velocity (b) for different turbulence models for an indoor flow situation. The model error can be seen as the variations between the turbulence models. (a) Source: Rong and Nielsen (2008), (b) Source: Wang and Chen (2009)

## Simulation setup

A CFD analysis is done by completing the following steps: build a geometry, mesh the geometry, set up the solver and solve the equations. The commercial software ANSYS, version 17.2, was used to complete all the parts of the analysis. The software packages from ANSYS made for 3D modeling (DesignModeler), meshing and solving (Fluent) were used. The CFD study analyzed the same three different cases that were also investigated experimentally:

1. 2D downward plane jet
2. Thermal plume from thermal manikin
3. Interaction between thermal plume from thermal manikin and downward plane jet
  - 3.1. Distance from thermal manikin centerline to jet centerline that corresponds to 20% draught rate
  - 3.2. Distance from thermal manikin centerline to jet centerline that corresponds to 10% draught rate

All simulated cases are compared to experimental and mathematical results in chapter 8. This chapter will go through the various setups and designs, considerations and limitations the thesis' CFD models have been subjected to.

### 6.1 Geometrical models

The three cases were simulated with different boundary conditions, meshes and geometries. The 3D-models of the three cases were made to be as similar to the experimental setup as possible. For instance, case 1, the jet case, had the simplest geometrical model with a box the size of the office room, a simple diffuser inlet and two holes in one of the walls functioning as exhausts. The main difference from the real-life setup was the complexity of the diffuser. The experimental

model was naturally following the laws of physics and had to be built in a way that would supply an air flow that matched the desired inlet condition of 1.5 m/s. The CFD model on the other hand, had the advantage of freely applying the desired inlet condition at a given face, and could therefore have a very simple geometry. The limiting factor was the shape of the supply opening, which should match that of the experimental model. To keep it both accurate and simple, the CFD diffuser was made to be a rectangular opening extruded from the ceiling to the correct height of 2.2 m from the ground, as seen in figure 6.1. The geometrical model of the plume case, case 2, included a manikin model that was constructed to resemble the thermal manikin used in the experiment. The model was slightly simplified however, due to the lack of a human laser scan and enough time to construct all the complex human geometries from scratch. The design of the manikin was based on a model used by a paper by Zhu et al. (2007), where the computational body was separated in 16 parts. In the thesis' situation, the desired surface area of the human was  $1.7m^2$ , which was slightly smaller than what Zhu et al. referred to as Smith's model, of  $1.85m^2$ . Therefore, the 16 body parts were made slightly smaller than this reference body. The body parts and their respective surface areas can be seen in table 6.1. The geometrical model used for case 3, plume vs. jet flow, was a combination of the models for case 1 and case 2. For case 3, the same two manikin locations of 0.34 m (20% DR, case 3.1) and 0.47 m (10% DR, case 3.2) from centerline of jet to centerline of manikin were simulated to study the flow around the manikin in proximity to the plane jet.

**Table 6.1:** The 3D model's human body components

<b>Body part</b>	<b>Surface area [<math>m^2</math>]</b>
Head	0.132
Neck	0.026
Upper body	0.322
Lower body	0.229
Left upper arm	0.102
Right upper arm	0.102
Left forearm	0.063
Right forearm	0.063
Left hand	0.036
Right hand	0.036
Left thigh	0.130
Right thigh	0.130
Left calf	0.109
Right calf	0.109
Left foot	0.054
Right foot	0.054
	1.699

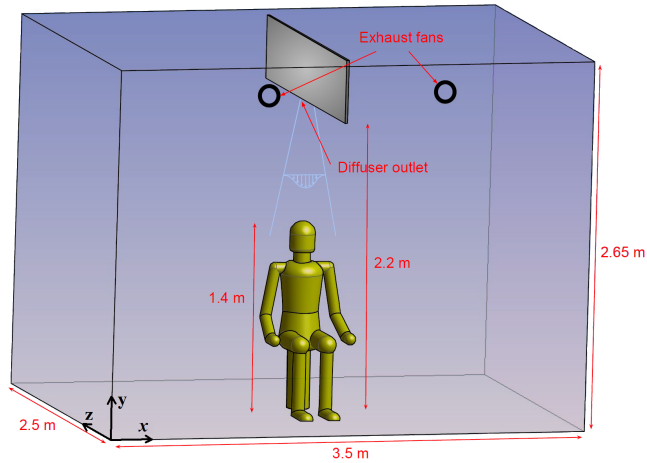


*Figure 6.1: CFD, geometrical setup*

## 6.2 Meshes

The meshes were naturally also different from case to case. For case 1, the room could be meshed with a structured mesh on the sides and with finer tetrahedral mesh in the center area where the main flow structure would be. An even finer tetrahedral mesh was used closer to the inlet in addition to 12 inflation layers from the face of the supply opening. Figure 6.3a and 6.3b display the mesh used for case 1. Figure 6.3b shows the mesh at a section mid-plane through the geometry. For case 2, in the bottom center of the mesh domain, a cube engulfed the manikin with tetrahedral mesh. The rest of the domain had structured mesh, which is better for simple geometries because fewer elements are needed for the same numerical accuracy. From the manikin's surface, 15 inflation layers were applied, and helped to resolve the viscous boundary layer and to get a  $y^+ \approx 1$ . Figure 6.2 shows a distribution of the  $y^+$  on the manikin's surface, and the value is generally lower than 1. The plume mesh can be seen in figure 6.3c and 6.3d.

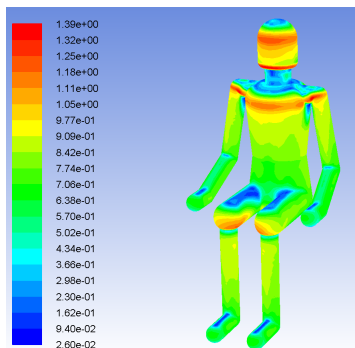


*Figure 6.2: Distribution of  $y^+$  at the manikin*

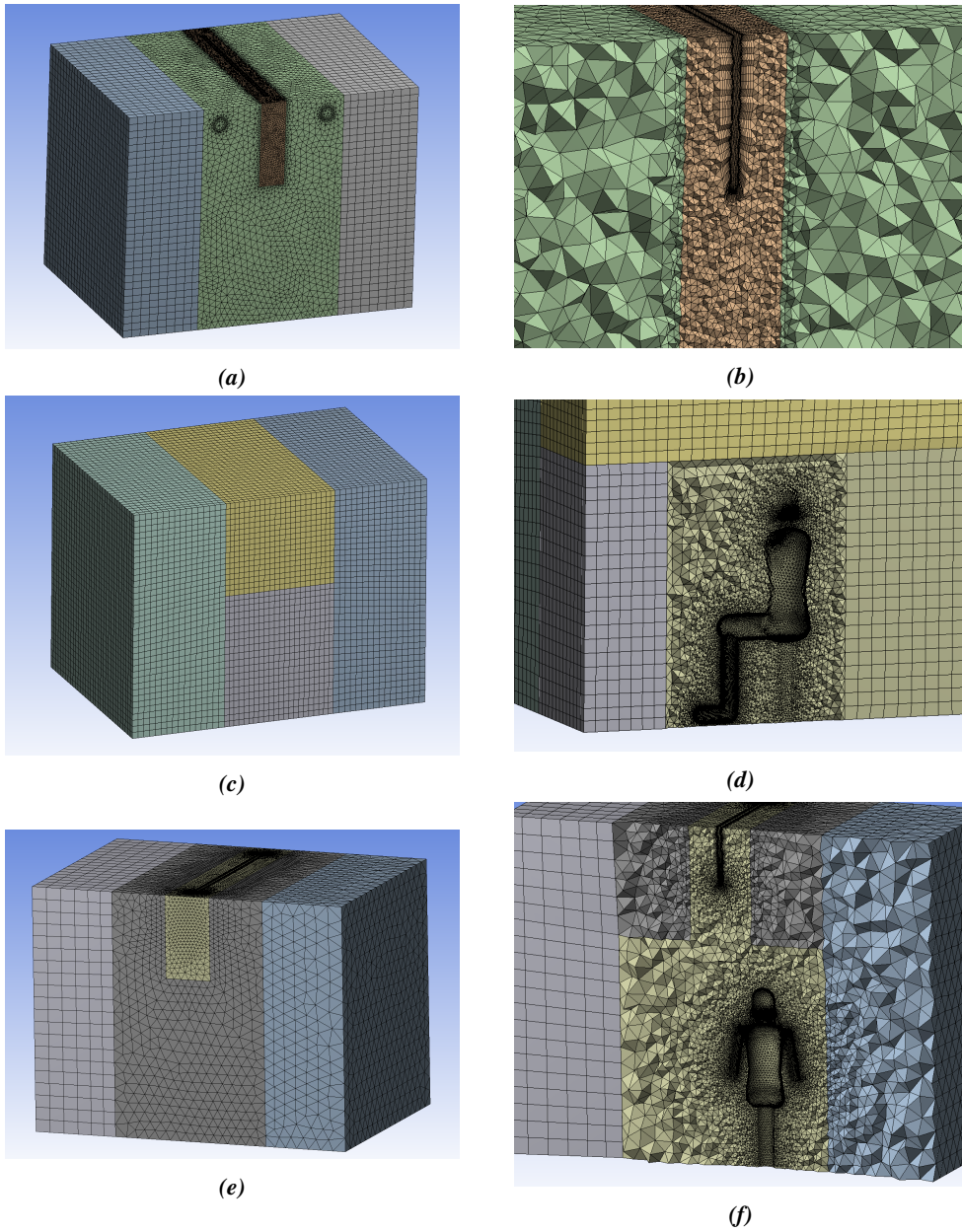


**Figure 6.3:** Mesh used for the CFD analysis of case 1, jet scenario, (a)+(b), case 2, plume scenario, (c)+(d), case 3.1, manikin at 0.34 m from jet (e)+(f)

The meshes used for case 3.1 and 3.2, the plume and jet situation, was a mix between the two meshes used for case 1 and 2. The meshes were completely equal except for the location of the manikin, where case 3.1 had the manikin 0.34 m next to the jet and case 3.2 had the manikin 0.47 m next to the jet. The meshes were split into 3 parts: the inner section covering both the

manikin and the diffuser outlet, the section surrounding the inner section and an outer section. The inner section was set to have 14 inflation layers from the manikin's body, with a first layer height of 0.8 mm to properly resolve the viscous sublayer and to get a  $y^+ \approx 1$  and a growth rate of 1.06. 12 inflation layers were also applied to the face of the diffuser outlet with a 1 mm first layer height and 1.2 growth rate. The other sections were set to have elements larger than the inner section's elements to ease unnecessary computational work. An element view of case 3.1, being very similar to case 3.2, can be seen in figure 6.3f. A wire-frame view of the same mesh is displayed in figure 6.4b.

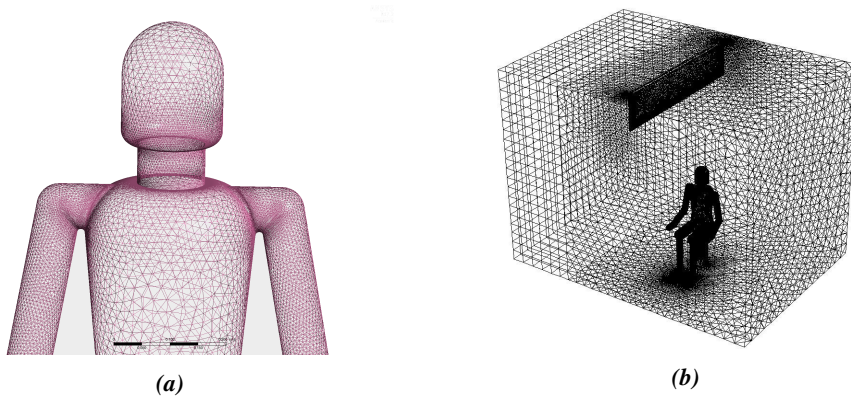


**Figure 6.4:** Manikin surface mesh (a) and case 3.1 surface mesh, manikin placed 0.34 m next to jet (b)

The meshing of the manikin was done in such a way that finer cells were put in areas with high curvature, like around the shoulders and at the chin, see figure 6.4a. This measure resulted in elements of higher quality because smaller elements would not have to skew and twist around the curves as much as larger elements. The large curve shaping the armpit was also a measure to increase the mesh element quality. By having a sharply curved armpit, which is normal when a person sits with his or her arm close to the body, the elements would be very skewed and of bad quality, inducing inaccurate results of flow and heat transfer in that area. The choice of approximating the human with simple geometrical building blocks, like cylinders and half-spheres, made the meshing of the body surface easier and of higher quality, but still able to attain the complexity of the human form. The only thing the author in retrospect would have added to the model, would have been nose, brows and ears to properly disrupt the flow past the curve of the head.

### 6.2.1 Grid independence check

A grid independence check was conducted for case 2, the plume case. The results from this check seemed sufficient to use for the plume vs. jet flow case, case 3, as well. The velocity at 0.2 m above the manikin's head, at  $z = 1.6$  m, was used as a control parameter. 5 different

meshes were checked to see when the velocity in this point did not notably change from one mesh refinement to the next. This can be seen in figure 6.5 where the change in percentage between the velocity at the point of interest in one mesh to the next finer mesh is given. The last two meshes at 1.8M elements and 2.0M elements yielded results with under 1% change from their previous refinement, and these meshes were therefore assumed to be grid independent. The 1.8M element mesh was used for the case 2 analysis to use the lowest necessary computational cost of the two grid independent solutions.

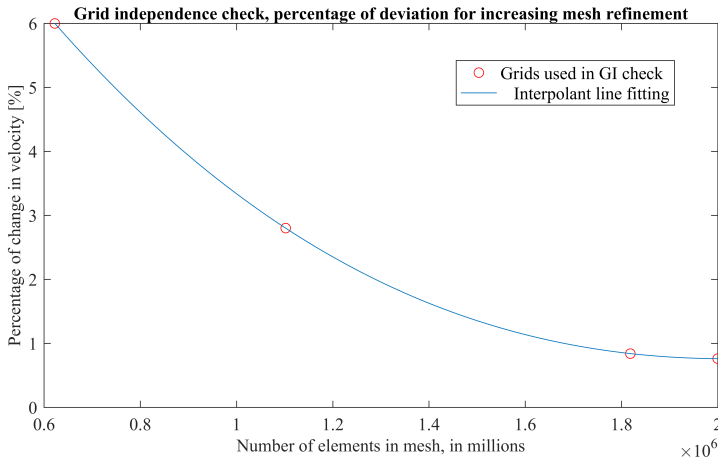


*Figure 6.5: Percentage change in velocity at the point of interest from one mesh refinement to the next*

### 6.3 Setup in Fluent

For the three cases, there were differences in the Fluent setup as well. All three cases were run with the RNG  $k-\epsilon$  turbulence model, due to its applicability for both natural convective flows, like the human plume, and jet flows. The enhanced wall treatment option was selected for the RNG  $k-\epsilon$  model. It was therefore desirable to have a  $y^+ \approx 1$  at walls of interest, like the manikin's body and the diffuser outlet. Due to the low-Reynolds number flows in this study, a value of 1 mm was calculated for the first cell height to give a value of  $y^+$  close to 1. After simulating the plume flow case, the human body surface was found to have a maximum  $y^+$  of 1.4. This was satisfactory and should have been small enough for the viscous sub-layer to be resolved and the flow and heat transfer to be captured.

All of the cases were solved with the coupled solver. When control variables, like velocity overhead or below the diffuser, heat transfer rate from body surface and volumetric inflow and outflow, approached a stable solution together with residuals below  $10^{-5}$ , the solution was assumed to be converged.

The boundary conditions for the three cases were different. For case 1, a velocity-inlet condition

of 1.5 m/s and a pressure-outlet condition were used together with isothermal conditions. For case 2, the experimental manikin model's surface area was split into three parts: head region, upper body and lower body, where the surface temperatures could be controlled individually to equal the experimental setup, as explained in chapter 3. Therefore, the CFD-model's 16 body parts were clustered into three larger parts with individual boundary conditions. The surface temperatures were set to 33°C for the head region, 32°C for the upper body and 31°C for the lower body. The choice of temperatures was a mix of what had been found in various literature. Dygert et al. (2009) used 32° on the whole body with an ambient temperature of 23°C, Tanabe et al. (2002) calculated the skin temperature by the use of a 65 node thermoregulatory method in an indoor environment of 30°C, and got temperatures of 35°C for the head and 33°C for the upper and lower body on average. Due to the ambient temperature being 23°C for the present experiment, it should have been safe to assume that the skin temperature in this climate was slightly lower. This assumption was backed up by Sørensen and Voigt (2003) who used an average skin temperature of 31°C with an ambient temperature of 19°C in their experiment. For case 3, all the BC's applied for case 1 and case 2 were applied. An overview of BC's and other important aspects connected to the simulation of the cases can be found in table 6.2.

**Table 6.2:** Important CFD aspects for the study. *OQ* = Orthogonal quality, *SK* = Skewness, *AR* = Aspect ratio

	Case 1 (Jet)	Case 2 (Plume)	Case 3 (Plume vs. Jet)
<b>Mesh quality</b>	OQ > 0.142 (min), 0.847 avg., SK < 0.9 (max), 0.254 avg., AR < 44.5 (max)	OQ > 0.115 (min), 0.897 avg., SK < 0.9 (max), 0.208 avg., AR < 42.8 (max)	OQ > 0.157 (min), 0.867 avg., SK < 0.899 (max), 0.245 avg., AR < 72.5 (max)
<b>Final mesh size</b>	1 514 733 elements, 377 305 nodes, 12 inflation layers at diffuser outlet, first layer 1 mm	1 999 652 elements, 718 795 nodes, 15 inflation layers at human body surface, first layer 0.8 mm	3 351 490 elements, 1 080 099 nodes, 14 inflation layers at human body surface, first layer 0.8 mm, 12 inflation layers at diffuser outlet, first layer 1 mm
<b>Boundary conditions</b>	Supply = 1.5 m/s and 0.8% turbulence intensity, pressure outlet for exhausts, isothermal conditions, no-slip at walls	$T_{skin} = 34, 32$ and $32$ °C, $T_{wall}$ and $T_{amb} = 23$ °C, no-slip at walls	Supply = 1.5 m/s and 23°C, pressure outlet for exhausts, $T_{skin} = 34, 32$ and $32$ °C, $T_{wall}$ and $T_{amb} = 23$ °C, no-slip at walls
<b>Turbulence model and related options</b>	RNG k- $\epsilon$ model with Enhanced Wall Treatment	RNG k- $\epsilon$ model with Enhanced Wall Treatment and differential viscosity scheme, gravity and full buoyancy effects, thermal effects on, energy eqn. enabled for heat transfer, Boussinesq density assumption	RNG k- $\epsilon$ model with Enhanced Wall Treatment and differential viscosity scheme, gravity and full buoyancy effects, thermal effects on, energy eqn. enabled for heat transfer, Boussinesq density assumption
<b>Solver setup</b>	First SIMPLE, then COUPLED solver with pseudo-transient, First-order upwind for momentum, otherwise default spatial discretization	First SIMPLE, then COUPLED solver with pseudo-transient with timescale factors of 1 to 0.01, Body Force Weighted pressure discretization, First-order upwind scheme for momentum to get a stable solution, otherwise default spatial discretization	COUPLED solver with pseudo-transient with a timescale factor of 1, Body Force Weighted pressure discretization, Second-order upwind scheme for momentum, otherwise default spatial discretization

# Simulation results

This chapter gives an overview of the results from the CFD study of the three cases first introduced in chapter 1.

## 7.1 Case 1: 2D downward plane jet

By the use of the mesh shown in chapter 6, the result of the simulated jet looked fairly similar to a real plane isothermal jet. The characteristic high velocity at the centerline and low spread angle could be seen. Figures 7.1a, 7.1b and 7.1c display velocity contours of the simulated plane jet. Figure 7.1d shows the turbulence intensity close to the diffuser outlet. Low turbulence intensities are found in the center and higher turbulence intensities on the sides, possibly due to the sharp edges of the outlet and the shear stresses with the ambient air. The turbulence intensities were generally a bit higher than expected. Deo et al. (2007) also got the same profile for turbulence intensity in his study of different geometries for turbulent plane jets.

To be able to find  $\alpha$  for the jet simulation, a similar approach to what was used for the experimental jet was used. Lines were drawn across the jet profile at 6 different heights in the CFD-post software of ANSYS 17.2. Each of the lines were segmented into 300 points, creating 6 matrices of 3x300 points, the 3 being a unit number, x-location and respective velocity. For each height's velocity-vector,  $U_m$ , being the point with the highest velocity-value, was found with the same MATLAB-script as before. The script divided  $U_m$  by 2, as in equation 4.1, and found  $U_{0.5}$ . The point with a velocity value closest to the calculated  $U_{0.5}$  was found with a for-loop and its respective location,  $x_{0.5}$ , was noted. Hence,  $b$ , was calculated by the use of equation 4.2. Lastly, the point with a location closest to the calculated  $b$  was found by plotting all the  $b$ -locations in a graph of x-location in the room vs. height above the floor, together with linear graph fitting, as seen in figure 7.2. The centerline of the jet was at  $x = 1.75$  m and the diffuser outlet at  $y = 2.2$

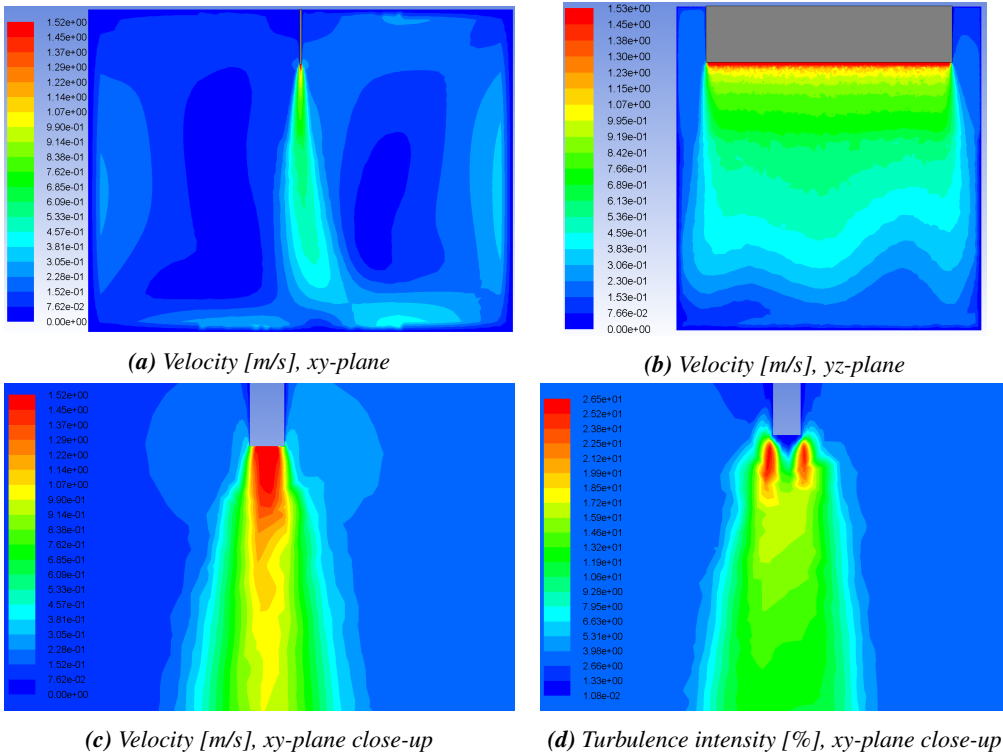


Figure 7.1: Velocity and Turbulence intensity contours close to the diffuser outlet of case 1

m. The MATLAB plotting software printed the equation for the linear graph fit, which was found to be  $y = -4.3x + 9.7$  and the angle to the centerline was then be found by  $\tan^{-1}(\frac{1}{4.3})$  to yield an angle of  $\alpha = 13.1^\circ$ . This spread angle proved to be fairly close to the spread angle of the experimental jet of  $13.4^\circ$ .

Figure 7.3a displays the velocity distributions at the 6 different heights used for the jet spread angle deduction. Figure 7.3b shows the distributions plotted dimensionless proving their uniformity and similar shape to other studies of velocity distributions for plane turbulent jets (Abramovich, 1963; Baturin, 1972). Figure 7.4 displays the centerline velocity development of the jet.

## 7.2 Case 2: Thermal plume from thermal manikin

The human plume simulation was satisfactory as well. Velocity contours can be seen in figure 7.5a and 7.5b. The highest velocity was found in front of the face in figure 7.5b. In a real scenario, the nose and eyebrows would disturb the rising plume flow, and the highest velocity would instead be found above the head of the occupant. However, a study by Wei et al. (2009) shows that the geometry of the manikin has little effect on the thermal plume magnitude further

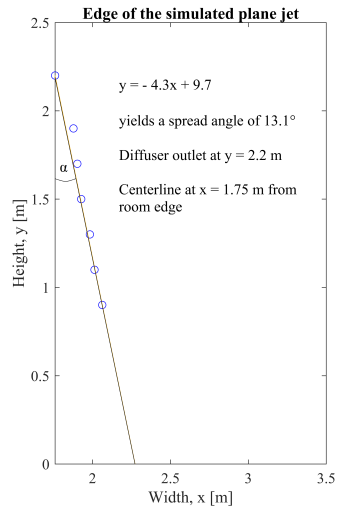


**Figure 7.2:** MATLAB deduced jet spread angle

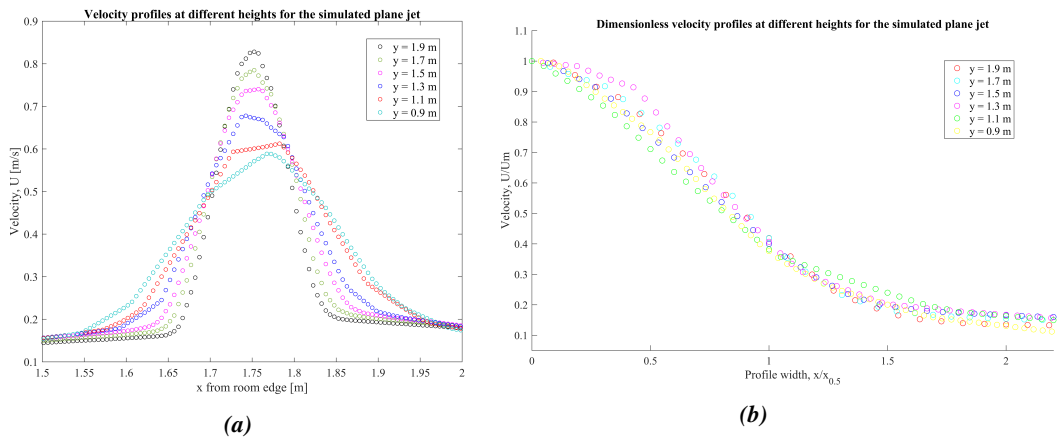


**Figure 7.3:** Velocity distributions at various heights above the floor (a), dimensionless representation (b)

away from the surface of the manikin. Therefore, the results from this CFD study were found to be acceptable some distance away from the manikin surface.

The shape of the plume resembled that of other simulation plume studies. The maximum velocity of 0.275 m/s (above the head) was within the norm for environments around  $20^\circ\text{C}$  (Sørensen and Voigt, 2003; Dygert et al., 2009). In environments with somewhat higher ambient temperatures, the literature report maximum plume velocities at around 0.25 m/s (Murakami et al., 2000; Kilic and Sevilgen, 2008; Liu et al., 2015; Zukowska et al., 2007). The centerline velocity development can be seen in figure 7.6 plotted from the head of the manikin at  $y = 1.4$  m to the ceiling at  $y = 2.65$  m. Figures 7.7a and 7.7b display the plume's velocity distributions at seven  $y$ -locations from  $y = 1.5$  m to  $y = 2.1$  m in the  $xy$ -plane, front view, and in the  $yz$ -plane, side view. Figure

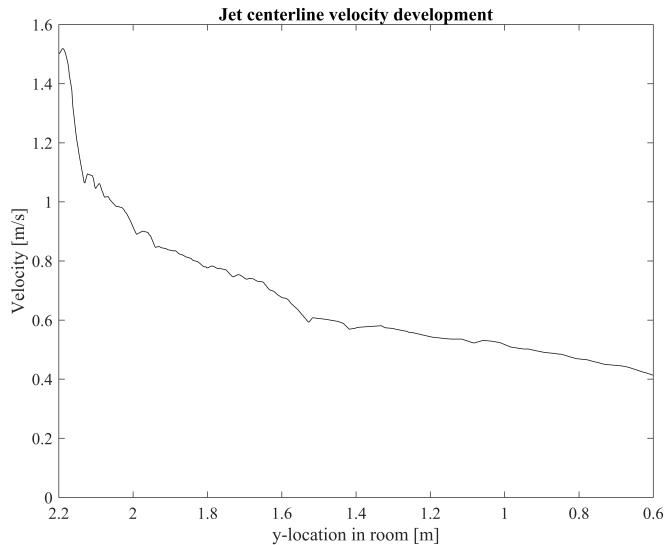


**Figure 7.4:** Jet centerline velocity development [m/s]

7.7a shows quite symmetrical profiles where for a certain height the velocity does not increase anymore. At  $y = 1.6$  and  $1.5$  m the distributions seems to behave somewhat differently. This can be because these heights are just above the head of the manikin where separation occurs, and the plume is not fully developed. Figure 7.7b shows a similar kind of plume axis wandering as was found in the experiment.

The spread of the simulated plume was also found by the same MATLAB-script used for the experimental plume in chapter 4. The two simulated plume-planes have spread angles smaller than the experimental plume-planes, which had  $11.3^\circ$  and  $10.5^\circ$  spread angle for the  $xy$ -plane and the  $yz$ -plane respectively. For the simulated plume, the plume in the  $xy$ -plane behaved a little differently than in the  $yz$ -plane. The edge of the simulated plume seemed to rise almost straight up and diminish slightly in width instead of growing larger and larger. By looking at figure 7.5b, the plume seems to rise straight up. The reason why the simulated plume grew differently in the  $xy$ -plane is not easy to determine. The turbulence model and options used can have an effect. Full buoyancy and thermal effects, for instance, were turned on. Maybe, these options overestimated the early growth of the plume. Either way, the spread angle of  $9.3^\circ$  should not be considered to be correct. The simulated plume in the  $yz$ -plane, however, seemed to spread out similar to the experimental plume, although with a somewhat smaller spread angle of  $6.8^\circ$ . A  $y_0$  of 1.2 m is also used for the simulated plume spread. Due to the uncertainties regarding the simulated plume, the spread angles of the experimental plume will be taken as the deduced plume spread angles of this thesis.

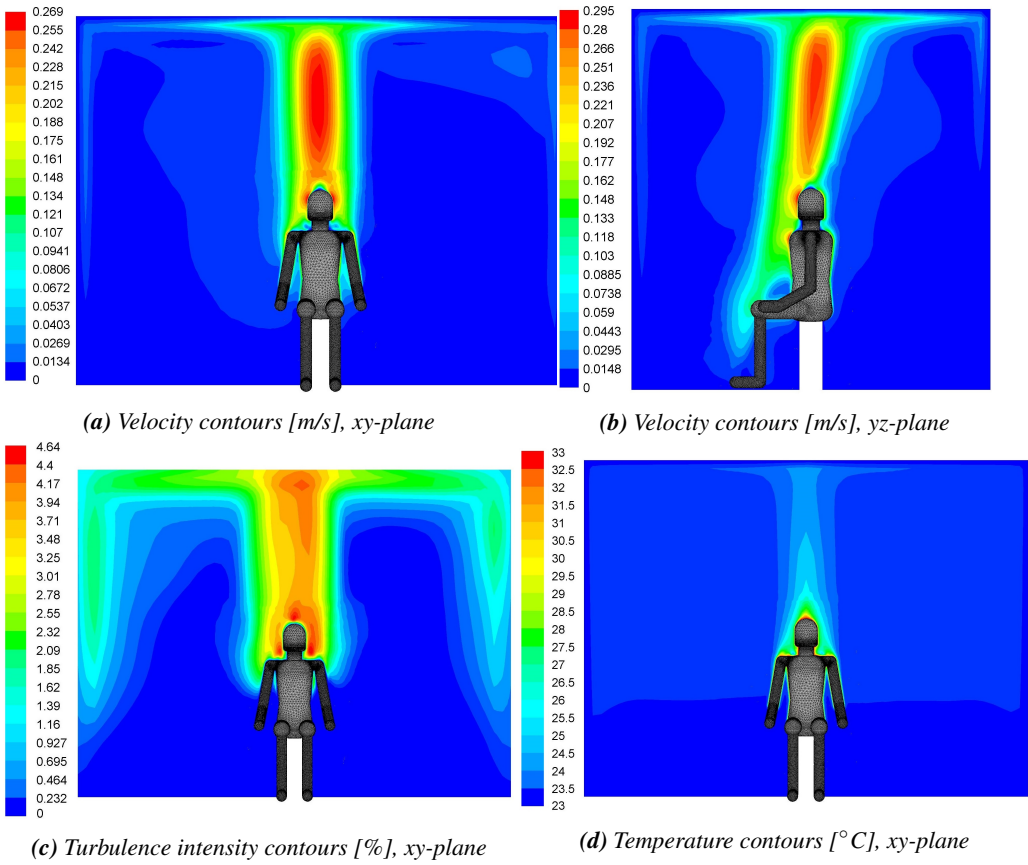


Figure 7.5: Velocity contours [m/s], turbulence intensity [%] and temperature [°C] contours, xy-plane

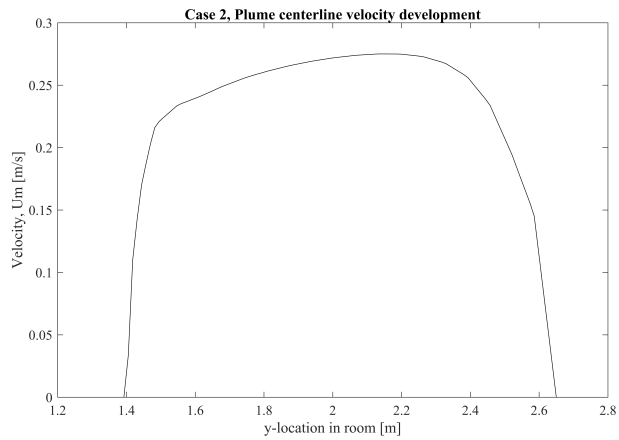


Figure 7.6: Plume centerline velocity development from head of manikin

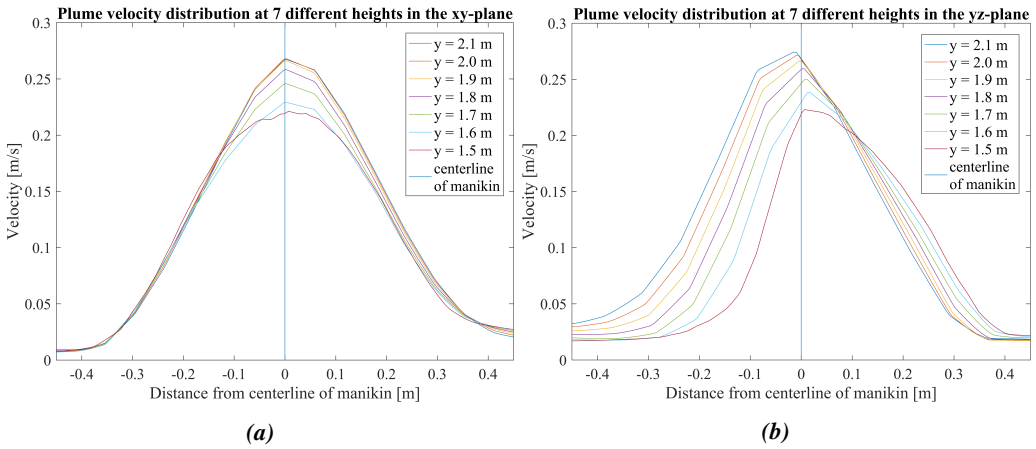


Figure 7.7: Velocity distribution for plume at seven different heights, case 2, xy-plane (a) and yz-plane (b)

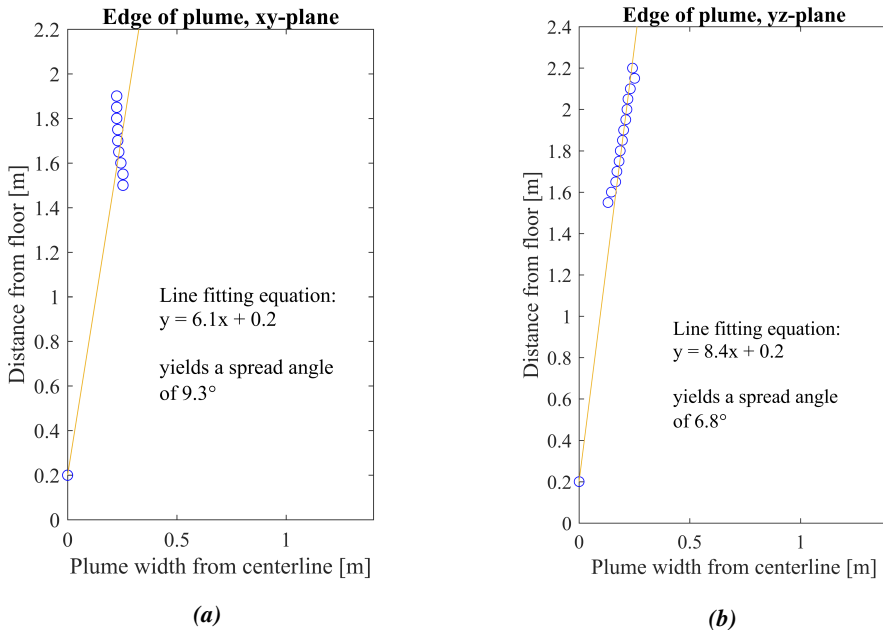


Figure 7.8: Calculated plume spread from simulation, case 2, xy-plane (a) and yz-plane (b)

### 7.3 Heat transfer

One way to validate results from the simulation for case 2 was to evaluate the manikin's heat transfer and heat transfer coefficient. For the simulated human manikin, the facet average of the convective heat transfer coefficient on the manikin's surface,  $h_c$ , was  $3.11 \text{ W/m}^2\text{K}$ . The facet average is the average value of the surface elements. This value was slightly lower than other

values found in the literature, but still fairly close. For example, Sørensen and Voigt (2003) got a similar result of a  $h_c$  of  $3.13 \text{ W/m}^2\text{K}$  where the ambient was at  $19.8^\circ\text{C}$  and the manikin's average surface temperature was at  $31^\circ\text{C}$ . Gao et al. (2006) got a  $h_c$  of  $3.51 \text{ W/m}^2\text{K}$  where the manikin had an average surface temperature of  $30.75^\circ\text{C}$  and the ambient a temperature of  $26^\circ\text{C}$ . de Dear et al. (1997) got a  $h_c$  of  $3.3 \text{ W/m}^2\text{K}$  in his experiment with a thermal manikin with a difference between the manikin's surface temperature and the ambient temperature of  $12^\circ\text{C}$ . The convective heat release from the manikin was simulated to be  $47.97 \text{ W}$ . This result is very close to  $47 \text{ W}$ , which is  $40\%$  (Sørensen and Voigt, 2003) of convective sensible heat release of the total sensible heat release of  $118 \text{ W}$ . Murakami et al. (2000) also got a similar convective heat release from a thermal manikin in similar ambient conditions of  $49.3 \text{ W}$ . In this study  $43.3\%$  of the total sensible heat release came from convection and  $56.7\%$  came from radiation.

This kind of evaluation was only done for case 2 because it was the most reproduced case. Several articles had done a similar study and therefore case 2 could be validated. Case 3, on the other hand, was an unique case, and could not be compared to the literature. In addition, its heavily unstable flow behavior influencing the convective heat transfer would make comparisons difficult. Case 1 did not contain any heat transfer, and was naturally not considered for this evaluation.

## 7.4 Case 3: Interaction between thermal plume and downward plane jet

The third case was split into two sub-cases, case 3.1 and 3.2. Case 3.1 was based on achieving a draught rate of  $20\%$  with a manikin centerline position of  $0.34 \text{ m}$  to the jet centerline. Case 3.2 was based on achieving a draught rate of  $10\%$  with a manikin centerline position of  $0.47 \text{ m}$  to the jet centerline. Having the manikin placed directly below the jet, as in figure 6.1, was also briefly investigated in the simulation part of the thesis. The simulation of the jet vs. plume flow was naturally more complex than case 1 and 2, and were time-consuming to finish. Due to opposing flows, there were severe transient behavior, and achieving a steady solution was impossible. Especially the iteration errors, as described in chapter 5.7, were large here due to the solver's inability to find a stable solution. The results should therefore be viewed critically. They can be viewed as being averages of the unsteady movement of the flow. One example that proves how difficult it was to determine a steady flow, can be seen in figure 7.9. Here, the instability of the calculated values for velocity was monitored at a point  $1.6 \text{ m}$  above the ground,  $0.2 \text{ m}$  above the manikin's head.

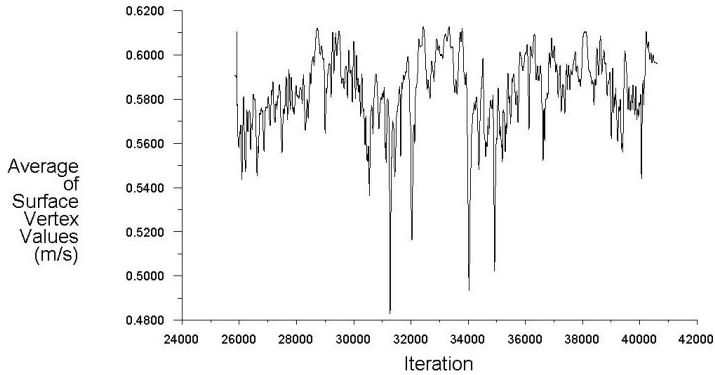


*Figure 7.9: Monitored velocity at 1.6 m above ground shows the flow is very unstable*

### 7.4.1 Manikin below jet

This special case was investigated briefly due to the possibility of visualizing jet impingement on top of the manikin's head. Viewing this impingement experimentally was difficult. A smoke test was performed with the manikin below the jet, but it was not especially successful. Part of the diffuser in front of the manikin supplied smoke in front of the manikin cross-section, making it difficult to see anything around the head and shoulder region. The project work last semester studied this case experimentally in more detail. A graph of measured velocity fluctuations above the manikin's head when subjected to the plane jet can be found in the conference paper in appendix C. The CFD simulation had a golden opportunity of visualizing the flow at the manikin cross-section. Velocity contours from the simulation can be seen in figure 7.10a and 7.10b, and turbulence intensity and pressure contours in figure 7.10d and 7.10c.

It can be seen by the velocity contours in 7.10a that the manikin's plume was destroyed completely by the downward jet. A slight upward flow was only seen under the arms and legs, and in some places, very close to the skin surface. Figure 7.11 shows the velocity vectors, colored by temperature, of the flow under the side chin. Circulating flow can be seen as the downward flow and drags the plume rising from the neck down into a swirl motion. The red and yellow colored vectors are the hottest vectors and are rising flow. The blue colored vectors are colder and are going down the head with the jet.

The opposing jet hit the manikin as an impinging jet due to the head and shoulders of the manikin, creating a slow circulating flow displayed as velocity streamlines in figures 7.12a and 7.12b. These figures show the flow velocity from the front. The view is sliced in two planes. The first sectioned view, sliced the flow along the manikin's shoulders at the centerline of the manikin, the second sectioned view sliced the thighs of the manikin at 0.25 m from the centerline. Velocity streamlines from the impinging flow can also be viewed from the side in figures 7.12d, and 7.12c. Here, the first plane slices the manikin and the jet at the centerline and the second plane at 0.1 m out from the side of the centerline.

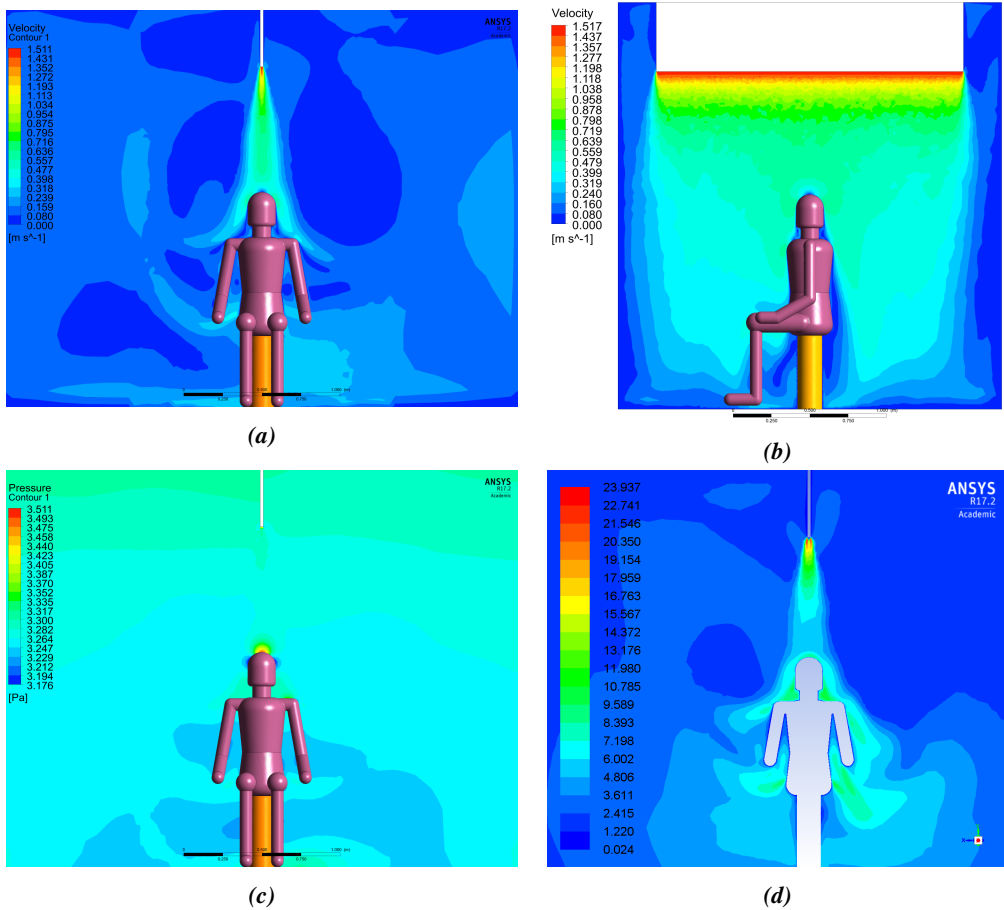


Figure 7.10: Velocity contours (a) and (b), pressure contour (c) and turbulence intensity (d)

### 7.4.2 Simulation results for case 3.1 and 3.2

The results from case 3.1 with centerline of manikin at 0.34 m next to jet centerline and case 3.2 with centerline of manikin at 0.47 m next to jet centerline are presented here. For a distance of 0.34 m between the manikin's centerline and the jet's centerline, a typical, normal occupant would generally not feel uncomfortable due to draught, assuming a  $DR = 20\%$  for category B standard in NS-EN7730 (2005), while a distance of 0.47 m is based on sensitive and fragile occupants with a maximum draught rate of 10%, category A. By verifying these pre-calculated distances means that the possibility to recommend how far away an occupant should be from a plane jet, for instance in a POV area, to avoid draught, arises. In chapter 4 both distances coincided quite well with experimental results.

Figures 7.13a and 7.13b display the velocity contours of case 3.1 and case 3.2 respectively. In case 7.13a the velocity at the shoulder is higher than 7.13b and therefore, a higher draught rate

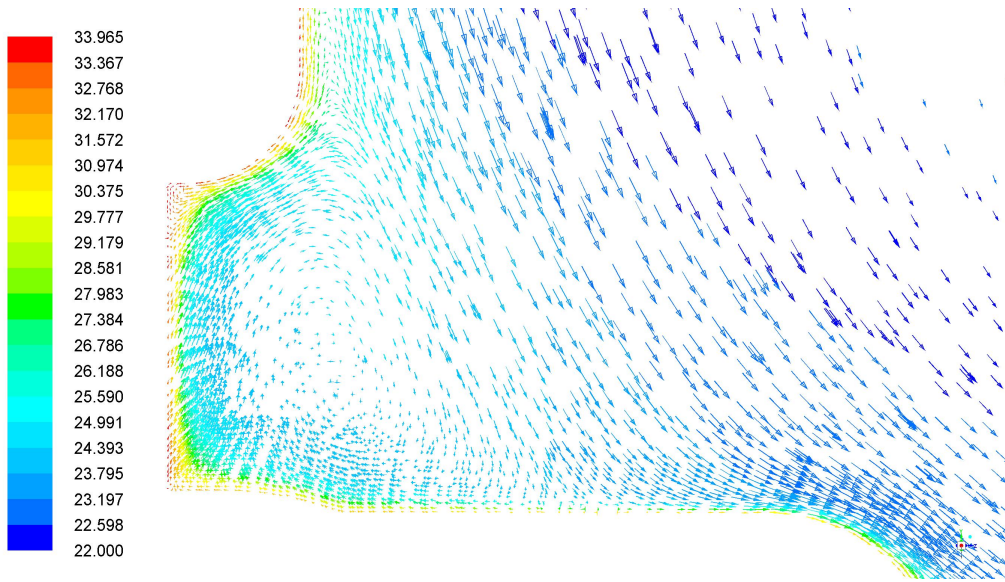


Figure 7.11: Velocity vectors colored by static temperature close to shoulder for manikin below jet

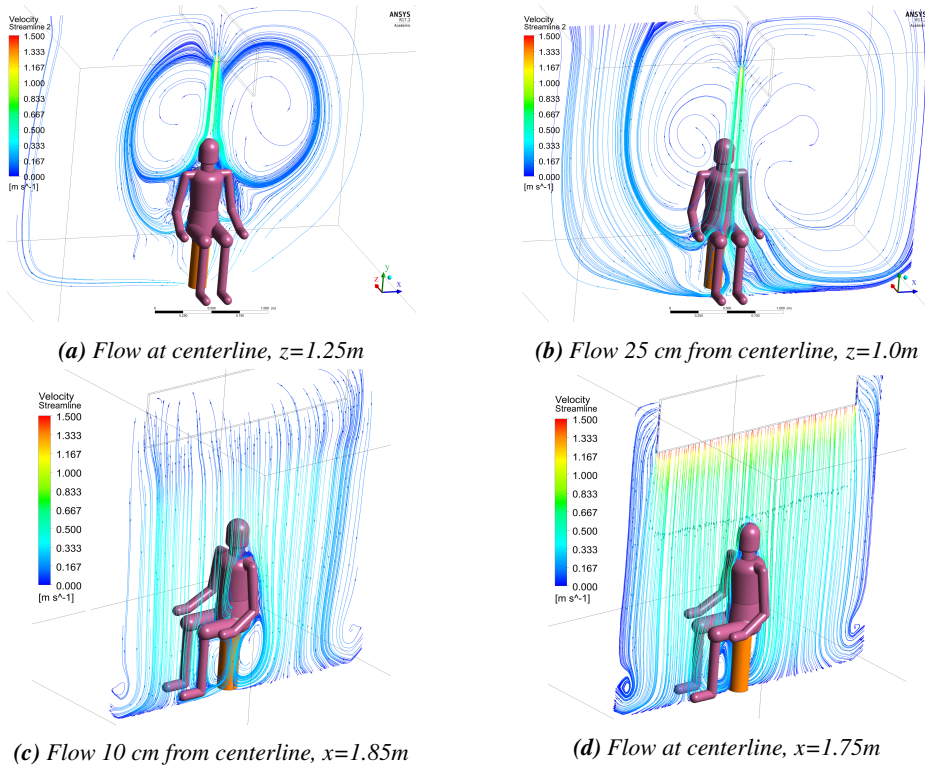
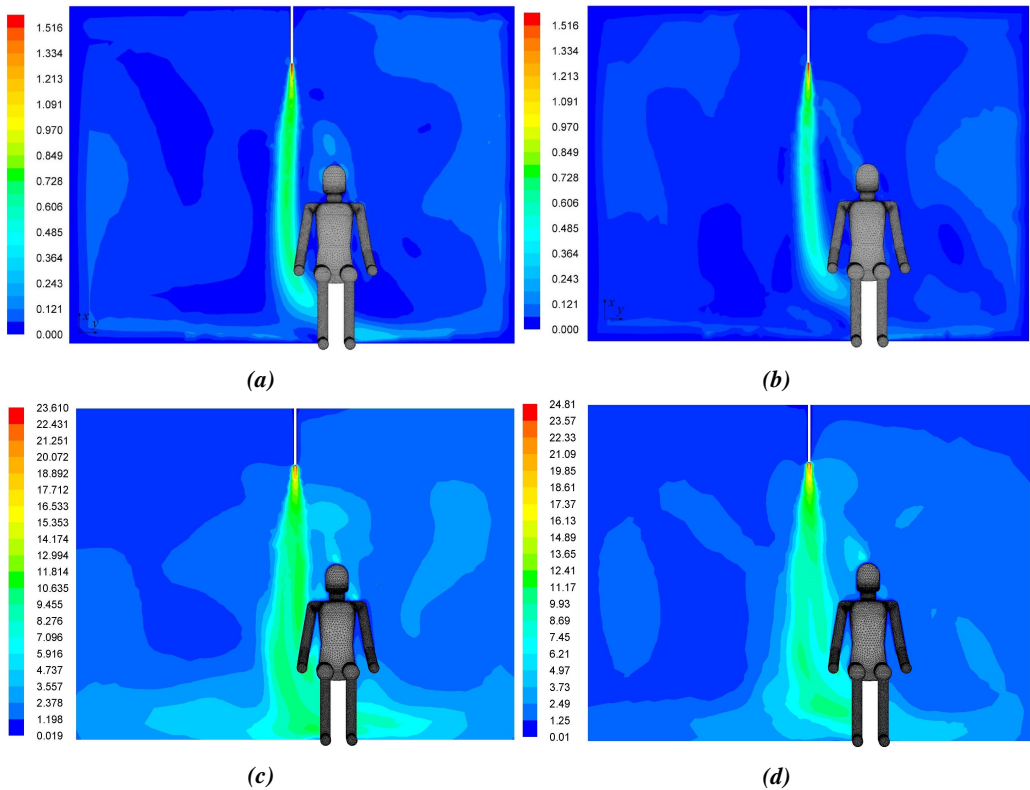


Figure 7.12: Velocity streamlines of manikin below jet

would be sensed here. The jets are slightly skewed, but that was also normal for the experimental jet. Therefore, this characteristic is not evaluated further.



**Figure 7.13:** Velocity contours [m/s] and turbulence intensity, case 3.1 (a) and (c) and case 3.2 (b) and (d)

Figure 7.14 displays the simulated jet centerline maximum velocity decay. Case 3.1 and 3.2 are compared and coincide quite well.

The velocity distribution simulated for case 3 at shoulder height,  $y = 1.1$  m, can be seen in figure 7.15. The velocity 5 cm from the shoulder was 0.241 m/s for case 3.1 and 0.082 m/s for case 2.2. Both velocities were below the requirement for  $DR = 20\%$  and  $10\%$  as seen in table 7.1. The simulated turbulence intensities were lower than  $10\%$ . Still,  $10\%$  had to be used in the DR-equation due to its boundary conditions. The simulation results seemed to suggest that the manikin could have been somewhat closer to the jet, and still be within the two DR-requirements. The experiment, however, proved the comfort distances of 0.34 m ( $20\%$  DR) and 0.47 m ( $10\%$  DR) to be decent recommendations.

Velocity vectors over the manikin's shoulder colored by temperature can be seen in figure 7.17 and 7.18. The size of the arrows corresponds to velocity magnitude. The difference between the two figures are quite clear. For case 3.1, the manikin is close to the jet and flow swirl can be seen at the shoulder where the rising plume is forced downwards by the jet flow. For case 3.2, the

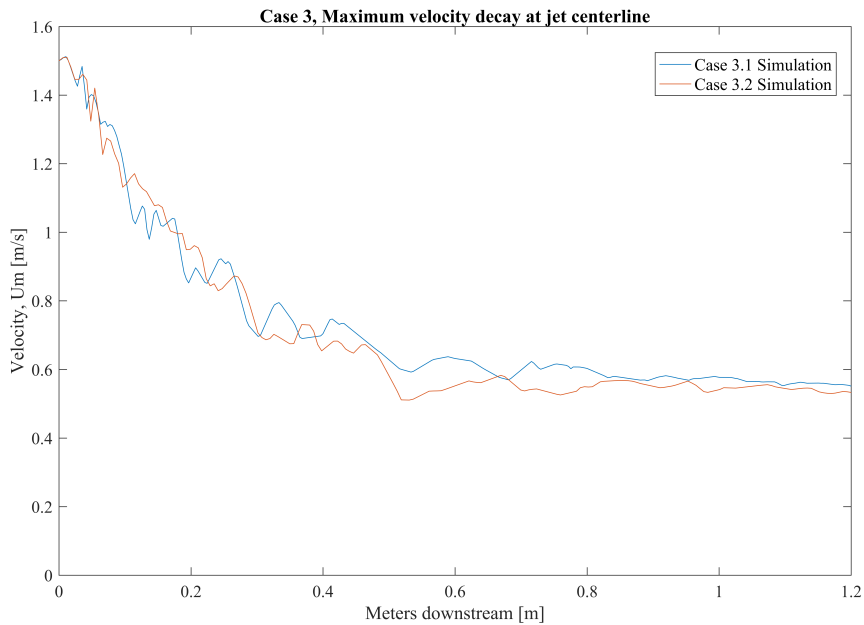


**Figure 7.14:** Jet centerline maximum velocity decay for case 3

swirl is not as abrupt, and lower swirl velocities can be seen. In this case, the plume entrains jet flow rather than the other way round, as in case 3.1. To the right of the manikin’s head the thermal boundary layer has grown bigger in both cases. This can be explained by the plume’s entrainment into the jet some distance above the head of the manikin, which drags the whole plume flow in the direction of the jet. This must also pull the boundary layer wider on the jet side and thinner on the ambient side. However, these are just suggestions on the authors part.

**Table 7.1:** Draught rate at shoulder for case 3.1 and 3.2

DR desired	CtoC distance	CtoS distance	Calc. velocity	Sim. velocity at shoulder	Simulated TU	Simulated DR <sup>1</sup>
20%	0.34 m	0.14 m	0.278 m/s	0.241 m/s	9.90%	15.9%
10%	0.47 m	0.27 m	0.143 m/s	0.082 m/s	6.33%	4.5%

Where CtoC distance is referring to centerline of jet to centerline of manikin, and CtoS distance is referring to centerline of jet to shoulder of manikin. The difference of 20 cm is due to the width of a shoulder from the manikin centerline.

<sup>1</sup>For simulated TU lower than 10%, 10% was used in DR-equation

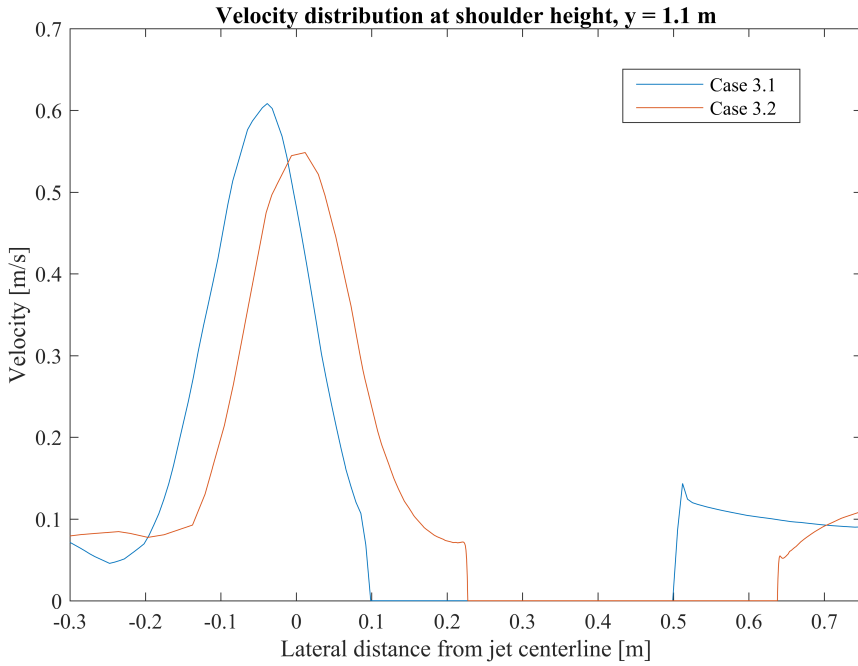


Figure 7.15: Velocity distribution laterally from shoulders at  $y = 1.1$  m for case 3.1 ( $x=0.34$  m) and 3.2 ( $x=0.47$  m)

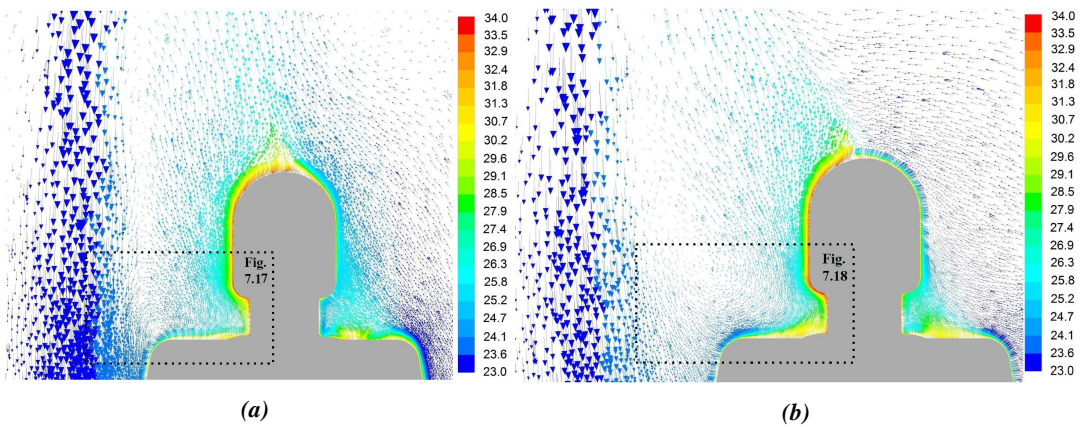
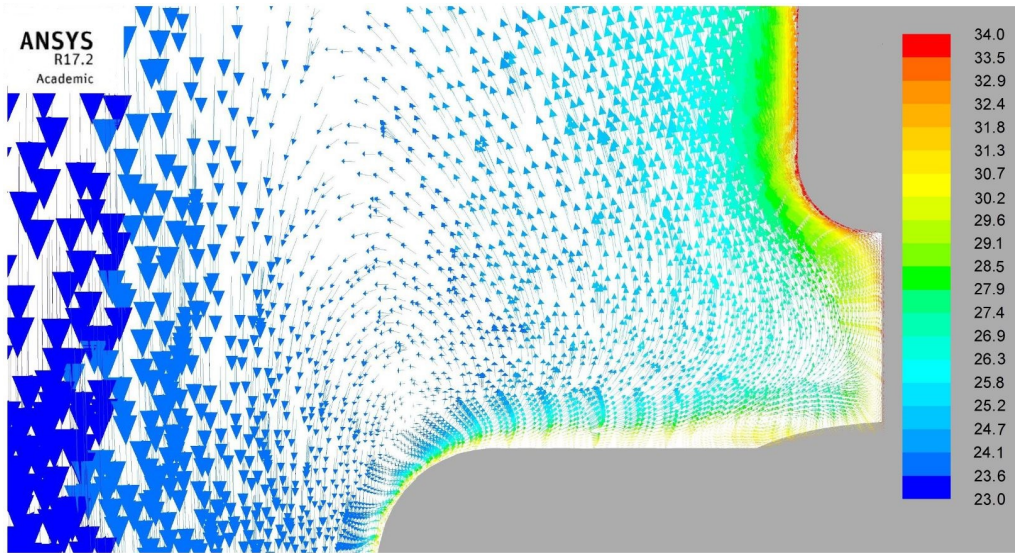
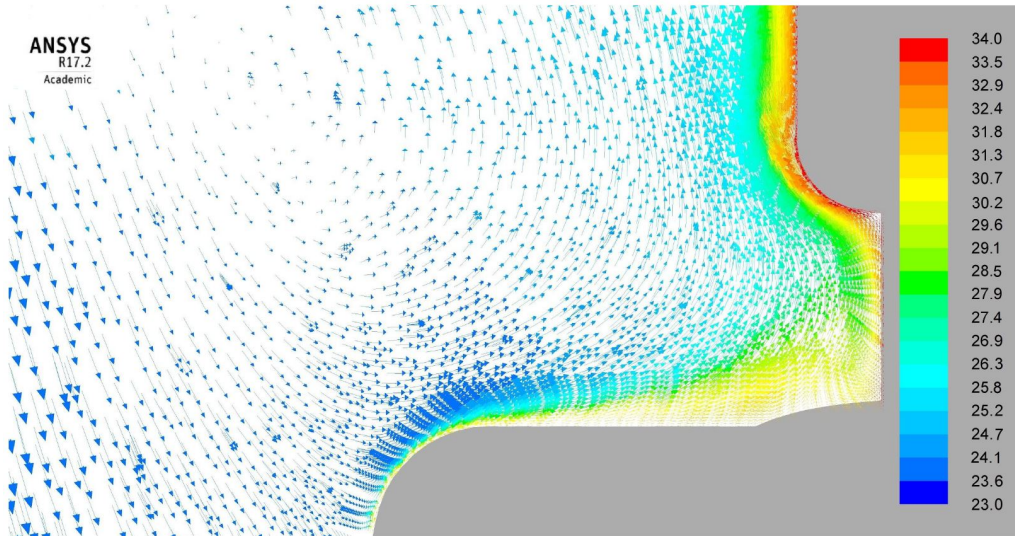


Figure 7.16: Velocity vectors colored by temperature, case 3.1 (a) and case 3.2 (b)



*Figure 7.17: Velocity vectors colored by temperature, close-up at shoulder, case 3.1*



*Figure 7.18: Velocity vectors colored by temperature, close-up at shoulder, case 3.2*

# Discussion

This chapter includes a thorough comparison of the experiment, the simulation and the mathematical model. Aspects of scientific methods that have some dubious characteristics, questionable conditions or have room for improvement will also be discussed.

## 8.1 Comparison of results

The plane jet has been an important aspect throughout this thesis due to its apparent influence on a nearby occupant's thermal comfort. Determining its centerline velocity decay plays a role in the jet's velocity distribution and hence, its outer boundary. Pinpointing the jet's edge and spread is important to be able to recommend a comfort distance for an occupant.

Figure 8.1 displays the centerline maximum velocity decay for the plane jet. Experimental, simulated and mathematical results are compared. The graph starts with the initial core region where  $U_0 = U_m$ , which lasts for approximately  $10 \cdot \frac{1}{2} \cdot h_0 = 0.1$  m (Abramovich, 1963). The simulated results only reached a core length of 0.02 m, but the experiment showed tendency of reaching the 0.1 m. The transitional region came next and Abramovich (1963) approximated the region to last 1.2 times the length of the core region. A model of the velocity distribution in this area was not found, and a graph fitting between the mathematical core region and the mathematical main region was determined instead. The transitional region was  $0.1 \cdot 1.2 = 0.12$  m for the experiment, which meant that the main region would start at  $0.1 + 0.12 = 0.22$  m downstream. Due to the shorter core region for the simulation, the transitional region became around  $1.2 \cdot 0.02 = 0.024$  m, and consequentially, a main region from  $0.02 + 0.024 = 0.044$  m. The comparison of the results in figure 8.1 shows that the simulation struggled to maintain a core region. For the flow 0.2 m downstream from the outlet, the fit between the simulation and the experiment was better. From 0.35 m downstream from the nozzle the three methods coincided

well. Between the three methods, the experiment and the mathematical model had the better fit. The experimental results seemed slightly lower than the other models overall, however not by a considerable amount.

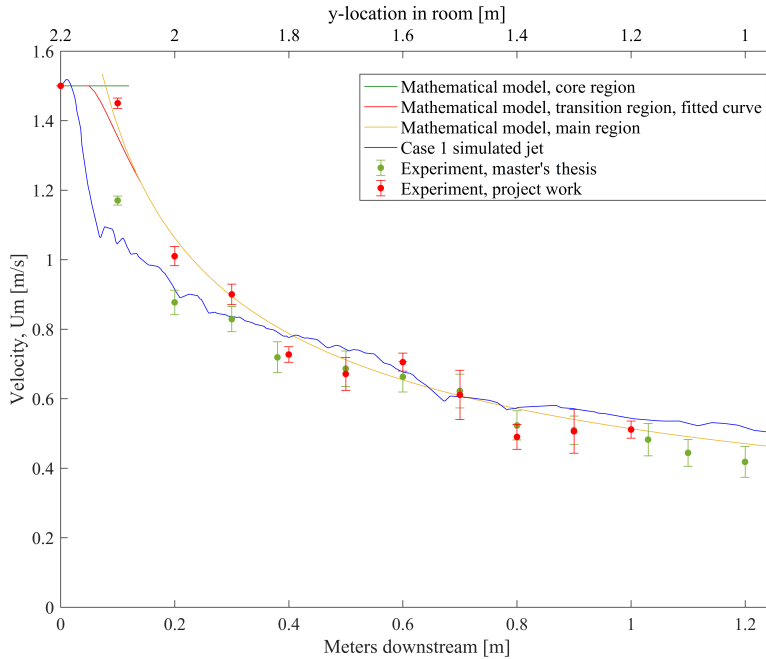


**Figure 8.1:** Jet centerline maximum velocity decay for case 1, comparison

A comparison of the plume centerline velocity was also performed. The simulated and the experimental results seemed to coincide quite well, except after roughly 0.55 m where the experimental results started to decline. There was another diffuser in the lab used for an unrelated experiment that shortened the total height above the manikin from the total room height of 2.65 m to 2.2 m. This meant that the experimental plume felt the ceiling earlier than the simulated plume, causing a deviation between the two. Two main mathematical models were tested, and none of them managed to describe the centerline velocity of the plume similar to the experiment and the simulation. The two models have already been introduced in chapter 2 as equation 2.9 and 2.8. The two equations were typically applied in the developed zone of the plume. At which height this zone starts, varies from geometry to geometry and heat power. The shape of the model is anyhow declining, which means that the zone must have started somewhere after the plume has had its maximum velocity. The equations gave generally too high velocities. To fit the experimental and numerical results, an similar equation to 2.9 and 2.8 are proposed. By changing the coefficient from equation 2.8 to 2.91, the equation looks like this:

$$U_m = 2.91 \left( \frac{g}{\rho c_p T} \right)^{\frac{1}{3}} \left( \frac{\dot{W}_c}{y_p} \right)^{\frac{1}{3}} = 0.87 \left( \frac{\dot{W}_c}{y_p} \right)^{\frac{1}{3}} \quad (8.1)$$

The empirical coefficient  $C$  is here 0.87. Assumptions made was a  $y_p$  of 1.2 ( $y_0$ ) m + 0.1 m to 0.9 m above the manikin. Otherwise, the same parameters as in table 2.1 were used. This proposed equation fits better to the experimental and numerical results, however only in the declining section of the plume, see figure 8.2. To cover the accelerating part of the plume, shown by the yellow line, an equation from a book of Baturin (1972) that characterized the accelerated section of a plume flow from a horizontal plate was used. It was defined as:

$$U_m = \sqrt{2g \frac{\Delta T}{T_{room}} \cdot y_p} \quad (8.2)$$

Where,  $\Delta T$  is the difference in temperature between the hot surface and the ambient. The other parameters have been introduced earlier. The model seemed to have the same trend as the numerical results for about 0.6 m before deviating from the jet. All the equations, however, were based on thermal currents from a point source, and not for a human, which must be why the discrepancies were so big. To bridge the two models, a fitting curve was placed to fit the experimental and numerical results better. The line is not ensuring a continuous curve between equation 8.2 and 8.1, especially not between 8.2 and the fitted curve. There was not enough time to improve this curve to full continuity. This should also be studied further.

Case 3 is a mix of case 1 and case 2. Therefore a comparison of the jet in case 3 was also conducted. Only the results from experiment and simulation were compared because no mathematical model was found to match case 3. It would be reasonable to assume that the manikin and its plume would slightly affect the jet. By looking at figure 8.3, the experiment fits very well with the simulation down to a  $y_j = 0.6$  m downstream of the diffuser. After 0.6 m, the experimental jet kept decreasing in velocity, while the simulation kept a somewhat even velocity at roughly 0.55 m/s. It must be mentioned that some distance later, the simulated jets also decreased in velocity. Figures 4.8a and 4.8b show that the simulated jet continues to move far down before breaking up. The reason for the difference in velocities is unclear. There can be errors in the simulation caused by the choice of turbulence model, model errors, iteration errors clearly shown in figure 7.9 or due to other options chosen in the solver. The uncertainties are higher for the simulated values, which means that ultimately, the experimental values are considered more trustworthy. When simulating the unsteady flow in case 3.1 and 3.2, the velocity contours almost changed from one iteration to the next. A steady solution was not possible to attain. The results shown in figures 4.8a and 4.8b, and the other figures in case 3, are only a few of many solutions. Some of the solutions were most likely closer to the experimental results than the ones chosen. It is impossible to know. A transient simulation should have been conducted, but the time was too short and the computational cost too big. An example of the instability in simulating case 3.1,

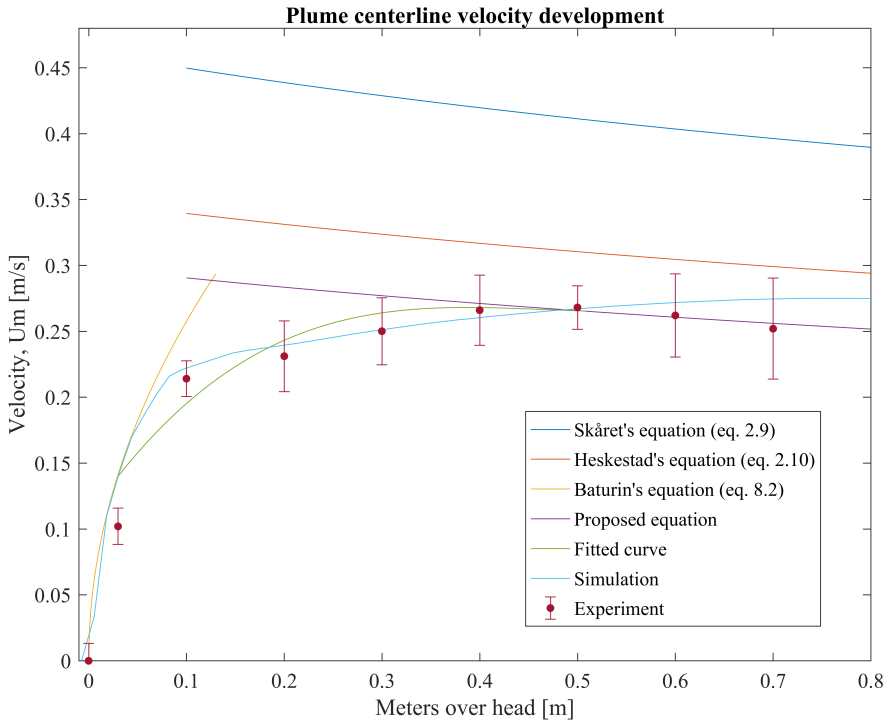


**Figure 8.2:** Plume centerline velocity development for case 2, comparison

can be seen in figure 8.4.

Draught in proximity to the shoulder was, as mentioned, a focus area. In the experiment and in the simulation, the shoulder region was defined at  $y = 1.1$  m. Velocity measurements were taken laterally out from the shoulder, with the first point being 1 cm from the surface, and the next points 5 cm apart. Figure 8.5 displays the velocities measured and simulated at  $y = 1.1$  m next to the shoulders. The high velocities on the left side of the figure is due to the jet. Generally higher simulated velocities were observed here. For case 3.1, the maximum was also slightly skewed from  $x = 0$ . The same goes for the experimental values, however they were skewed the other way, towards the shoulder. This discrepancy is most likely due to the swaying of the experimental jet already mentioned earlier in this chapter.

## 8.2 Limitations of the experimental setup

The manikin was considerably improved from the project work, which can be seen in the conference paper in appendix C. Some parts, however, still had room for improvement. One disappointing element was the piecewise heat foil coverage of the manikin's surface area. The heat

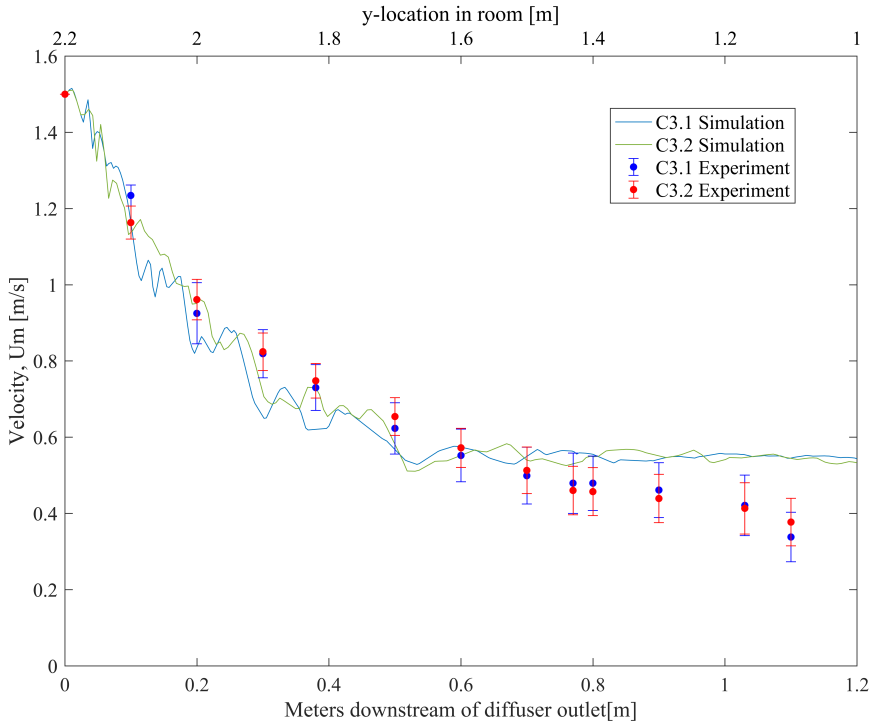


**Figure 8.3:** Jet centerline maximum velocity decay for case 1, comparison

foil did not cover all areas, and its stiff structure did not manage to adapt to the curves of the manikin surface, leading to irregular heating of the manikin. Hence, the light bulb on the inside was crucial to be able to spread the heat evenly. In spite of the internal fan, the air did not pass that much through to the lower body of the manikin due to the strong natural buoyancy of the hot air. Furthermore, a perforated plate separated the upper body and the lower body which the air had to pass through to reach the legs. A higher pressure was therefore required for the flow to achieve a successful spread to the legs. Another unfortunate element was the failure of the upper body heat foil circuit, due to a broken electrical connection somewhere. Fortunately, the upper body was the part of the manikin enjoying most of the heat from the light bulb, and conclusively resulted in achieving the desired surface temperature. The arms, which were part of the upper body circuit, did not have an internal passage to the torso. Only heat foil was meant to heat them. This failed when the upper body heat foil failed. Consequently, the arms did not contribute to the plume flow, which perhaps resulted in a slightly narrower plume. The arm foil's heat output would have been 7.6 W. The skin temperature on the upper body was slightly higher than 32 degrees, especially the parts of the stomach close to the light bulb, which will have covered the heat lost from the arms. It can, for instance, be assumed that the manikin sat with its arms in front of the body with the hands resting on the thighs, which would have resulted in a plume very similar to the measured plume.

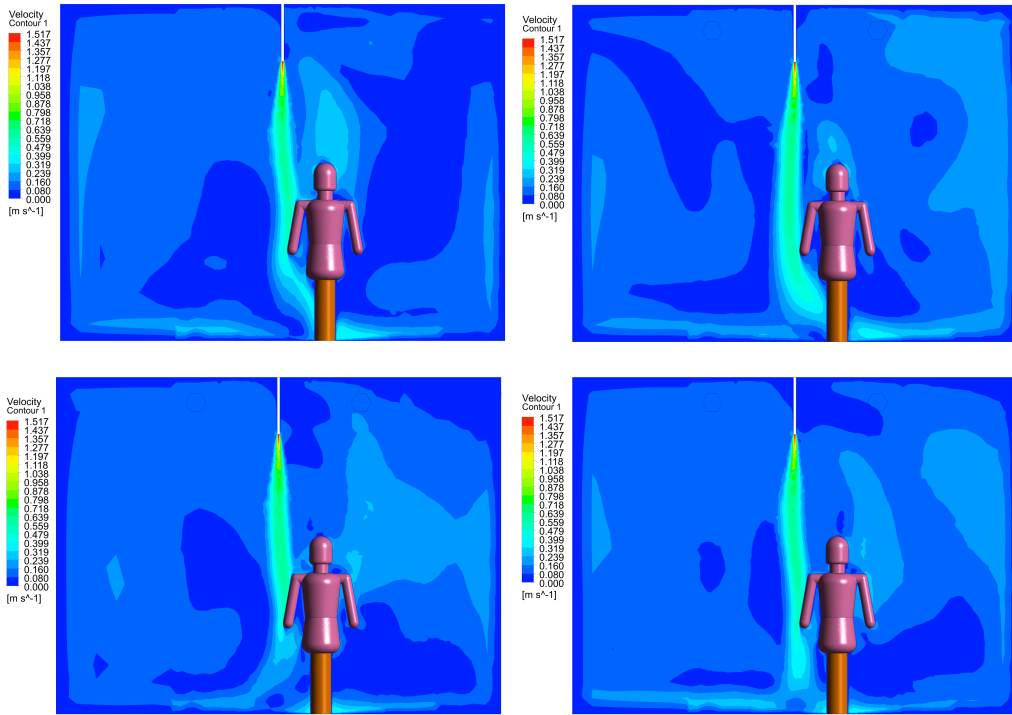


Figure 8.4: Velocity contour for 4 different iterations of case 3.1. The chosen case is at top right

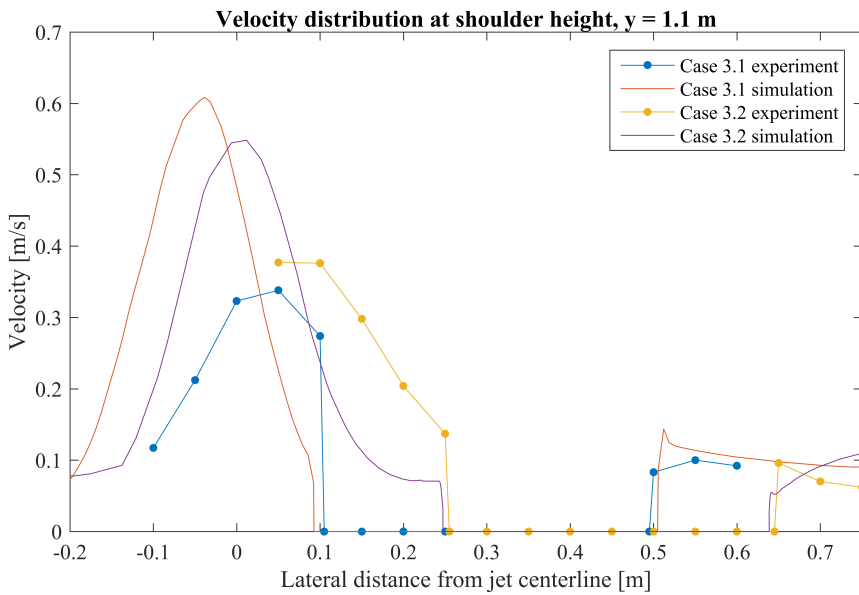


Figure 8.5: Jet centerline maximum velocity decay for case 1, comparison

Other parts that could have been improved, was the use of more anemometers, preferably of the same brand. This improvement would have resulted in less moving of the anemometer stand, and the accuracy of the measurement locations would most likely be better. Also, if a traverse stand had been used, it would have been easier to adjust the anemometers to the correct measuring locations, resulting in the measurement taking being both smoother and swifter. Maintaining an even temperature of 23° in the room was problematic for case 2 and 3, because the thermal manikin kept increasing the room air temperature. Therefore, the room had to be aired now and then. This could have been a source of error for measurements taken just before and just after such an airing, because the temperatures were not necessarily equal.

As thoroughly emphasized in the scientific conference paper based on the project work's results, see appendix C, the anemometers only measured speed and not velocity due to their omnidirectional probe. This made it difficult to know in case 3 in which direction the flow was going, and which flow type, jet or plume, was dominating. This was the main reason CFD was used in this thesis. The vector plots in chapter 7 shows the complex movement of the jet that the omnidirectional probes could not register. To validate the simulation results, however, particle image velocimetry or other experimental methods that can register flow direction should be conducted for the same setup.

### 8.3 Momentum evaluation

One parameter that has not been considered during the experiment, due to its effect being minor for low temperature differences between flows, is momentum. How great or how little the effect momentum had on the flow, however, is briefly reviewed make sure it could be neglected. The plume was hot and had a lower density than the jet flow. This meant that the jet would need less velocity to achieve the same amount of momentum as the plume. This can be shown by the momentum equation:

$$\begin{aligned} M &= \dot{m}_j U_j = \dot{m}_p U_p \\ &= \rho_j A_j U_j^2 = \rho_p A_p U_p^2 \end{aligned} \quad (8.3)$$

Where  $M$  is momentum,  $\dot{m}$  is air mass flow rate,  $\rho$  is density,  $A$  is cross-sectional area and  $U$  is velocity. Subscripts  $j$  and  $p$  stand for jet and plume respectively. To find  $U_j$  for a certain momentum magnitude,  $\rho_p$  had to be found. As the pressure difference between the two flows compared to the ambient pressure was negligible, one could use the assumption of  $\rho_j T_j = \rho_p T_p$  from the ideal gas law.  $T_p$  was also unknown, however, and had to be found first. Skåret (2000) supplied a method for calculating the difference between room temperature and plume temperature,  $\Delta T_m$ , at the plume's centerline for various heights,  $y_p$ , from the plume source. The height chosen to be investigated was  $y = 1.1$  m from the floor, which is at the manikin's shoulder. From the source of the plume, this equaled  $1.2\text{m} - 0.3\text{m} = 0.9$  m because the source was 1.2 m below the head of

the manikin, which was at  $y = 1.4$  m from the floor.

$$\begin{aligned}
 \Delta T_m &= \frac{1.09}{C_b^{\frac{4}{3}} (\rho_r c_p \sqrt{g\beta})^{\frac{2}{3}} (y)^{\frac{5}{3}}} \dot{W}_c^{\frac{2}{3}} \\
 &= \frac{1.09}{0.238^{\frac{4}{3}} (1.2 \cdot 1.005 \sqrt{9.81 \cdot \frac{1}{296}})^{\frac{2}{3}} (0.9)^{\frac{5}{3}}} \\
 &= 3.184^\circ C
 \end{aligned} \tag{8.4}$$

$\Delta T_m$  is equal to  $T_p - T_{room}$ . The rest of the parameters are the same as in equation 2.9. Then, if  $T_{room}$  was 23 °C,  $T_{plume}$  is 26.184 °C at head level.  $\rho_j = 1.192$  kg/m<sup>3</sup> which gave a  $\rho_p = 1.192 \frac{23+273}{26.184+273} = 1.179$  kg/m<sup>3</sup> by the ideal gas assumption. Therefore, the jet velocity needed for the jet momentum to equal the plume's momentum with a plume velocity of 0.138 m/s, being the experimental plume velocity measured just over the shoulder was:

$$\begin{aligned}
 \rho_j A_j U_j^2 &= \rho_p A_p U_p^2 \\
 \Rightarrow U_j &= \sqrt{\frac{1.179}{1.192}} 0.138 = 0.137 \text{ m/s} \\
 \Delta U &= 0.001 \text{ m/s}
 \end{aligned} \tag{8.5}$$

$A_p = A_j$  is assumed to be able to compare the momentum of the flows. Since there was a velocity difference of only 0.001 m/s due to density differences between the jet and the plume, the effect from the jet's additional momentum compared to the plume's, could be concluded to be insignificant in this study.

## 8.4 Draught related discussion

One of the sub-objectives in the thesis was determining a comfort distance to the plane jet. The two draught rate tables in chapters 4 and 7 have been merged to give an overview and a comparison of the results, see table 8.1. The simulation results seems to suggest that the manikin's comfort distance could be shortened. Where the draught rate was assumed to be 10%, the simulation got 4.5%. The same discrepancy was found for the category B criteria of 20%. The experiment, however, got results that coincided very well with the pre-calculated DR-values and velocities. The simulated jet and plume case had issues with jet instabilities and swaying. These issues were most likely due to errors related to the CFD calculations as described in chapter 5.7. For the thesis' simulations, iteration errors would be substantial because the flow was unsteady. The simulations could also have been influenced by model errors from the choice of RNG k- $\epsilon$  turbulence model and discretization errors from the mesh not being constructed correctly. Due to these errors, the uncertainty with the simulated results were greater than for the experimental

results. The experimental values were therefore assumed to be able to confirm the mathematical suggestion of the two comfort distances. The difference between center to center distance and

*Table 8.1: Draught rate at shoulder for case 3.1 and 3.2*

<b>DR desired</b>	<b>CtoC<sup>1</sup> distance</b>	<b>CtoS<sup>2</sup> distance</b>	<b>Calc. velocity</b>	<b>Meas. vel. shoulder</b>	<b>Sim. vel. shoulder</b>	<b>Meas. TU</b>	<b>Sim. TU</b>	<b>Meas. DR</b>	<b>Sim. DR<sup>3</sup></b>
20%	0.34 m	0.14 m	0.278 m/s	0.274 m/s	0.241 m/s	16.17%	9.90%	21.7%	15.9%
10%	0.47 m	0.27 m	0.143 m/s	0.137 m/s	0.082 m/s	25.81%	6.33%	10.7%	4.5%

center to shoulder distance is 20 cm, which is the width of a shoulder. The manikin is measured to be 40 cm across at the shoulders. In a practical aspect, knowing the comfort distance between the jet centerline and the edge of the shoulder could be useful.

The author would recommend the use of a safety factor when recommending a comfort distance to the plane jet. Not only due to the vast interpersonal differences that exist from person to person and amount of clothes worn, but also because the flow is unsteady by nature and might sway to one side or the other also in experimental cases, especially if subjected to disturbances like the opening of a door. This phenomenon was experienced in between measurements when the door to the experimental office was opened. The simulations also showed an unstable jet swaying from side to side, often exposing the shoulder of the manikin to higher velocities than desired. A safety factor of 20% is suggested, which would result in comfort distances of 0.408 m for case 3.1 and 0.564 m for case 3.2. A study on determining this factor, however, should be conducted.

In chapter 2, Fanger (1972) proposes three criteria that together, in most cases, lead to thermal comfort. One of them is related to air velocity, saying that an air velocity below 0.25 m/s should, in addition to the other criteria, fulfill thermal comfort. The comfort criteria of 20% DR was calculated to allow a maximum velocity of 0.278 m/s. It should therefore be expected that Fanger's proposition was valid for the comfort criteria of 20%. A quick calculation of DR for ambient temperature of 23 °C, turbulence intensity of the average of experimental and simulated Tu at the shoulder  $16.17 + 9.9/2 = 13\%$  and average velocity of 0.25 m/s, resulted in a draught rate of 17.6%. This confirms Fanger's proposition for the scenario studied in this master's thesis.

## 8.5 Validity of equations and deduction of comfort distances

Mathematical models are only that - models. They rarely fit a real-life situation perfectly. Usually, the model can describe some parts of the physical behavior better than others. Just like equation 2.3 for jet centerline velocity only fits the jet's main region. Therefore, the model's

<sup>1</sup>Centerline of jet to centerline of manikin

<sup>2</sup>Centerline of jet to shoulder of manikin

<sup>3</sup>10% TU was used in DR-equation where TU-values were lower than 10%

results should not be considered blindly. A good example of this is the draught rate equation, eq. 2.10. It is only valid for  $60\% > Tu > 10\%$  and for  $0.5 \text{ m/s} > v > 0.05 \text{ m/s}$ , according to NS-EN7730 (2005). Unfortunately, some of the simulated results showed values outside the validity limits of the equation.

The deduction of the comfort distances also assumed several aspects, as most models. Firstly, it used the DR-equation for finding the maximum velocities allowed to have a draught rate of 10% and 20%. When using the draught rate equation, a turbulence intensity had to be assumed. 10% was chosen, and proved to be somewhat low after the experimental results had been examined. Luckily, due to lower measured velocities than the calculated velocities at the recommended comfort distances, the desires of 10% and 20% draught rate were still met. The plane jet velocity distribution equation, equation 2.1, could have been used after knowing the maximum DR velocities to find the respective comfort distances. However, equation 2.1 required the knowledge of the edge of the jet. As explained in chapter 4 and 7 when finding the jet spread, the edge  $b = 0.44 \cdot x_{0.5}$ . Unfortunately, the jet's  $x_{0.5}$  was unknown before conducting measurements, and the comfort distances were needed prior to the experiment to know where to place the manikin. Simulation results for the plane jet were used to find the comfort distances. This meant that the manikin's plume was not considered. Before knowing where to place the manikin, the manikin plume's influence on the plane jet would be difficult to deduce. The plane jet's velocity distribution were plotted for  $y = 1.1 \text{ m}$  above ground, which was the shoulder height of the manikin. Figure 8.6 shows how the comfort distances from centerline of jet to shoulder of manikin were found. A MATLAB-script printed the accurate intersection between the velocity distribution curve and the two DR-velocity-curves. To find the distance from centerline of jet to centerline of manikin, 20 cm were added to the comfort distances to yield 0.34 m and 0.47 m for a DR of 20% and 10% respectively.

The comfort distances proved to be verified by the experimental results, due to too high TU values and too low velocities balancing the DR-result. The reason for the velocities at the proposed comfort distances were measured to be slightly lower than the calculated velocities, could be due to the thermal plume of the manikin reducing the velocity magnitude at that height. The plume was not considered during the comfort distance deduction, as mentioned. Despite this, the deduced comfort distances coincided quite well with the experimental results, meaning that the plume could not have had a significant impact on the plane jet flow. The deduction method used seems to function well as a first-guess method of comfort distance for a given draught rate.

## 8.6 Applicability for real life scenarios

The plane jet could be used for protected occupied zone ventilation, POV, mentioned in chapter 2. POV is typically used to divide a room into protected occupied zones. An example of these zones

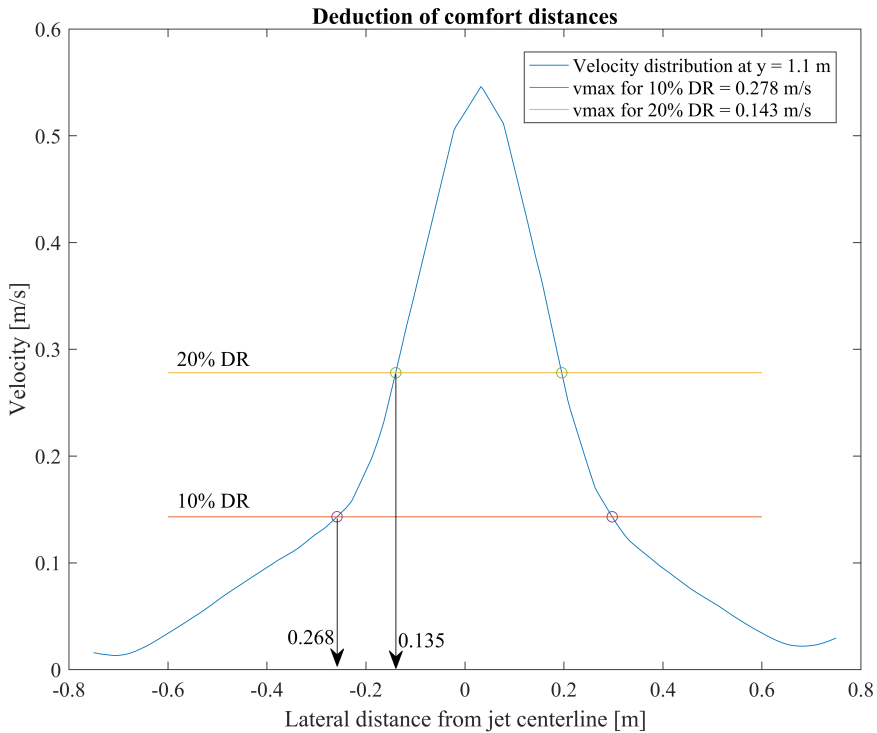


**Figure 8.6:** Deduction of comfort distances for DR = 10% and DR = 20%

can be office booths. The POV can protect the seated occupants from possible contaminated room air, but could cause draught if seated too close to the jet. The occupant in such a booth would most likely sit by a table. Zukowska (2011) found in her PhD studies that in case of a real office scenario where an occupant would sit by a desk, that a distance of 10 cm between the desk and the abdomen would not cause any considerable change in the plume flow from the person. Therefore, the draught study done in this thesis could be applied in this case. Closing the gap, however, resulted in a stronger, more symmetrical and wide plume with a 50% greater volume flux at 0.7 m above the head of the occupant. Using the suggested comfort distance in this scenario, might not be the appropriate comfort distance. More experiments and studies regarding different room setups and their influence on thermal comfort and plane jet should be conducted.

To both avoid draught sensation and improve the local air quality, the author recommends using the POV ventilation together with the comfort distances suggested, if used in a facility with the same indoor conditions as used in this thesis. It could be imagined that the plane jet should not be placed at locations where people frequently move in and out, as they could drag unhealthy air and particles from a contaminated zone to a clean zone. The POV would be best suited, for

instance, in front of a reception desk, studied by an earlier master's student from NTNU (Szopa, 2015), between booths in an office, as mentioned, or at the door to an operating theater.

## 8.7 Further work

The methods used in this master's thesis have room for improvement. This list shows a few things that should be considered if the topic of the thesis is to be further investigated. Recommendations on additional scientific methods to use and other relevant fields of study are also included.

- Use real honeycomb instead of straws in the diffuser outlet.
- Use a second perforated plate in the diffuser. If that is not good enough, have smaller pieces of plexi-glass on top of one of the plates to slow down the high-flow areas.
- Have an air cooler available in the lab to quicker adjust the ambient air temperature to the desired temperature before doing measurements.
- Use a thermal manikin with evenly distributed heat foils covering the entire surface area. Preferably, use a proper thermal manikin made for studying thermal comfort.
- Use a traverse stand for the anemometers. Also, more anemometers would speed up the experiment sessions and reduce the necessary reallocation of the anemometer stand.
- Use a more accurate velocity measurement technique that also measures direction. Like Particle Image Velocimetry, Lazer Doppler Velocimetry or ultrasonic anemometers (Licina et al., 2015).
- Measure plane jet influence on human thermal plume from a non-isothermal plane jet.
- Study on how different room setups can influence thermal comfort and plane jet.
- Deduce a new correlation for centerline velocity development for the human plume.
- Deduce mathematical models for the plume and jet interaction studied in case 3.
- Deduce comfort distances to the jet for other plane jet velocities than 1.5 m/s.
- Measure particle spread and protection efficiency by the use of a thermal manikin next to a plane jet.
- Use real human subjects during experiment and compare to thermal manikin results.
- Record human thermal plume and plane jet flow with thermal camera to visualize the cooling of the human thermal plume.
- If using CFD, test different turbulence models for all three cases to find which model captures the physics the best by verifying against experimental results.
- Do a transient simulation of the human plume and the human plume vs. plane jet flow.

## Conclusion

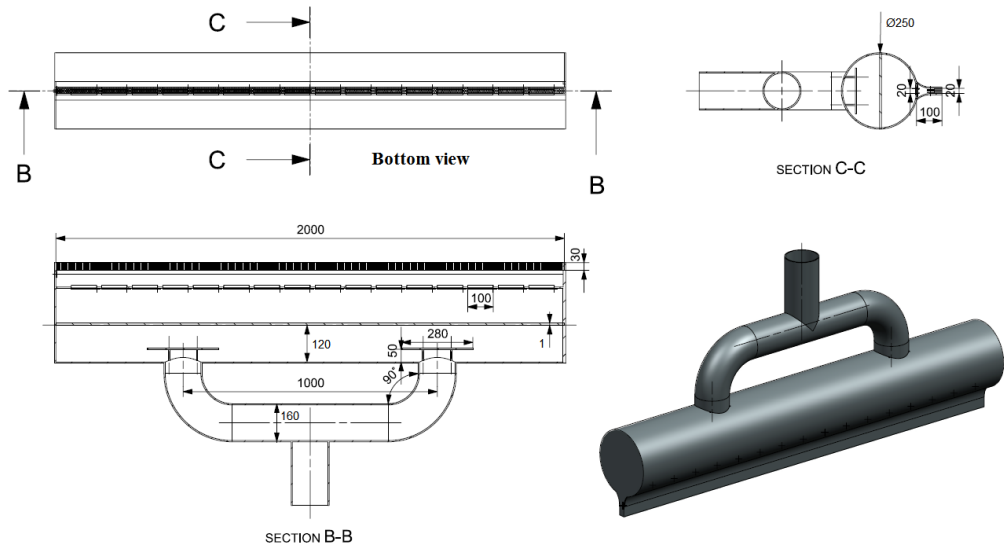
This master's thesis has numerically and experimentally investigated the airflow distribution in close proximity to the human body with a downward plane jet. The thesis has studied three main cases. The first case investigated the plane jet, the second case investigated the thermal plume from a sedentary, seated thermal manikin, and the third case investigated the interaction between the downward plane jet and the thermal manikin's plume at two different manikin positions next to the jet. The thesis has also determined plausible comfort distances of a seated thermal manikin to a plane jet where uncomfortable draught is avoided. Two comfort criteria for draught have been investigated. The first criteria regarded 20% draught rate, categorized as category B by NS-EN7730 (2005). This criteria is usually applied to new buildings used by normal, healthy occupants. A comfort distance of 0.14 m was found, and was the distance between the plane jet's centerline and the occupant's nearest shoulder. The second criteria regarded 10% draught rate, categorized as category A by NS-EN7730 (2005). This criteria is mostly used in buildings or rooms with sensitive and fragile occupants, like the young and the elderly. A comfort distance was in this case found to be 0.27 m between the centerline of the jet to the shoulder of the occupant. An ambient temperature of 23°C and an isothermal plane jet with an outlet velocity of 1.5 m/s, and outlet at a height 0.8 m above the head of the manikin, was assumed. These were the experimental and numerical conditions considered during the thesis. The experimental measurements of draught rate proved to agree well with the desired draught rates of 20% and 10% at the proposed comfort distances. The comfort distances were therefore assumed to be verified for the situation studied. The simulation underestimated the draught rates at the comfort distances getting values of 15.9% and 4.5%.

Generally, the results from the simulations agreed well with the experiments. The uncertainties were high for the simulations, due to the unsteady flows being simulated. Achieving a steady state solution, especially for case 3, was not possible. The asset with using CFD was its ability to produce vector plots for the three cases to visualize flow directions, which were impossible

with the omnidirectional anemometers used in the experiments. This also meant that the flow patterns produced with CFD could not be experimentally verified at the time. The comparison of the mathematical models to the experimental and numerical results showed agreement only in some areas, mainly due to the validity limits of the models not covering the entire flow regions being studied.

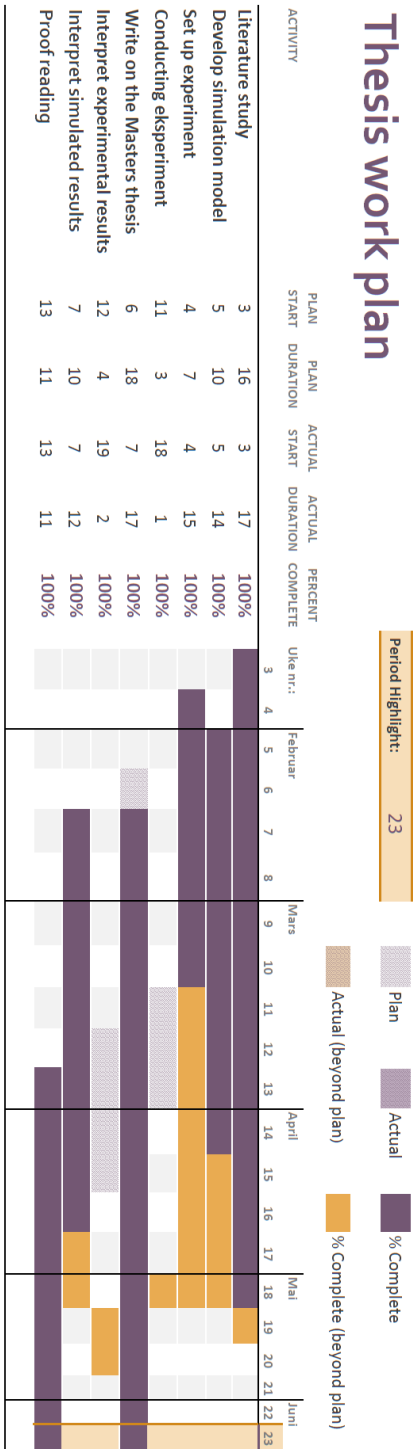
To verify the results from the experiments and simulations, more experiments should be conducted. High accuracy and measurement precision are necessary to produce reliable experimental results. Despite the uncertainty in the numerical and experimental results, the outcome of this study can still be useful in both a practical and a theoretical aspect. The thesis recommends comfort distances from an occupant to a plane jet for different comfort criteria, which can benefit the protected occupied zone ventilation business. By having a well-functioning POV system, the health and productivity of occupants can be improved, as it contributes to restrict the spread of epidemic respiratory diseases and harmful pollution. Additionally, the results presented in this thesis can hopefully be utilized in several other applications, as studies of the human thermal plume and the plane jet were also conducted.

## Appendix A: Technical drawing, diffuser



**Note:** The drawing was made for the diffuser used in the project work. The same diffuser was used in the master's thesis, however the t-pipe was turned  $90^\circ$  to increase the distance from the diffuser to the floor.

# Appendix B: Gantt chart



## **Appendix C: Conference paper**

See next page



## **Experimental Study of the Airflow Distribution Close to the Human Body with a Downward Plane Jet**

Marie Steffensen<sup>1\*</sup>, Amar Aganovic<sup>1</sup>, Guangyu Cao<sup>1</sup>

<sup>1</sup>Norwegian University of Science and Technology (NTNU), Trondheim, Norway

\*Corresponding email: [marie2steff@gmail.com](mailto:marie2steff@gmail.com)

### **SUMMARY**

The objective of the study is to investigate the effect of a downward plane isothermal air jet on an occupant's thermal comfort by conducting experimental measurements and employing a mathematical model. The study investigates two interacting and opposing flows - the thermal plume generated by a thermal manikin and a downward plane jet discharged from a plane diffuser at 1.5 m/s. A thermal comfort criterion of a draught rate of 10% at the closest comfort distance (CCD) to the jet's centerline was used. A corresponding distance of 0.134 m was found by using the measured air velocity, the respective turbulence intensity and the air temperature above the head of the manikin. The results from this study can contribute to a plausible suggestion where to place a plane jet if the jet may be used as a ventilation solution, like a personalized ventilation system, or in a protected occupied zone ventilation system.

### **KEYWORDS**

*Thermal comfort, draught, thermal plume, indoor climate, isothermal plane jet*

### **1 INTRODUCTION**

This study focuses on a ventilation solution, namely an isothermal plane jet, serving as a blocking mechanism of pollutant movement. The downward plane jet is discharged from a ceiling-mounted slot diffuser, and can be used in hospitals to shield staff and visitors from sick patients e.g. in waiting rooms, receptions or entrances to operating rooms. It can also be used as a shielding mechanism for workers in an open plan office. The plane jet can be placed between booths to hinder cross-contamination of harmful airborne particles emitted from other co-workers or indoor processes, as Cao et al. (2014) has investigated. The indoor climatic parameters thermal comfort and the spread of airborne pollution, are especially relevant in this study. Due to a limited time frame however, only the matters regarding thermal comfort has been considered at this time. One important thermal comfort parameter, that is the main focus in the study, is to avoid draught due to the plane jet. Draught is an indoor situation that gives local thermal discomfort, and is usually referred to as unwanted local convective cooling of a person. In heated or cooled buildings and transport vehicles, it is one of the most frequent causes of complaint (Awbi, 2003). Therefore, draught can be considered as an important factor to have eliminated from an indoor situation. One of the research questions posed in this study is: "How close to the plane jet can a person be without feeling draught?". To be able to answer this question, both an experimental situation and a mathematical model were developed and

compared. The experiment included a plane jet diffuser, issuing an isothermal plane jet at 1.5 m/s and a thermal manikin, producing a hot thermal plume. The draught supposedly felt by the thermal manikin when situated below and from the side to the jet was estimated by the use of the draught rate-parameter (DR) from the International Standard ISO 7730 (ISO7730, 2005). To calculate the draught rate for a given location, the velocity, turbulence intensity and room temperature were assessed during the experiment. Thereafter, the mathematical model was compared to the experimental results.

## 2 MATERIALS/METHODS

Both a mathematical model and an empirical model were developed during this study. Due to complex flows and the inability to express the explicit flow movement, mathematical simplifications have been used in the mathematical model. For instance, the detailed structure of the vortices that occur as the air jet hits the manikin's thermal plume were not considered. The mathematical model therefore only gave a pinpoint on which velocities to expect when measuring the flow around the manikin during the experiment.

### Mathematical model

The model consists of equations for velocity distributions both for the jet and the plume, centerline velocity development, also for the jet and the plume, turbulence intensity calculation, draught rate calculation, and an estimate of the distance between the manikin's shoulder and the jet's centerline that will yield 10 % draught rate or less - the closest comfort distance (CCD). Several equations for each parameter were examined, and the most relevant ones were chosen. According to Skåret (2000), the velocity distribution for both the plane jet and the plume can be approximated by a common equation by Abramovich (1963):

$$\frac{U}{U_m} = \left(1 - \left(\frac{x}{b}\right)^{1.5}\right)^2 \quad (1)$$

Where  $U$  is the velocity at a certain distance  $x$  from the centerline,  $U_m$  is the velocity at the centerline, the maximum velocity for a given  $y$ -value downstream of the nozzle, and  $b$  is the horizontal distance from the centerline to the jet's outer edge. The  $y$ -value is defined as the distance downstream from the outlet, plus  $y_p$ , the distance from the source of the jet to the outlet.

For the centerline velocity development for a plane free isothermal jet, an equation given by Skåret (2000) was used:

$$\frac{U_m}{U_0} = \sqrt{\frac{h_0 \rho_0 i}{y \rho_r \varepsilon I_4 2 \tan \alpha}} = K \sqrt{\frac{h_0}{y}} \quad (2)$$

Where  $h_0$  is the width of the diffuser opening,  $y$  is the distance in the  $y$ -direction from the source of the jet,  $\rho_0$  is the air density at the nozzle outlet,  $\rho_r$  is the air density of the ambient room air,  $\varepsilon$  is the contraction coefficient,  $I_4$  is a constant related to the free plane jet equal to 0.316,  $i$  is a coefficient related to eventual impact losses the jet might experience at the outlet and  $\alpha$  is the spread angle of the jet from the centerline, here  $12.5^\circ$ . In this study, the  $K$  for a free plane jet was found to be 2.69. In other studies, Gutmark (1976) has found  $K$  to yield 2.43, while Skistad (1995) and Awbi (2003) used a  $K$  equal to 2.7 and 2.67 respectively.

The underlining criterion from which the different thermal comfort conditions were based upon, is the draught rate equation from ISO7730 (2005):

$$DR = (34 - t_{a,l})(\bar{v}_{a,l} - 0.05)^{0.62} (0.37 \bar{v}_{a,l} Tu + 3.14) \quad (3)$$

Where  $t_{a,l}$  is the local air temperature between 20 °C and 26 °C,  $\bar{v}_{a,l}$  is the local mean air velocity < 0.5 m/s,  $Tu$  is the local turbulence intensity [%] between 10% and 60%, if unknown, 40% may be used. The equation is valid for people with sedentary activity, 1.2 MET = 70 W/m<sup>2</sup>, which is the assumed activity level of the manikin. The DR-equation relates to a draught sensation typically felt at the neck. To satisfy the comfort criteria of 10% DR, the closest comfort distance (CCD) was specified. The CCD is assumed to reach from the manikin's shoulder to the jet's centerline. Calculating the CCD was done by determining the velocity,  $\bar{v}_{a,l}$ <sup>1</sup> from equation 3 by trial and error with input settings of DR = 10 %,  $t_{a,l}$  = 22 °C and  $Tu$  for a desired area. Sequentially, the CCD was found by reorganizing equation 1.

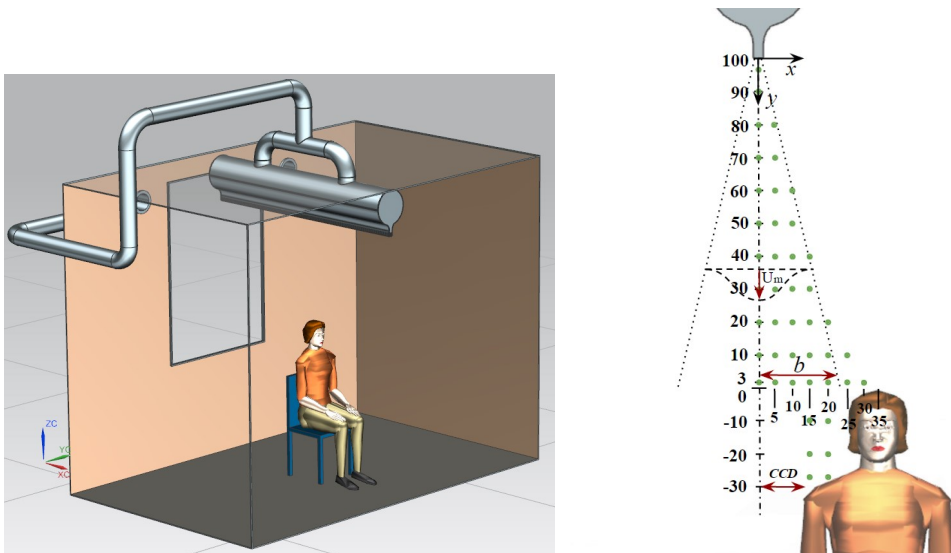


Figure 1: Facility layout (left). Measuring layout with dots representing the measuring points (right)

### Experimental setup

The experimental facility resembled an office space with dimensions 3.50 m · 2.50 m · 2.65 m (l·w·h), and was located in a laboratory at Norwegian University of Science and Technology. A diffuser supplying a plane jet was made on beforehand and placed as seen in Figure 1 (left). A layout of the measured locations can also be seen in Figure 1 (right). The manikin's position in the figure is one of several positions the manikin had during the process of finding the CCD. The diffuser's nozzle outlet was made to have dimensions 0.02 m · 2.0 m, and the diffuser body to have a diameter of 250 mm. The diffuser was made such that the jet being issued at 1.5 m/s had an even velocity, ± 0.1 m/s, throughout the length of the nozzle. Several elements were implemented, amongst a perforated plate with Ø4 mm holes and a solidity ratio of 54% placed along the middle of the diffuser duct, diffusing the passing air. A honeycomb pattern at the nozzle outlet contributed to a low turbulence jet, increasing the accuracy of the velocity measurements taken during the experiment. A sectioned view of the diffuser can be

<sup>1</sup> The  $\bar{v}_{a,l}$  found was used as U in equation 1 in the following step.

seen in Figure 2 (right). A thermal manikin was made with an internal 100W light bulb, and dressed in a clothing level equal to 1 *clo*. See figure 2 (left). The room temperature was kept at  $22 \pm 0.1$  °C with no significant thermal stratification. To keep the room balanced, a couple exhaust fans were installed at one wall to extract the same amount of air being supplied by the diffuser,  $216 \text{ m}^3/\text{h}$ . All measuring instruments used were either calibrated before use or by their manufacturer.

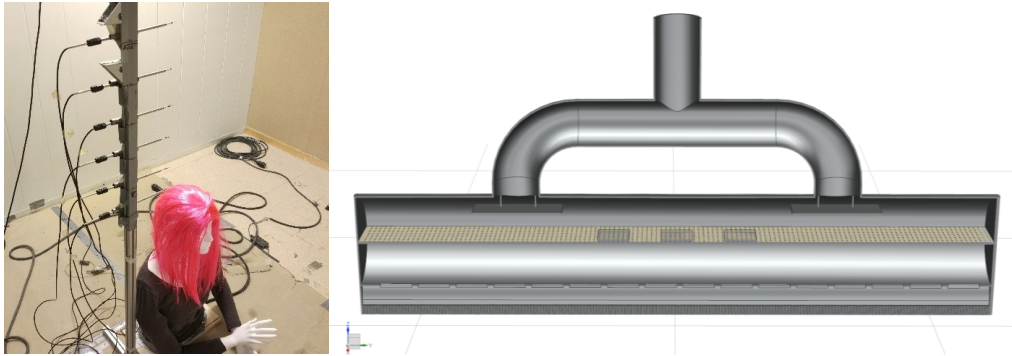


Figure 2: Measuring-setup in the lab (left). 3D-model of the diffuser design, sectioned view (right)

The experiment investigated the jet's velocities separate from the manikin's plume velocities, before conducting measurements of the impinging flows' (jet VS. plume) velocities. The separate tests of the jet flow and the plume flow served as reference scenarios, and were used for comparison to the impinging flows scenario (jet VS. plume).

### 3 RESULTS AND DISCUSSION

The results from the measurements of the downward jet flow's centerline velocity agree well with the mathematical model's equation 2, with an  $R^2$ -value of 0.92, indicating that the model were appropriate for the experiment. As equation 2 has been validated extensively by others (Cao et al., 2014, Skistad, 1995, Awbi, 2003), it also suggests that the diffuser functioned as designed. Table 1 shows that the rising plume decreased the velocity of the downward jet when comparing the jet flow scenario to the impinging flow scenario. At the head of the manikin, at  $y = 1.0$  m, the jet's centerline velocity decreased from 0.511 to 0.444 m/s. Another parameter in table 1 worth noting, is the turbulence intensity. The turbulence intensity used for the pre-experiment mathematical model was 40% as recommended by ISO7730 (2005) for unknown turbulence intensities.

Table 1: Comparison of parameters from mathematical model, jet flow and jet + plume flow at  $y = 1.0\text{m}$

	$U_m$ [m/s]	$Tu$ [%]	$DR$ [%]	CCD	$U_{max}$ for $DR \leq 10\%$
Math. model	0.56	40	77.1	0.154	0.11
Jet flow	$0.511 \pm 0.002$	2.48 (<10)	37.3	0.141	0.142
Impinging flows (Jet VS. plume)	$0.444 \pm 0.002$	12.6	34.7	0.134	0.138

After conducting experiments, the measured turbulence intensities were found to be much lower than the assumed 40%. Consequently, the calculated  $DR$  at the jet's centerline was drastically reduced from 77.1%, but not to a satisfactory level from a thermal comfort perspective, as both 37.3% and 34.7% > 10%. This only meant that even with the lower turbulence intensities, the manikin would still supposedly feel uncomfortable if placed directly below the plane jet diffuser. However, it is worth mentioning that humans typically are more sensitive to draught

from below to the head and draught on the back of the neck, which are the types considered by the  $DR$ -equation, than draught downward on the head, as is the case in this study, or draught towards the face (Awbi, 2003).

The decrease in  $DR$ , as seen in table 1, led to a reduction in the manikin's minimum distance to the jet, the  $CCD$ , from 0.154 m to 0.141 m and an increase in the maximum allowed velocity from 0.11 m/s to 0.142 m/s when not considering the plume's interference. The jet flow also proved to have the lowest turbulence intensity of 2.48%. When considering the plume together with the jet flow, the turbulence intensity was measured to be substantially higher, 12.6%, as the impinging flows were opposing each other. Despite a higher turbulence intensity, the reduction in the velocity at the head,  $U_m$ , from 0.511 m/s to 0.444 m/s resulted in a reduction in the  $DR$  below the jet's centerline to 34.7%, the  $CCD$  to 0.134 m and  $U_{max}$  to 0.138 m/s. It is worth noting that the comfort criterion of 10%  $DR$  is valid for a category A building, where the indoor climate situation is suitable for sensitive people, old people and children (ISO7730, 2005). It can also be used for clean rooms. In other words, a climatic situation suitable for literally all types of people. For a normal indoor climate, category B, ISO7730 (2005) recommends a maximum of 20%  $DR$ .

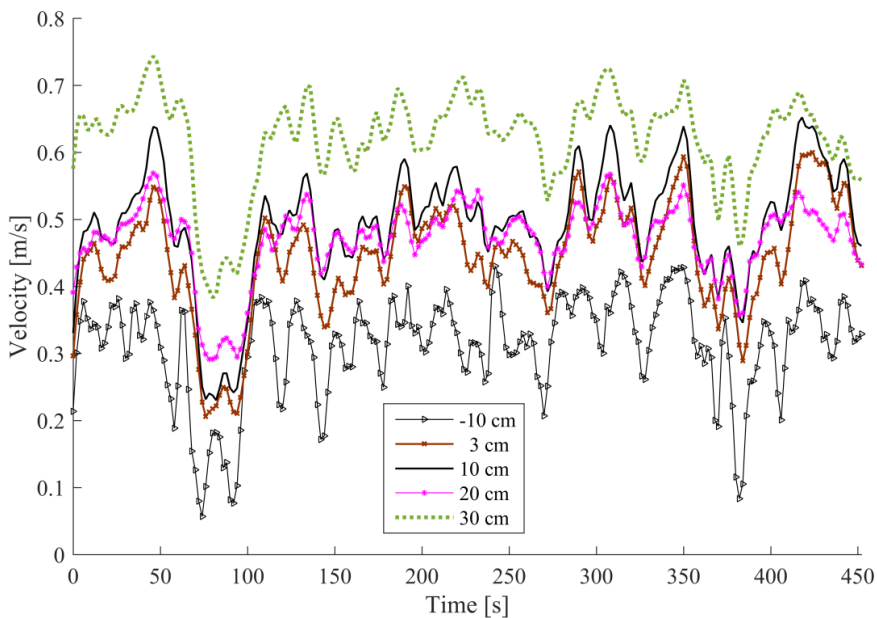


Figure 3: Impinging airflows (jet VS. plume) measured with the manikin below the jet's centerline over the course of 8 minutes, -10 to 30 cm above the head

An overall view of the velocity fluctuation of the impinging flows (jet VS. plume) can be seen in Figure 3. Velocities at 5 different heights over the manikin's head have been recorded over the course of 8 minutes. In this scenario, the manikin was sitting directly below the jet's centerline. From the graph, it looks like the jet is covering the plume like a lid until the plume has built up enough pressure to break through the jet flow. This would explain the infrequent dips in the graphs that affects the flow at all heights. In the dips, the velocity is sharply reduced, indicating that a strong upward flow is slowing the jet down. More research should be conducted to better capture this unsteady, complex flow scenario.

#### 4. PRACTICAL LIMITATIONS

The thermal plume generated by the thermal manikin, deviated somewhat from its mathematical model. This was caused by the unevenness of the manikin's surface temperature. As the light bulb was positioned inside the stomach, and only a narrow passage through the manikin's neck linked its inner upper body and its inner head, only a limited amount of hot air passed through to the inside of the head. Consequentially, the head was around 10 degrees lower on the surface than the upper body. The thermal plume created by the thermal manikin was therefore somewhat erroneous, and this could be seen when comparing the measured plume velocities to the calculated velocities. The peak velocity was, for instance, expected to be found above the head of the manikin, as in the mathematical model, but it was found over the shoulders instead during the experiment. The slightly erroneous thermal plume was still useful in the study of the impinging flows. A factor that made the deduction work of the flow movement hard, was the lack of knowing the flow direction of the measured velocities. The measuring equipment only measured the velocity magnitude, as an omnidirectional hot-wire anemometer was used. This is partly why the jet flow and the plume flow were measured separately at first, so that they could serve as reference scenarios when processing the impinging flows' measurement data.

#### 5 CONCLUSIONS

The influence of the thermal plume on the downward plane jet is seemingly important for an occupant's thermal comfort when residing close to the jet. However, many factors play important roles in determining whether thermal comfort is achieved or not. For a sedentary, sitting occupant, draught might be the most disturbing sensation caused by a downward, isothermal plane jet. With a discharge velocity of 1.5 m/s from a plane diffuser, an occupant 1.0 m below the slot opening should be able to sit 0.134 m away from the centerline of the jet, without feeling thermally uncomfortable due to draught. The experiment could be improved further to better characterize this comfort distance. By having an evenly heated manikin and utilizing more advanced measurement equipment, the experiment would more precisely be able to capture the complex flow pattern of the impinging jet and plume flow. Also, measuring of the spread of indoor pollutants, like particulate matters, would be a natural way forward, as the plane jet may be able to prevent the transmission of indoor pollutants from one area to another.

#### 6 REFERENCES

- ABRAMOVICH, G. N. 1963. *The Theory of Turbulent Jets*, The M.I.T press, The Massachusetts Institute of Technology, Cambridge Massachusetts.
- AWBI, H. B. 2003. *Ventilation of Buildings*, Taylor and Francis.
- CAO, G., SIRÉN, K. & KILPELÄINEN, S. 2014. Modelling and experimental study of performance of the protected occupied zone ventilation. *Energy and Buildings*, 68, Part A, 515-531.
- GUTMARK, E. A. W., I. 1976. The planar turbulent jet. *Journal of Fluid Mechanics*, 73, pp. 465-495.
- ISO7730 2005. International Standard ISO 7730:2005. *Ergonomics of the thermal environment - Analytical determination and interpretation of thermal comfort using calculation of the PMV and PPD indices and local thermal comfort criteria*. 3 ed.: The International Organization for Standardization.
- SKÅRET, E. 2000. *Ventilasjonsteknisk håndbok*, Norges byggforskningsinstitutt.
- SKISTAD, H. 1995. *RE: Industriventilasjon, Heft 1: Innblåsning og avsug*.

## Appendix D: Additional experimental results

Processing of the experimental data was very time consuming. Especially preparing the data to use in the contour plots took a long time, because the plots were constructed from all the measured values. The values in each location had to be extracted and averaged from 44 and 51 different excel-files each with loggings of 5 locations and 3 locations from the new anemometers (AirDistSys) and the old anemometers (TSI) respectively. The contour plot for case 1 alone consisted of 319 average velocity values, which had to be manually inserted into a txt.-file for the MATLAB script to read. When making contour plots of turbulence intensities as well, the same process had to be repeated for TU-values. Contour-plot of experimental turbulence intensities were only made for case 1. If more time had been available, plots for case 2 and 3 could also have been constructed. The figure on the next page displays the turbulence intensities for case 1. Roughly 2/3 of the figure is covered by measurements from the AirDistSys anemometers, which sampled velocity 8 times every second. Every 2 second, a velocity average of the 16 samples was logged and standard deviation, turbulence intensity and draught rate was calculated. Totally 300 velocity values were logged at each location during 10 minutes. These average values were then averaged again to get one velocity and turbulence intensity value at each location. This process was done for all locations. The last 1/3 of the figure covering the right side, were measured by the TSI anemometers. 20 velocity samples were averaged every second and logged. These anemometers however, did not calculate the turbulence intensity per logging as the AirDistSys, which meant that TU had to be manually calculated from the velocity loggings. After obtaining all the TU-values, a contour plot could be constructed. Because the contours only shows averages of averages, the contours should be viewed critically. It can be seen in Figure ?? that there is low turbulence intensity in the middle of the jet, as expected. However at the boundaries, there are higher TU spread seemingly random, except near the ceiling. The author can see no apparent reason for why some areas have such a high turbulence intensities other than random air movement from entraining air, or disturbances in the flow from the exhaust fans. The author can also have made mistakes during calculations.

Table A1 shows measured parameters for case 1, the jet, at the centerline. Unfortunately, as explained, there was only time to process the first case.

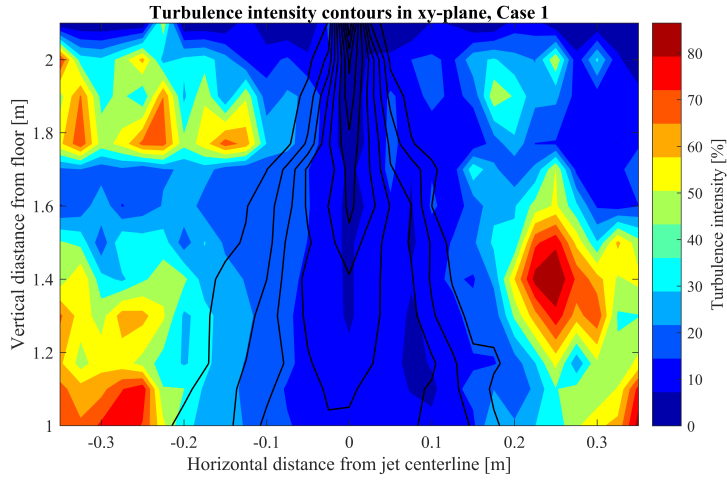


*Table A1: Parameters of interest for the jet flow, case 1*

Height, $y$ [m]	Mean velocity [m/s]	SD [m/s]	Turbulence intensity [%]	Draught rate [%]
2.1	1.180	0.0131 (1.1%)	1.112	89.06
2.0	0.877	0.0354 (4.0%)	4.039	61.03
1.9	0.829	0.0366 (4.4%)	4.410	58.49
1.82	0.719	0.0446 (6.2%)	6.209	49.73
1.7	0.686	0.0511 (7.4%)	7.493	45.59
1.6	0.663	0.0441 (6.7%)	6.666	42.10
1.5	0.622	0.0485 (7.8%)	7.831	41.37
1.4	0.523	0.0421 (8.0%)	8.060	34.96
1.3	0.509	0.0406 (8.0%)	8.007	33.90
1.17	0.482	0.0467 (9.7%)	9.737	32.19
1.1	0.444	0.0385 (8.7%)	8.675	29.53
1.0	0.412	0.0441 (10.7%)	10.773	28.02

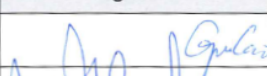
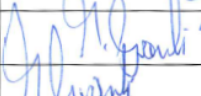
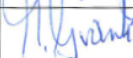
## Risk Assessment Report

### Klimarom VVSLab Diffuser experiment with air curtain

Prosjektnavn	Experimental study of the airflow distribution in close proximity to the human body with a downward plane jet
Apparatur	Klimarom VVSLab - Diffuser experiment with air curtain
Enhet	NTNU
Apparaturansvarlig	Guangyu Cao
Prosjektleder	Guangyu Cao
HMS-koordinator	Morten Grønli
HMS-ansvarlig (linjeleder)	Olav Bolland
Plassering	Klimarom, Varmetekniske laboratorier
Romnummer	C247C, 2. etg i klimalab, Varmetekniske laboratorier
Risikovurdering utført av	Marie Steffensen

#### Approval:

Apparatur kort (UNIT CARD) valid for:	9 måneder
Forsøk pågår kort (EXPERIMENT IN PROGRESS) valid for:	9 måneder

Rolle	Navn	Dato	Signatur
Prosjektleder	Guangyu Cao	18.11.2016	
HMS koordinator	Morten Grønli	18.11.-2016	
HMS ansvarlig (linjeleder)	Olav Bolland		

---

## TABLE OF CONTENTS

1	INTRODUCTION .....	1
2	ORGANISATION .....	1
3	RISK MANAGEMENT IN THE PROJECT .....	1
4	DESCRIPTIONS OF EXPERIMENTAL SETUP.....	2
5	EVACUATION FROM THE EXPERIMENTAL AREA .....	3
6	WARNING .....	3
6.1	Before experiments.....	3
6.2	Abnormal situation.....	3
7	ASSESSMENT OF TECHNICAL SAFETY .....	4
7.1	HAZOP.....	4
7.2	Flammable, reactive and pressurized substances and gas .....	4
7.3	Pressurized equipment.....	4
7.4	Effects on the environment (emissions, noise, temperature, vibration, smell) .....	4
7.5	Radiation .....	5
7.6	Chemicals.....	5
7.7	Electricity safety (deviations from the norms/standards) .....	5
8	ASSESSMENT OF OPERATIONAL SAFETY .....	5
8.1	Procedure HAZOP .....	5
8.2	Operation procedure and emergency shutdown procedure.....	5
8.3	Training of operators.....	6
8.4	Technical modifications.....	6
8.5	Personal protective equipment.....	6
8.6	General Safety .....	6
8.7	Safety equipment .....	6
8.8	Special predations .....	6
9	QUANTIFYING OF RISK - RISK MATRIX.....	6
10	REGULATIONS AND GUIDELINES .....	7
11	DOCUMENTATION.....	7

## 1 INTRODUCTION

This experiments purpose is to investigate the interaction between an air curtain in a room and the thermal plume rising from an occupant sitting either below the curtain or to the side from it. The experiment will be conducted in the middle of the small office in the Klimalab.

The experiment will be conducted in several steps:

- **Presetting** of the air curtain nozzle by measuring the velocity at the outlet to be sure there is an even outflow. Adjust the fan to get the desired value for the flow velocity. **Calibrating** the anemometers and the thermal manikin.
- Placing the thermal manikin at three assigned locations relative to the diffuser – below, right next to and a bit further to the one side. **Carry out the experiment** by positioning the anemometers and thermometers for each of the manikin positions.

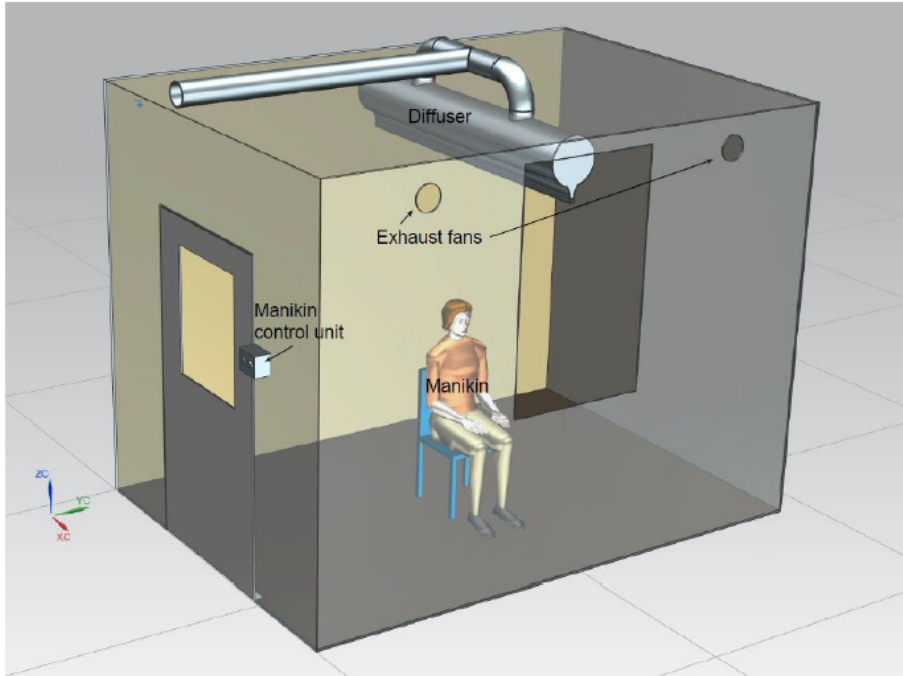
## 2 ORGANISATION

Rolle	
Prosjektleder	Guangyu Cao
Apparaturansvarlig	Guangyu Cao
Romansvarlig	Lars Konrad Sørensen
HMS koordinator	Morten Grønli
HMS ansvarlig (linjeleder):	Olav Bolland

## 3 RISK MANAGEMENT IN THE PROJECT

Hovedaktiviteter risikostyring	Nødvendige tiltak, dokumentasjon	DATE
Prosjekt initiering	Prosjekt initiering mal	11.10.16
Veiledningsmøte Guidance Meeting	Skjema for Veiledningsmøte med pre-risikovurdering	11.10.16
Innledende risikovurdering Initial Assessment	Fareidentifikasjon – HAZID Skjema grovanalyse	11.10.16
Vurdering av teknisk sikkerhet Evaluation of technical security	Prosess-HAZOP Tekniske dokumentasjoner	11.10.16
Vurdering av operasjonell sikkerhet Evaluation of operational safety	Prosedyre-HAZOP Opplæringsplan for operatører	
Sluttvurdering, kvalitetssikring Final assessment, quality assurance	Uavhengig kontroll Utstedelse av apparaturkort Utstedelse av forsøk pågår kort	

## 4 DESCRIPTIONS OF EXPERIMENTAL SETUP



Location of the room, is the little room inside the KlimaLab at VAT laboratories, 2<sup>nd</sup> floor.

The experimental setup will be like the figure above. There will be measurements of the airflow distribution close to the manikin, and temperature in the room. Airflow measurements will be done by the use of omnidirectional anemometers. Air will enter the room by the plane diffuser, and get extracted by the exhaust fans on the back wall. The manikin will be fitted with heat foil which covers its surface to better simulate a real human. The heat foils can be controlled with dimmers. The foils are using 230V current, and as long as they are plugged in as there is a risk of shock if the heat foil panels are not properly insulated or if there is a cut in the foil that can expose the metal. Therefore, safety measures are necessary to comply with safety regulations. A switch on the door to the little room will shut off the current when someone enters the room. The heat foils will be connected to a control unit with an on/off switch and a fuse in case of short-circuiting. To get the correct heat output, the previously used light bulb inside the manikin will also be used. This light bulb is controlled by a Variac-unit where the input voltage can be adjusted.

Instrumentation to be used:

- Thermometer
- Anemometers
- Pre-made diffuser

- Fan controlling the volume flow out of the diffuser
- Exhaust fan x2
- Heated manikin, heat foil and light bulb, at approx. 50+50 W
  - Manikin foil control unit with switch and fuse.
- Smoke machine for flow visualization

## 5 EVACUATION FROM THE EXPERIMENTAL AREA

Evacuate at signal from the alarm system or local gas alarms with its own local alert with sound and light outside the room in question, see 6.2

Evacuation from the rigging area takes place through the marked emergency exits to the assembly point, (corner of Old Chemistry Kjelhuset or parking 1a-b.)

### Action on rig before evacuation:

In case of evacuation, the fans and the thermal manikin should be shut down and unplugged. The measurements stop.

## 6 WARNING

### 6.1 Before experiments

Send an e-mail with information about the planned experiment to:

[iept-experiments@ivt.ntnu.no](mailto:iept-experiments@ivt.ntnu.no)

#### The e-mail must include the following information:

- Name of responsible person:
- Experimental setup/rig:
- Start Experiments: (date and time)
- Stop Experiments: (date and time)

You must get the approval back from the laboratory management before start up. All running experiments are notified in the activity calendar for the lab to be sure they are coordinated with other activity.

### 6.2 Abnormal situation

#### FIRE

If you are NOT able to extinguish the fire, activate the nearest fire alarm and evacuate area.

Be then available for fire brigade and building caretaker to detect fire place.

If possible, notify:

NTNU	SINTEF
Morten Grønli, Mob: 918 97 515	Harald Mæhlum, Mob: 930 14 986
Olav Bolland: Mob: 918 97 209	Petter Røkke, Mob: 901 20 221
NTNU – SINTEF Beredskapstelefon	800 80 388

#### GAS ALARM

If a gas alarm occurs, close gas bottles immediately and ventilate the area. If the level of the gas concentration does not decrease within a reasonable time, activate the fire alarm and

evacuate the lab. Designated personnel or fire department checks the leak to determine whether it is possible to seal the leak and ventilate the area in a responsible manner.

Alert Order is in the above paragraph.

#### **PERSONAL INJURY**

- First aid kit in the fire / first aid stations
- Shout for help
- Start life-saving first aid
- **CALL 113** if there is any doubt whether there is a serious injury

#### **OTHER ABNORMAL SITUATIONS**

##### **NTNU:**

You will find the reporting form for non-conformance on:

<https://innsida.ntnu.no/wiki/-/wiki/Norsk/Melde+avvik>

##### **SINTEF:**

Synergi

## **7 ASSESSMENT OF TECHNICAL SAFETY**

### **7.1 HAZOP**

*See Chapter 13 "Guide to the report template".*

The experiment set up is divided into the following nodes:

Node 1	Test rig in Klimalab
Node 2	

**Attachments, Form: Hazop\_mal**

**Conclusion: (Safety taken care of)**

### **7.2 Flammable, reactive and pressurized substances and gas**

Are any flammable, reactive and pressurized substances and gases in use?

NO	
----	--

### **7.3 Pressurized equipment**

Is any pressurized equipment in use?

NO	
----	--

### **7.4 Effects on the environment (emissions, noise, temperature, vibration, smell)**

Will the experiments generate emission of smoke, gas, odour or unusual waste?

Is there a need for a discharge permit, extraordinary measures?

NO	
----	--

**Attachments:**

**Conclusion:**

## 7.5 Radiation

*See Chapter 13 "Guide to the report template".*

NO	
----	--

**Attachments:**

**Conclusion:**

## 7.6 Chemicals

Will any chemicals or other harmful substances be used in the experiments? Describe how the chemicals should be handled (stored, disposed, etc.) Evaluate the risk according to safety datasheets, MSDS. Is there a need for protective actions given in the operational procedure?

NO	
----	--

**Attachments:**

**Conclusion:**

## 7.7 Electricity safety (deviations from the norms/standards)

NO	
----	--

**Attachments:**

**Conclusion:** The use of electrical equipment in this experiment complies with the standards and regulations in terms of touch danger.

# 8 ASSESSMENT OF OPERATIONAL SAFETY

Ensure that the procedures cover all identified risk factors that must be taken care of. Ensure that the operators and technical performance have sufficient expertise.

## 8.1 Procedure HAZOP

*See Chapter 13 "Guide to the report template".*

The method is a procedure to identify causes and sources of danger to operational problems.

**Attachments:** HAZOP\_MAL\_Prosegyre

**Conclusion:** Simple misunderstandings will not lead to dangerous situations. Form not filled.

## 8.2 Operation procedure and emergency shutdown procedure

*See Chapter 13 "Guide to the report template".*

The operating procedure is a checklist that must be filled out for each experiment.

Emergency procedure should attempt to set the experiment set up in a harmless state by unforeseen events.

**Attachments:** Procedure for running experiments

**Emergency shutdown procedure:** In case of emergency, fans should be switched off and manikin turned off if possible before leaving the rig.

### 8.3 Training of operators

The operator should know how to use the anemometers, how to adjust the watt level on the thermal manikin and how to operate both exhaust fans and supply fan. Training should be completed before the actual measurements begin. The operator should also be responsible and tidy, so that no accidents occur. In case of evacuation, the operator should turn off the manikin and the fans and leave the building.

### 8.4 Technical modifications

- *Technical modifications made by the operator (e.g. Replacement of components, equal to equal)*
- *Technical modifications that must be made by Technical staff (for example, modification of pressure equipment).*
- *What technical modifications give a need for a new risk assessment (by changing the risk picture)?*

### 8.5 Personal protective equipment

- *Use gloves when there is opportunity for contact with hot/cold surfaces.*

### 8.6 General Safety

An operator should always be present to follow the measurements. However, there is no risk involved when leaving the rig for a few moments. Door to the room must always be closed during measurements. No entry allowed at that point.

### 8.7 Safety equipment

Not required

### 8.8 Special predations

## 9 QUANTIFYING OF RISK - RISK MATRIX

*See Chapter 13 "Guide to the report template".*

The risk matrix will provide visualization and an overview of activity risks so that management and users get the most complete picture of risk factors.

IDnr	Aktivitet-hendelse	Frekv-Sans	Kons	RV
	<i>Rotating exhaust fans, danger of contact</i>	1	C	C1
	<i>Shock damage from touching exposed metal</i>	1	D	D1

## 10 REGULATIONS AND GUIDELINES

Se <http://www.arbeidstilsynet.no/regelverk/index.html>

- Lov om tilsyn med elektriske anlegg og elektrisk utstyr (1929)
- Arbeidsmiljøloven
- Forskrift om systematisk helse-, miljø- og sikkerhetsarbeid (HMS Internkontrollforskrift)
- Forskrift om sikkerhet ved arbeid og drift av elektriske anlegg (FSE 2006)
- Forskrift om elektriske forsyningsanlegg (FEF 2006)
- Forskrift om utstyr og sikkerhetssystem til bruk i eksplosjonsfarlig område NEK 420
- Forskrift om håndtering av brannfarlig, reaksjonsfarlig og trykksatt stoff samt utstyr og anlegg som benyttes ved håndteringen
- Forskrift om Håndtering av eksplosjonsfarlig stoff
- Forskrift om bruk av arbeidsutstyr.
- Forskrift om Arbeidsplasser og arbeidslokaler
- Forskrift om Bruk av personlig verneutstyr på arbeidsplassen
- Forskrift om Helse og sikkerhet i eksplosjonsfarlige atmosfærer
- Forskrift om Høytrykksspyling
- Forskrift om Maskiner
- Forskrift om Sikkerhetsskiltning og signalgivning på arbeidsplassen
- Forskrift om Stillaser, stiger og arbeid på tak m.m.
- Forskrift om Sveising, termisk skjæring, termisk sprøyting, kullbuemeisling, lodding og sliping (varmt arbeid)
- Forskrift om Tekniske innretninger
- Forskrift om Tungt og ensformig arbeid
- Forskrift om Vern mot eksponering for kjemikalier på arbeidsplassen (Kjemikalieforskriften)
- Forskrift om Vern mot kunstig optisk stråling på arbeidsplassen
- Forskrift om Vern mot mekaniske vibrasjoner
- Forskrift om Vern mot støy på arbeidsplassen

Veiledninger fra arbeidstilsynet

se: <http://www.arbeidstilsynet.no/regelverk/veiledninger.html>

## 11 DOCUMENTATION

- Tegninger, foto, beskrivelser av forsøksoppsetningen
- Hazop\_mal
- Sertifikat for trykkpåkjent utstyr
- Håndtering avfall i NTNU
- Sikker bruk av LASERE, retningslinje
- HAZOP\_MAL\_Prosedyre
- Forsøksprosedyre
- Opplæringsplan for operatører
- Skjema for sikker jobb analyse, (SJA)
- Apparatorkortet
- Forsøk pågår kort

### ATTACHMENT E: PROCEDURE FOR RUNNING EXPERIMENTS

<b>Prosjekt</b> <i>Experimental study of the airflow distribution in close proximity to the human body with a downward plane jet</i>		
<b>Apparatur</b> Klimarom VVSLab - Diffuser experiment with air curtain	<b>Dato</b>	<b>Signatur</b>
<b>Prosjektleder</b> Guangyu Cao	17.11.2016	Gyu Cao

	Conditions for the experiment:	Completed
	Experiments should be run in normal working hours, 08:00-16:00 during winter time and 08.00-15.00 during summer time. Experiments outside normal working hours shall be approved.	X 12.12.16
	One person must always be present while running experiments, and should be approved as an experimental leader.	X
	An early warning is given according to the lab rules, and accepted by authorized personnel.	X
	Be sure that everyone taking part of the experiment is wearing the necessary protecting equipment and is aware of the shut down procedure and escape routes.	X
	<b>Preparations</b>	<b>Carried out</b>
	Post the "Experiment in progress" sign.	✓
	Hang up black blanket (to be able to see smoke profile)	✓
	Turn on the fan to supply air through the diffuser nozzle, and check outlet velocity at 10 different locations that the flow has an even velocity	✓
	Measure initial air temperature in the room. Check at 3-4 different heights to be sure there is little thermal stratification	✓
	Measure all wall surface temperatures in case of radiation influence on the thermal manikin	✓
	Place anemometers and manikin at starting locations	✓
	Heat up manikin to the correct temperature, turn on the air curtain, heat it to 21°C (room temp.) and adjust it to have a velocity of 1.5 m/s at the outlet	✓
	<b>During the experiment</b>	
	Measure velocity at all relevant locations	✓
	Check that the temperature in the room is the same as the air curtain temperature.	✓
	<b>End of experiment</b>	
	Turn off fans and heat source	✓
	Remove all obstructions/barriers/signs around the experiment.	✓
	Tidy up and return all tools and equipment.	✓
	Tidy and cleanup work areas.	✓
	Return equipment and systems back to their normal operation settings (fire alarm)	✓
	<b>To reflect on before the next experiment and experience useful for others</b>	

	Was the experiment completed as planned and on scheduled in professional terms?	OK, but delayed
	Was the competence which was needed for security and completion of the experiment available to you?	✓
	Do you have any information/ knowledge from the experiment that you should document and share with fellow colleagues?	✓

Operator(s):

Navn	Dato	Signatur
Marie Steffensen	14.11.2016	Marie Steffensen

# Bibliography

- Abramovich, G. N., 1963. *The Theory of Turbulent Jets*. The M.I.T press, The Massachusetts Institute of Technology, Cambridge Massachusetts.
- Aftab, S. M. A., Mohd Rafie, A. S., Razak, N. A., Ahmad, K. A., 2016. Turbulence model selection for low reynolds number flows. *PLoS ONE* 11 (4), e0153755.
- ANSYS, 2016. *ANSYS Documentation Guide 17*. ANSYS Inc., 17th Edition.
- Awbi, H., 1989. Application of computational fluid dynamics in room ventilation. *Building and Environment* 24 (1), 73 – 84.
- Awbi, H. B., 2003. *Ventilation of Buildings*, 2nd Edition. Taylor and Francis.
- Bar-Ilan, J., 2008. Which h-index? a comparison of wos, scopus and google scholar. *Scientometrics* 74 (2), 257–271.
- Baturin, V. V., 1972. *Fundamentals of Industrial Ventilation*, 3rd Edition. Vol. 8 of *Heating, Ventilation and Refrigeration*. Pergamon Press.
- Bibsys, 2016. Søkjetjenesten oria.no. Accessed 26.09.16.  
URL <http://www.bibsys.no/produkter-tjenester/produkter/soketjenesten-oria/>
- Borges, C. P., Quintela, D. A., Brites, G. N., Gaspar, A. R., Costa, J. J., 2002. Analysis of thermal plumes generated by a seated person, a thermal manikin and a dummy. In: *Roomvent 8th International Conference*, Copenhagen, Denmark, September 2002.
- Cao, G., Nielsen, P. V., Jensen, R. L., Heiselberg, P., Liu, L., Heikkinen, J., 2015. Protected zone ventilation and reduced personal exposure to airborne cross-infection. *Indoor Air* 25 (3), 307–319.
- Cao, G., Sirén, K., Kilpeläinen, S., 2014. Modelling and experimental study of performance of the protected occupied zone ventilation. *Energy and Buildings* 68, Part A, 515–531.

- Cebeci, T., Shao, J. P., Kafyeke, F., Laurendeau, E., 2005. *Computational Fluid Dynamics for Engineers*. Horizons publishing.
- Cengel, Y. A., Cimbala, J. M., 2010. *Fluid Mechanics - Fundamentals and Applications*, 2nd Edition. McGraw-Hill.
- Chapman, D., 1979. Computational aerodynamics development and outlook. *AIAA Journal* 17 (12), 1293–1313, cited By 0.
- Chen, Q., Xu, W., 1998. A zero-equation turbulence model for indoor airflow simulation. *Energy and Buildings* 28 (2), 137 – 144.
- Corgnati, S. P., da Silva, M. G., 2011. Indoor climate quality assessment. *Rehva Guidebook* no. 14.
- Craven, B. A., Settles, G. S., Mar. 2006. A computational and experimental investigation of the human thermal plume. *Journal of Fluids Engineering* 128 (6), 1251–1258.
- Crowe, C. T., Elger, D., Williams, B. C., Roberson, J. A., 2010. *Engineering Fluid Mechanics*, 9th Edition. John Wiley & Sons.
- Davidson, L., Nielsen, P. V., Sveningsson, A., 2003. Modification of the v2f model for computing the flow in a 3d wall jet. *Proceedings of the International Symposium on Turbulence, Heat and Mass Transfer*, October 12 - 17, 2003, Antalya, Turkey.
- de Dear, R. J., Arens, E., Hui, Z., Oguro, M., 1997. Convective and radiative heat transfer coefficients for individual human body segments. *International Journal of Biometeorology* 40 (3), 141–156.
- Deo, R. C., Mi, J., Nathan, G. J., 2007. The influence of nozzle-exit geometric profile on statistical properties of a turbulent plane jet. *Experimental Thermal and Fluid Science* 32 (2), 545 – 559.
- Dokka TH, T. P., 2002. A simplified model for human induced convective air flows - model predictions compared to experimental data. In: *Proceedings of Room Vent 2002, 8th International Conference on Air Distribution in Rooms*. pp. p 269–272.
- Dygert, R. K., Russo, J. S., Dang, T. Q., Khalifa, H. E., 2009. Modeling of the human body to study the personal micro environment. *ASHRAE Transactions* 115 (2), 407 – 420.
- Fanger, P. O., 1972. *Thermal Comfort - Analysis and Applications in Environmental Engineering*. McGraw-Hill.
- Foster, A., Swain, M., Barrett, R., D'Agaro, P., James, S., 2006. Effectiveness and optimum jet velocity for a plane jet air curtain used to restrict cold room infiltration. *International Journal of Refrigeration* 29 (5), 692 – 699.

- Gao, N., Niu, J., 2004. Cfd study on micro-environment around human body and personalized ventilation. *Building and Environment* 39 (7), 795 – 805.
- Gao, N., Niu, J., Zhang, H., 2006. Coupling cfd and human body thermoregulation model for the assessment of personalized ventilation. *HVAC&R Research* 12 (3), 497–518.
- Gao, N. P., Niu, J. L., 2005. Cfd study of the thermal environment around a human body: A review. *Indoor and Built Environment* 14 (1), 5–16.
- Germano, M., Piomelli, U., Moin, P., Cabot, W. H., 1991. A dynamic subgrid-scale eddy viscosity model. *Physics of Fluids A* 3 (7), 1760.
- Gibson, M. M., Launder, B. E., 06 1978. Ground effects on pressure fluctuations in the atmospheric boundary layer. *Journal of Fluid Mechanics* 86 (3), 491–511.
- Goodfellow, H., Tähti, E., 2001. *Industrial Ventilation - Design Guidebook*. Academic Press.
- Gutmark, E., Wygnanski, I., 1976. The planar turbulent jet. *Journal of Fluid Mechanics* 73 (3), 465–495.
- Hargreaves, D. M., Scase, M. M., Evans, I., 2012. A simplified computational analysis of turbulent plumes and jets. *Environmental Fluid Mechanics* 12 (6), 555–578.
- Heskestad, G., 1984. Engineering relations for fire plumes. *Fire Safety Journal* 7 (1), 25 – 32.
- Homma, H., Yakiyama, M., 1988. Examination of free convection around occupant's body caused by its metabolic heat. *ASHRAE Transactions* (94), 104–124.
- Incropera, F., Dewitt, D. P., Bergman, T. L., Lavine, A. S., 2013. *Principles of Heat and Mass Transfer*, 7th Edition. John Wiley & Sons, p. 594-630.
- Jones, W. P., 2001. *Air Conditioning Engineering*, 5th Edition. Taylor and Francis, chapter 4.
- Kilic, M., Sevilgen, G., 2008. Modelling airflow, heat transfer and moisture transport around a standing human body by computational fluid dynamics. *International Communications in Heat and Mass Transfer* 35 (9), 1159 – 1164.
- Kong, M., Zhang, J., Wang, J., 2015. Air and air contaminant flows in office cubicles with and without personal ventilation: A cfd modeling and simulation study. *Building Simulation* 8 (4), 381–392.
- Kuznik, F., Rusaouën, G., Brau, J., 2007. Experimental and numerical study of a full scale ventilated enclosure: Comparison of four two equations closure turbulence models. *Building and Environment* 42 (3), 1043 – 1053.
- Kuznik, F., Rusaouën, G., Hohotá, R., 2006. Experimental and numerical study of a mechanically ventilated enclosure with thermal effects. *Energy and Buildings* 38 (8), 931 – 938.

- Launder, B., Sharma, B., 1974. Application of the energy dissipation model of turbulence to the calculation of flow near a spinning disk. *Letters in Heat and Mass Transfer* 1(2), November 1974, 131–137.
- Launder, B., Spalding, D., 1974. The numerical computation of turbulent flows. *Computer Methods in Applied Mechanics and Engineering* 3 (2), 269 – 289.
- Licina, D., Melikov, A., Sekhar, C., Tham, K. W., 2015. Human convective boundary layer and its interaction with room ventilation flow. *Indoor Air* 25, 21–35.
- Licina, D., Pantelic, J., Melikov, A., Sekhar, C., Tham, K. W., 2014. Experimental investigation of the human convective boundary layer in a quiescent indoor environment. *Building and Environment* 75, 79–91.
- Lilly, D. K., 1992. A proposed modification of the germano subgrid-scale closure method. *Physics of Fluids A: Fluid Dynamics* 4 (3), 633–635.
- Liu, Y., Liu, Z., Luo, J., 2015. Numerical investigation of the unsteady thermal plume around human body in closed space. *Procedia Engineering* 121, 1919 – 1926, the 9th International Symposium on Heating, Ventilation and Air Conditioning (ISHVAC) joint with the 3rd International Conference on Building Energy and Environment (COBEE), 12-15 July 2015, Tianjin, China.
- Makhoul, A., Ghali, K., Ghaddar, N., 2013. Desk fans for the control of the convection flow around occupants using ceiling mounted personalized ventilation. *Building and Environment* 59, 336–348.
- Makhoul, A., Ghali, K., Ghaddar, N., 2015. Low-mixing coaxial nozzle for effective personalized ventilation. *Indoor and Built Environment* 24 (2), 225–243.
- Mazej, M., Butala, V., 2011. Investigation in the characteristics of the personal ventilation using computational fluid dynamics. *Indoor and Built Environment* 21 (6), 749–771.
- Menter, F. R., 1994. Two-equation eddy-viscosity turbulence models for engineering applications. *AIAA Journal* 32 (8), 1598–1605.
- Munson, B., Young, D., Okiishi, T., 2002. *Fundamentals of Fluid Mechanics*, 4th Edition. John Wiley & Sons.
- Murakami, S., Kato, S., Zeng, J., 2000. Combined simulation of airflow, radiation and moisture transport for heat release from a human body. *Building and Environment* 35 (6), 489 – 500.
- Nielsen, P. V., 2015. Fifty years of cfd for room air distribution. *Building and Environment* 91, 78 – 90, fifty Year Anniversary for Building and Environment.

- NS-EN7730, 2005. Ergonomics of the thermal environment - analytical determination and interpretation of thermal comfort using calculation of the pmv and ppd indices and local thermal comfort criteria, ns-en iso 7730.
- Rohdin, P., Moshfegh, B., 2007. Numerical predictions of indoor climate in large industrial premises. a comparison between different k–ε models supported by field measurements. *Building and Environment* 42 (11), 3872 – 3882.
- Rong, L., Nielsen, P. V., 2008. Simulation with different turbulence models in an annex 20 room benchmark test using ansys cfx 11.0. DCE Technical Report, Aalborg University 46.
- Rouse, H., Yih, C. S., Humphreys, H. W., 1952. Gravitational convection from a boundary source. *Tellus* 4 (3), 201–210.
- Seim, B. G., 2009. Study of hydrofoil wakes using piv and cfd. Master's thesis, Norwegian University of Science and Technology.
- Shur, M., Spalart, P., Strelets, M., Travin, A., 1999. Detached-eddy simulation of an airfoil at high angle of attack. In: Rodi, W., Laurence, D. (Eds.), *Engineering Turbulence Modelling and Experiments 4*. Elsevier Science Ltd, Oxford, pp. 669 – 678.
- Skistad, H., 1995. Industriventilasjon, hefte1: Innblåsning og avsug.
- Skåret, E., 2000. Ventilasjonsteknisk håndbok. Norges byggforskningsinstitutt, håndbok 48.
- Sørensen, D. N., Voigt, L. K., 2003. Modelling flow and heat transfer around a seated human body by computational fluid dynamics. *Building and Environment* 38 (6), 753 – 762.
- Storleer, R., 2016. Endnote kurs, ntnu.
- Szopa, A. B., 2015. Experimental study of the performance of protected zone ventilation used for a reception space. Master's thesis, Norwegian University of Science and Technology (NTNU).
- Tanabe, S., Kobayashi, K., Nakano, J., Ozeki, Y., Konishi, M., 2002. Evaluation of thermal comfort using combined multi-node thermoregulation (65mn) and radiation models and computational fluid dynamics (cfd). *Energy and Buildings* 34 (6), 637 – 646, special Issue on Thermal Comfort Standards.
- Tieszen, S., A. Ooi, P. D., Behnia, M., 1998. Modeling of natural convection heat transfer. *Proceedings of the Summer Program for Center of Turbulence Research*.
- Turner, J. S., 1973. *Buoyancy effects in fluids*. Cambridge University Press.
- Veselý, M., Zeiler, W., 2014. Personalized conditioning and its impact on thermal comfort and energy performance – a review. *Renewable and Sustainable Energy Reviews* 34, 401–408.
- Wang, M., Chen, Q., 2009. Assessment of various turbulence models for transitional flows in an enclosed environment (rp-1271). *HVAC&R Research* 15 (6), 1099–1119.

- Wang, M., Chen, Q. Y., 2010. On a hybrid rans/les approach for indoor airflow modeling (rp-1271). *HVAC&R Research* 16 (6), 731–747.
- Wei, Y., Xudong, Y., Ming, S., 2009. How to simplify computer simulated persons (csps) for modeling personal microenvironments: Comparison and case studies. *ASHRAE Transactions* 115 (1), 473 – 483.
- White, F. M., 2006. *Viscous fluid flow*, 3rd Edition. McGraw-Hill.
- Xu, W., Chen, Q., 2001. A two-layer turbulence model for simulating indoor airflow: Part i. model development. *Energy and Buildings* 33 (6), 613 – 625.
- Yakhot, V., Orszag, S. A., Oct 1986. Renormalization-group analysis of turbulence. *Physical Review Letters* 57, 1722–1724.
- Yang, B., Melikov, A. K., Sekhar, C., 2009. Performance evaluation of ceiling mounted personalized ventilation system. *ASHRAE Transactions* 115.
- Zhai, Z. J., Zhang, Z., Zhang, W., Chen, Q. Y., 2007. Evaluation of various turbulence models in predicting airflow and turbulence in enclosed environments by cfd: Part 1—summary of prevalent turbulence models. *HVAC&R Research* 13 (6), 853–870.
- Zhang, Z., Zhang, W., Zhai, Z. J., Chen, Q. Y., 2007. Evaluation of various turbulence models in predicting airflow and turbulence in enclosed environments by cfd: Part 2—comparison with experimental data from literature. *HVAC&R Research* 13 (6), 871–886.
- Zhu, S., Kato, S., Ooka, R., Sakoi, T., 2007. Development of a computational thermal manikin applicable in a nonuniform thermal environment—part 1: Coupled simulation of convection, radiation, and smith’s human thermal physiological model for sensible heat transfer from a seated human body in radiant environment. *HVAC&R Research* 13 (4), 661–679.
- Zukowska, D., 2011. *Airflow interactions in rooms – convective plumes generated by occupants*. Phd thesis, International Center for Indoor Environment and Energy, Technical University of Denmark.
- Zukowska, D., Melikov, A., Popiolek, Z., 2007. *Thermal plume above a simulated sitting person with different complexity of body geometry*, 1st Edition. Vol. 3. FINVAC ry, pp. 191–198.
- Zukowska, D., Popiolek, Z., Melikov, A., 2010. Determination of the integral characteristics of an asymmetrical thermal plume from air speed/velocity and temperature measurements. *Experimental Thermal and Fluid Science* 34 (8), 1205 – 1216.